Investigation of an Intumescent Coating System in Pilot and Laboratory-scale Furnaces

Nørgaard, Kristian Petersen

Publication date:
2014

Document Version
Publisher's PDF, also known as Version of record

Investigation of an Intumescent Coating System in Pilot and Laboratory-scale Furnaces

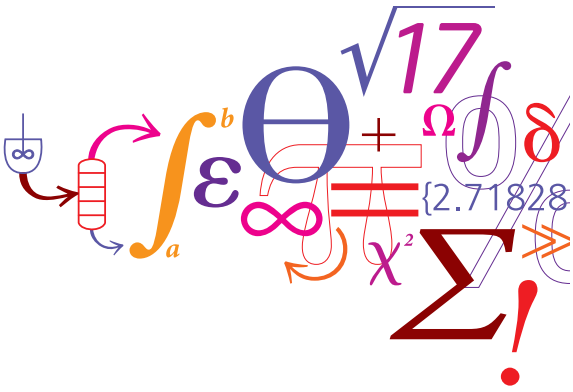

Kristian Petersen Nørgaard

Ph.D. Thesis

February 2014

DTU Chemical Engineering
Department of Chemical and Biochemical Engineering

Investigation of an Intumescent Coating System in Pilot and Laboratory-scale Furnaces

Ph.D. Thesis

Kristian Petersen Nørgaard

February 28, 2014

Supervisors:

Søren Kiil

Kim Dam-Johansen

Pere Català

CHEC Research Centre

Department of Chemical and Biochemical Engineering

Technical University of Denmark, DTU, Denmark

DTU Chemical Engineering
Department of Chemical and Biochemical Engineering

Address: Centre of Combustion and Harmful Emission Control
Department of Chemical and
Biochemical Engineering
Technical University of Denmark
Søltofts Plads, Building 229
DK-2800 Kgs. Lyngby
Denmark
Phone: +45 4525 2800
Fax: +45 4525 4588
Web: www.chec.kt.dtu.dk

Print: J&R Frydenberg A/S
København
March 2015

ISBN: 978-87-92481-59-7

Table of Contents

Preface

This dissertation is the result of three years of work on the project "Investigation of an Intumescent Coating System in Pilot- and Laboratory-scale Furnaces". The majority of the work has been performed in the CHEC research group at The Department of Chemical and Biochemical Engineering, Technical University of Denmark. Experiments have also been performed in Spain at Hempel A/S and at DTU FOOD. The work was supervised by Associate Professor Søren Kiil, Professor Kim Dam-Johansen, and Fire Protection R&D Manager in Hempel A/S, Pere Català. The work has been funded by the Technical University of Denmark and The Hempel Foundation.

Over the course of the past three years, different people have been involved in the work and contributed in one way or another. Some people deserve a special acknowledgement for making this work possible. Søren has been the main supervisor of this project and it has been a very good experience working with you. There have always been quick and highly relevant suggestions and I really appreciate the collaboration and everything I have learned from you. I would also like to thank Kim for giving me the opportunity in the first place to pursue this project. Especially I have enjoyed all our meetings, discussions and generation of ideas, which has been a fantastic experience. Pere has indeed shaped the project with his ideas, suggestions and comments and I have learned a lot from our co-orperation. Also, I have felt very welcome during my stays in Barcelona and my work with Pere's team has been an extraordinarily good experience. I feel deep gratefulness for all the guidance provided by Adria, Erik, Joan, Jose, Maite, Michael, Miguel, Lars, and Xavier and for letting me be a part of your team during my stays at Hempel. Your very fast responses and advice to every question I have e-mailed to you during this project is highly appreciated. The students I have supervised, Kristian Rønnedal, Andreu Franco and Noelia Rubio, deserve sincere thanks for their tremendous efforts. I would also like to thank all the students, Ph.D. students, technicians and staff in CHEC. It has been great working with such dedicated and competent people and over the past three years I have come to consider you as dear friends. Jakob Christensen has been invaluable in this project especially with his help on plotting techniques and by being a very good friend. I would also like to thank my friend Jacob Brix for his friendship and advice during my project. Sincere thanks goes to my parents and parents in law for all their help making it possible to work whenever needed. I would also like to send thanks to my

daughter Anja for being a constant source of happiness. Finally, and most of all, I would like to thank my wife for everything, your understanding and support during this project.

In the thesis, references are given at the end of each chapter.

Kristian Petersen Nørgaard
Kgs. Lyngby, February 28, 2014

Summary

Steel is an incombustible substrate, but at elevated temperatures structural steel suffers from a drastic reduction in mechanical strength. In the event of a fire, the reduced strength may lead to collapse of the structure. A method to prolong the time before steel reaches the critical temperature (450 - 600 ^{o}C), at which the collapse may occur, is the use of a fire protective intumescent coating, which swells when exposed to temperatures above about 200 ^{o}C. The swelling of the intumescent coating happens according to a complex sequence of chemical reactions, whereby the coating forms a porous char, which thermally insulates the substrate. In addition to the coating itself, several process parameters influence the performance of the intumescent coating. Such parameters may for instance be the interaction with an underlying anticorrosive primer, the heating rate employed, or the oxygen content in the fire. In this work, focus has been on process parameters for an intumescent coating for so-called cellulosic fires.

The thesis contains five chapters, where Chapter 1 is a literature survey providing background knowledge on coatings, intumescent coatings in particular, and fire scenarios. In Chapter 2, the effects of coating thickness and gas-phase oxygen concentration on two epoxy primers used in an intumescent coating system were investigated. It was found that primers with a too high thickness failed in the presence of oxygen. In nitrogen, the primer did well, except for a single case, which showed a minor delamination at the edges. In addition, it was shown that the thermogravimetric behavior of the primer and intumescent coating alone could not be used for explaining the entire coating system performance. A novel experimental method, which may potentially be developed into a fast screening method of primers for intumescent coatings, is also described. Upon heating in nitrogen, a color change of the primer from red to black was observed. Potentially, this may be used as an indicator to whether a primer under an intumescent coating has been exposed to oxygen or not in gas-fired furnace experiments.

In Chapter 3, a mathematical model of an intumescent coating exposed to heating in a pilot-scale gas-fired furnace is presented. The model takes into account convective heat transfer to the char surface, conduction inside the char, and the char expansion rate. Model validation was done against experimental char expansion rates and temperatures of the steel substrate and at intra-

char positions. The model was solved in a discretized and non-discretized version and a good qualitative description of the temperature curves was found. An important learning was that temperatures measured inside the char are very important for a proper model validation. Due to its simplicity and few input parameters, the model (non-discretized version) shows a good potential as a practically applicable engineering model. Results suggest that oxygen mass transport is not a limiting factor for the char oxidation reactions. An investigation of the repeatability of the experimental temperatures showed that temperatures close to the char surface were somewhat more uncertain than the steel temperature and char temperatures close to the steel substrate.

Chapters 4 and 5 are concerned with the development of a fast screening method for the extent of expansion and char strength of intumescent coatings. The method is relevant for investigation of special cases, where the char is damaged by moving objects during a fire. The method uses the concept of shock heating to avoid long heating up and cooling down times of a furnace. In Chapter 4, it was found that for measuring char strength reliably at room temperature, dried samples were required. Chapter 5 discusses shock heating in various oxygen concentrations and verified that the expansion is affected by the gas composition. Experimental data showed that under a high heating rate, the char strength could not meaningfully be correlated to the degree of expansion. Furthermore, it was found that at the high heating rates employed thin films (147 µm) would contract horizontally while expanding vertically. This was not the case with a coating thickness of 598 µm. The strength of the char in the vertical direction was also investigated. It was found that the outer crust of the char had the highest mechanical strength and a weak zone, in the central region of the char, was identified.

Dansk resumé (Summary in Danish)

På trods af at stål ikke er et brandbart materiale, vil bærende stål ved forhøjede temperaturer opleve en drastisk reduktion i den mekaniske styrke. I tilfælde af brand kan denne reducerede styrke føre til at strukturen kollapser. En metode til forlængelse af perioden før stålet når den kritiske temperatur (450 – 600 ^{o}C), hvor kollapset sker er anvendelse af brandbeskyttende coatings der expanderer ved påvirkning af temperaturer over 200 ^{o}C. Ekspansionen af brandbeskyttende coatings sker via en kompleks serie af kemiske reaktioner, hvorved den ekspanderende coating danner porøs koks, der termisk isolerer substratet. Udover selve den brandbeskyttende coating har en mængde procesparametre indflydelse på, hvor godt det dannede kokslag beskytter stålet. Eksempler på sådanne parametre er interaktionen med en antikorrosiv primer, den anvendte opvarmningshastighed og iltkoncentrationen i brandområdet. I dette projekt har fokus været på brandbeskyttende coating egnet til såkaldte ”cellulosebrande”, hvor den transiente temperaturstigning svarer til almindelige bygningsbrande.

Afhandlingen består af 5 kapitler. Kapitel 1 udgør et litteraturstudium indeholdende baggrundsviden om coatings, særligt om brandbeskyttende coatings samt brandforløb. I kapitel 2 undersøges effekter af coatingtykkelse og iltkoncentration i gasfasen på to epoxy primere anvendt i et brandbskyttende coatingsystem. Det påvistes, at primere med for høj lagtykkelse fejlede ved tilstedeværelsen af ilt. I nitrogen klarede primerne sig godt, undtagen i et enkelt tilfælde hvor mindre delaminering ved kanterne blev observeret. Ydermere blev det vist, at det individuelle massetabsforløb af primer og brandbeskyttende coating ikke kunne anvendes til at forklare coatingsystemets samlede ydelse. En ny eksperimentiel metode, der potentielt kan udvikles til en hurtig screeningsmetode af primere til brandbeskyttende coatings er ligeledes beskrevet. Endvidere blev en farveændring fra rød til sort under opvarmning i nitrogen observeret. Potentielt kan dette muligvis bruges til at bestemme om primeren blev udsat for ilt under eksperimenter i en gasfyret ovn. I kapitel 3 præsenteres en matematisk model over en brandbeskyttende coating opvarmet i en pilot-skala gasfyret ovn. I modellen inkluderes konvektiv varmetransport til koksoverfladen, varmeledning gennem koksen og koksekpansionshastigheden. Validering af modellen blev udført mod koksekspansionshastigheden samt ståltemperaturer og temperaturer målt inde i koksen. Modellen blev løst både i en diskretiseret og ikke-diskretiseret version og en

god kvalitativ beskrivelse af temperaturkurverne blev fundet. En vigtig opdagelse var, at temperaturer målt inden i selve koksen er vigtige for en pålidelig modelvalidering. Grundet sin enkelthed og få input parametre udviser modellen potentiale til at blive en praktisk anvendelig ingeniørmodel. Desuden blev det sandsynliggjort, at massetransport af ilt fra koksoverfladen og ind i kokslaget ikke er en hastighedsbestemmende faktor for koksoxidationsreaktionerne. En undersøgelse af pilotforsøgenes repeterbarhed viste, at temperaturer målt nær koksoverfladen var mere usikre end kokstemperaturer nær stålet samt selve stålets temperatur. Kapitel 4 og 5 omhandler udviklingen af en hurtig screeningsmetode til at måle ekspansion samt styrken af koks fra brandbeskyttende coating. Metoden anvender konceptet "chokopvarmning" for at undgå lange opvarmnings- og nedkølingstider af store ovne og er endvidere relevant for undersøgelse af specielle tilfælde, hvor koks skades af objekter i bevægelse under en brand. I kapitel 4 blev det vist, at for at opnå pålidelige målinger af koksstyrken ved stuetemperatur var tørre prøver nødvendige. I kapitel 5 diskuteres chokopvarmning ved forskellige iltkoncentrationer og det blev vist, at ekspansionen er afhængig af gassammensætningen. Ved hjælp af de eksperimentielle data blev det påvist, at under de høje opvarmningshastigheder kunne koksstyrken ikke korreleres med koksens ekspansionsgrad. Tilmed blev det observeret, at under de høje opvarmningshastigheder ville tynde film (147 µm) trække sig sammen horizontalt og ekspandere vertikalt. Dette var dog ikke tilfældet ved en tykkelse på 598 µm. Koksstyrken i den vertikale retning blev også undersøgt og det blev vist, at den yderste del udviste den største mekaniske styrke.

Chapter 1 – Literature survey

1.1 Introduction

In this chapter, a literature survey on coatings, fire development, and intumescent coatings is presented. The aim of the literature survey is to give a general overview of relevant topics related to intumescent coatings and provide the reader with the necessary background information for getting the full benefit of the subsequent chapters in the thesis. In Chapters 2-5, which describe the mathematical modeling and experimental work of the Ph.D. project, more concise reviews of specific literature, relevant for each chapter, are provided in the introduction.

1.2 History and market of intumescent coatings

Commercial reference to intumescent fire protective coatings was first given with the 1938 patent by Tramm[1]. What is considered as the classical review of intumescent coatings was written by Vandersall[1,2] in 1971 and a recent review was published by Weil[2] in 2011. In recent years, after the attack on the world trade center, research on thermal protection of steel structures has intensified[3]. The development in the intumescent coatings market is shown in Figure 1.1. The growth rate from 2011-2015 is in good agreement with an annual growth rate in the use of flame retardant of 4.8% per year as estimated by Amir et al.[4]. The global market for flame retardants in 2009 is estimated to 2.2 million tons[4].

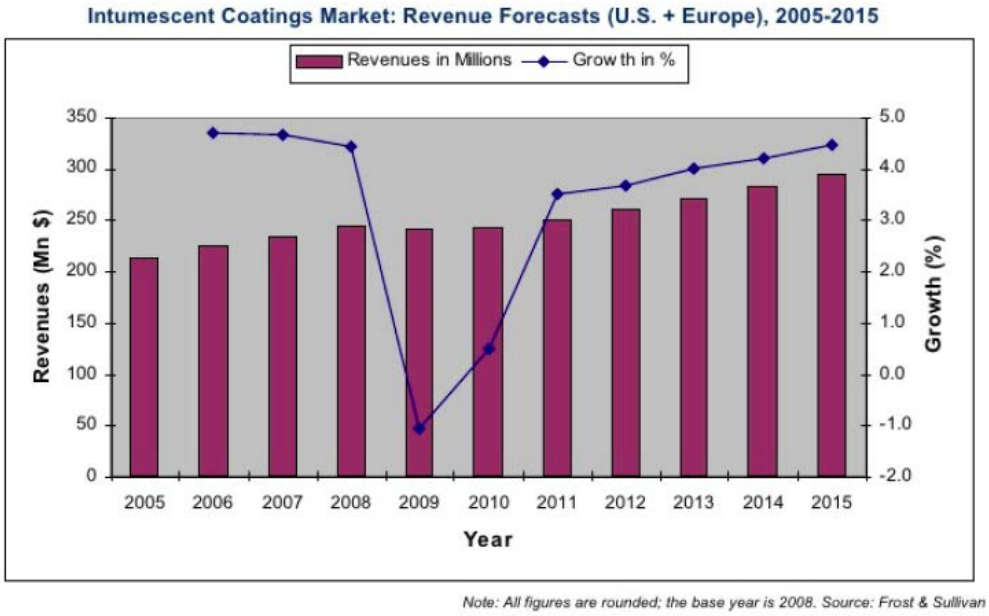

Figure 1.1. Development in intumescent coatings market. The financial crisis in 2008 can be clearly seen. Frost and Sullivan[5].

1.3 General introduction to coatings

Coatings are used for reasons of appearance or protection of a substrate (e.g. steel or wood) and may be divided into different categories based on their composition (e.g. inorganic or organic), their intended use (e.g. protective or decorative) or their appearance (e.g. clear or pigmented). Coatings are complex chemical mixtures, but a division of the compounds into four categories can be done, i.e. 1) volatile compounds (solvents), 2) binders, 3) pigments, and 4) additives. After the coating has been applied to the substrate and cured, a hard protective dry film is left behind[6].

Volatile compounds (solvents)

The volatile compounds that evaporate during and after application of the coating are referred to as solvents. The term solvent is used irrespectively of whether or not the binder is dissolved by the compound. The purpose of the solvent is to reduce the viscosity of the coating during application and film formation. However, the choice of solvent for a given coating is important because parameters related to application such as leveling of the film and adhesion are affected by the choice of solvent[6]. Another issue related to solvents is the possibility of solvents being trapped in

the film which can cause a range of undesired problems for the dried coating[7]. Organic solvents used for coatings are divided into three different groups[6]: 1) "weak hydrogen bonding solvents" which are either aliphatic (e.g. mineral spirits) or aromatic (e.g. xylene). In this group the aliphatic type has the advantage of being cheaper whereas the aromatic type dissolves more different resins. 2) "hydrogen bond acceptor solvents" (e.g. acetone) may for instance be used due to their high electrical conductivity, which is used for making solvent mixtures suitable for electrostatic spray application. 3) "hydrogen-bond donor-acceptor solvents" (e.g. propylene glycol) may for instance be used in a mix with water for latex paints.

Pigments

Pigments are fine particles which are insoluble in the other coating materials. The pigments serve one or more of the four purposes: 1) provide color, 2) hide the substrate by affecting the opacity of the dry film, 3) change the performance properties of the coating, and 4) change the application properties of the coating[6]. The pigments used in coatings form a colloidal dispersion and are divided into four different groups[6]: 1) white pigments (e.g. TiO_2) which are used to give hiding power and are not only used in white coatings. 2) color pigments (e.g. Fe_2O_3) which affect the color and opacity of the coating. When selecting the color pigments, considerations relating to factors such as dispersion properties, exterior durability, chemical resistance, solvent solubility and toxic and environmental hazards should be considered. 3) inert pigments may serve different purposes, such as adjusting rheological properties of the fluid coating, gloss and mechanical properties of the film. However, the main purpose is to occupy volume in the film and reduce cost of the coating. Therefore, the inert pigments are also referred to as fillers or extenders. 4) functional pigments are used to modify the appearance, film properties or application characteristics of the coating. An example of changes in performance properties due to pigments is anticorrosive coatings which provide cathodic protection via pigments[8].

Binders

As the name implies, the binder is used to "bind" the other compounds in the film after the solvent has evaporated. The binder adheres to the surface and forms a solid coating film. The binder and binder precursors are also referred to as resins[6]. Binders used in intumescent coatings are typically based on acrylic polymers and epoxy networks.

Additives

Additives are added to coatings in small amounts to achieve certain properties. They can consist of a wide range of chemical compounds and affect very different properties. An example of a property affected by additives is a change in the rheological properties of the coating by thickeners (e.g. organoclay). Modified rheological properties are for instance of importance for storage due to slower sedimentation of pigments[9]. Another example is the use of silicone which affects the surface slip of the coating[9]. Other examples of additives are antifoaming agents, fungicides and biocides which act as preservatives, and absorbers of ultraviolet radiation which decrease the rate of photoinitiated coating degradation[6,10].

Application of coatings

To obtain a solid coating film, the coating needs to be applied to the substrate. Before application is performed it is important to make sure the substrate is appropriately prepared and cleaned[6]. A method for substrate preparation could be sandblasting which also leaves the surface rough. Cleaning of metal is especially important[6]. After the surface cleaning the coating may be applied to the substrate. Means for this are, among others, brushes, pads, and hand rollers. When selecting the appropriate brush, factors such as handle size and width of the brush should be taken into account. Spray application is another method, which is faster and can also be used for substrates with irregular shapes. In the spray application the coating is atomized into droplets that deposit on the surface. Enhanced application of the coating by spray may be achieved by electrostatic spray where the droplets are charged before they meet the substrate. If the coating has a high viscosity, heating may be used before spray application[6].

1.4 Mechanisms of fire prevention

Depending on the expected fire scenario, different ways of obtaining fire protection (for developed fires) or fire retardancy (related to ignition) can be used. When using fire retardant polymers, three distinctions can be made: inherently flame retardant polymers, chemically modified polymers, and polymers with flame retardant additives[11,12].

- **Inherently flame retardant polymers** are almost inflammable in nature and have application temperatures ranging up to about 300 ^{o}C. The degradation temperature of these polymers is reported to be about 350 ^{o}C[11].

- **Chemically modified polymers** are obtained by incorporation of flame retardants into the polymers by copolymerization. The flame retardants can for instance be based on P, Si, B, N. Halogens can also be used, but due to undesired side effects other alternatives are being investigated[11].
- **Flame retardants as additives to polymers** obtain their fire retardant ability in different ways. One way is to form a protecting layer which captures gasses. This makes the coating swell[11] and form an intumescent char. Another way is by additives that react endothermically when exposed to heat and thereby cool the polymer below the ignition temperature[11]. A third kind of additive is used to dilute a polymer with an inert substance or a substance that produces inert gasses.

In the literature, intumescent coatings, the topic of this work, are often regarded as a subtopic of the overall field of fire/flame retardancy[11, 13, 14]. For a recent review of flame retardant polymeric coatings see Liang et al.[15].

1.5 Intumescent coatings

A special kind of coatings which are investigated in this project are intumescent coatings. To intumesce means to swell or expand. If a fire takes on and the temperature increases, the intumescent coating will begin to swell and form a porous insulating char as shown in Figure 1.2.

Figure 1.2. Photograph showing cross-section of expanded intumescent char after heating in gas-fired furnace. The photo is taken after an experiment in this Ph.D. study. The height of the char is approximately 7.5 cm.

The swelling happens according to a complex series of reactions, which will be described in detail in Chapter 2 (section 2.4). However, very briefly described intumescent coatings basically contain at least five compounds, blowing agent, carbon source, acid source, binder and pigments. As the temperature increases, the acid source decomposes and releases an acid, which reacts with the carbon source to form a phosphorous ester. Meanwhile, the binder melts and the phosphorous ester decomposes and reacts with the pigments. At the same time, gasses released from the blowing agent are trapped in the melted binder and the char expands which results in an insulting layer between the fire and substrate[16]. For illustrative purposes, the principle of intumescence can be compared to the rise of dough during baking[3]. The intumescent char layer also limits the oxygen mass transport between the substrate and air, which is particularly important when the underlying substrate is combustible[17]. A simple two step drawing of the intumescence mechanism is shown in Figure 1.3.

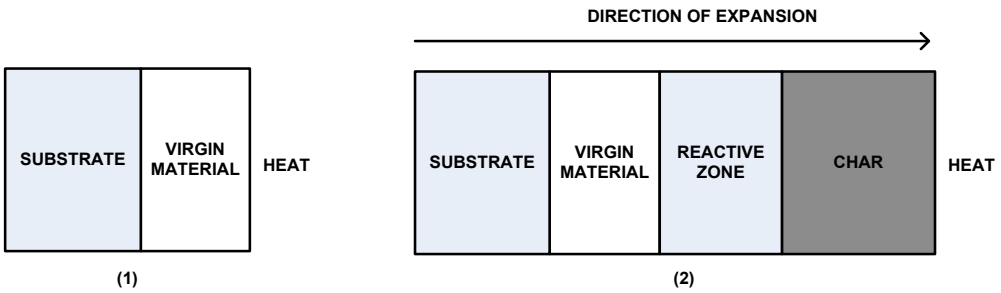

Figure 1.3. Drawing of the intumescent mechanism. The left hand illustration (1) shows the initial situation and the right hand one (2) shows the expanding coating. After Butler[17]. Figure is not to scale.

1.6 Standards and fire scenarios

A special requirement to intumescent coatings, compared to other protective coatings, is the necessity for third party approval before the coating can be marketed. The third party approval is obtained by following certain standards of which the exact procedure often vary between countries. A short introduction to the most common standards relating to approval of intumescent coatings is given in this section. In addition to the standards for testing and approval of intumescent coatings, numerous standards for other fire retardant materials exist, as described by Wilkie[13], where 49 standards are described with a wide range of parameters from flammability of furniture to the release of toxic gasses in a fire. It is noted that in the literature, research on intumescent coatings is often performed by testing materials according to standards or slightly modified versions of the standards. The standards described in this section are based on intumescent coatings for steel structures.

In general, intumescent coatings are applied to steel substrates and a fire test is performed in a gas-fired furnace. The temperature of the steel substrate is measured and the time to reach a certain critical steel temperature is recorded. The critical steel temperature is usually in the range 450-600^{o}C. This temperature range is chosen because steel looses its structural strength at this critical temperature and cannot support the load anymore[18, 19]. However, the exact critical temperature varies, as for instance according to the North American standards (UL), where the critical steel temperature is 538 ^{o}C for steel columns and 593 ^{o}C for steel beams[18, 20].

1.7 Types of fires

It is common to divide fire environments, relevant for intumescent coatings, into two categories described by so-called hydrocarbon- and cellulosic fires[19, 21-23]. The cellulosic type is encountered where the fuel is of cellulosic basis (e.g. wood and paper), whereas hydrocarbon fires are encountered in the oil and gas industry[23].

Fire development of cellulosic fires

A cellulosic fire can roughly be divided into three periods[12]: ignition, a developing fire, and a fully developed fire. In addition, a decay period can also be included in the fire description[18]. The development of a cellulosic fire is illustrated in Figure 1.4. The temperature rises to 1100 °C in about 3 hours[18], as will be addressed in the next section. In addition to changes in temperature, the heat flux and length scale, due to flame spread, increases with time, whereas the ventilation typically decreases[12].

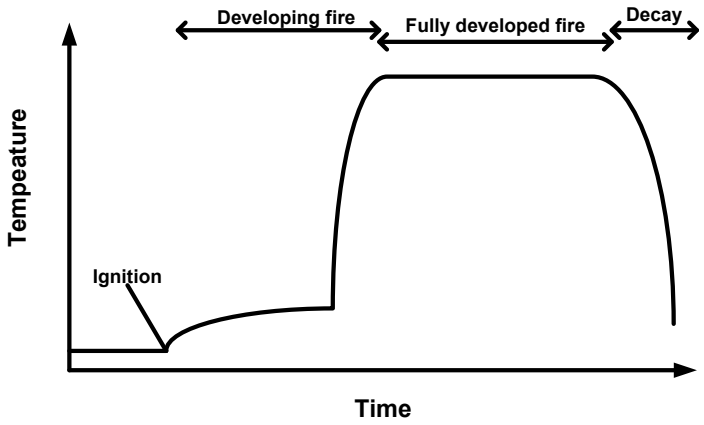

Figure 1.4. Illustration of cellulosic fire development after Schartel and Hull[12] and Lie[18]. Temperature and time on the axes are shown in arbitrary units. The steep increase before the fully developed fire is the flash over point, which is generated because walls and hot smoke radiates heat back to the fire and accelerates the reactions[24].

A frequently used standard for describing cellulosic fires is the ISO 834 standard from International Organization for Standardization. ISO 834 describes the temperature as function of time following the temperature-time curve[18]

$$T = 345 \cdot \log_{10}(8t + 1) + T_0 \quad (1\text{-}1)$$

where t is time in minutes, T is the temperature of the fire in ^{o}C and T_0 is the initial temperature in ^{o}C. The expression for the ISO 834 standard is originally derived from an enthalpy balance of an enclosure and represents a heating rate that is not likely to be exceeded when a building is on fire[18]. The details of the enthalpy balance are unknown and it is noted that several uncertainties in the proposed heating curve, for instance the ventilation and the window area in the room, will affect the temperature significantly[18]. Apart from the ISO 834 curve, another important temperature-time dependency is the ASTM E119. The severity of the ISO and the ASTM standards have been investigated and it was shown that the ASTM E119 standard is slightly more severe than the ISO 834[25]. However, the difference is small and can probably be neglected for most purposes.

An important guideline in relation to approval of intumescent coatings in Europe is the ETAG 018 - PART 2[26]. This document describes different guidelines for the approval of fire protection for steel substrates. In addition to the measurement of the steel temperature, the guideline also prescribes tests for weathering durability and the combination of topcoats and primers with intumescent coatings[26]. For the weathering durability, the exposure in approval tests varies depending on the expected use of the coating (e.g. exposed to rain or not).

Standards related to hydrocarbon and jet fires

Apart from protection of building elements, the protection of substrates in the petrochemical industry is very important. In this area, substrates may be exposed to hydrocarbon fires, which are rapid temperature rise fires where the temperature increases to about 1100 ^{o}C within the first 5 minutes[23]. Standards relating to this area differ from the ISO 834 standard by a faster temperature increase and the possibility of high speed flames. A standard, OTI 95 634, is described in Jimenez et al.[27]. In this standard, a heat flux between 200 and 250 kW/m^2 is obtained by burning 0.3 kg/s propane at a distance of 1 m from the sample. The heating rate in this fire is more than 200 ^{o}C/min and reaches 1000 ^{o}C within four minutes. Subsequently, a steady state temperature between 1100 or 1200 ^{o}C is reached. Erosive jet flames can reach 150 m/s and are used to simulate leakages from high pressure hydro-carbon gas containing vessels[19, 21]. Other similar standards for hydrocarbon fires are the UL 1709 and ISO 22899-1:2007. A comparison of the UL1709 and the ISO 834 curve is

seen in Figure 1.5. From the figure it is interesting to notice that the initial heating rates of the two curves are almost identical.

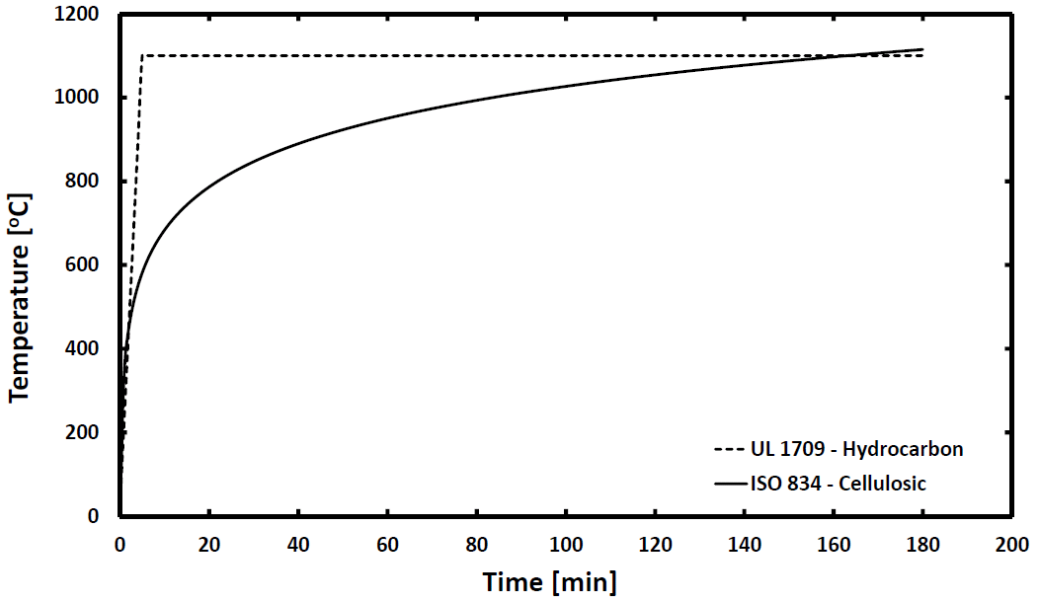

Figure 1.5. Intended temperature development of the UL 1709 and the ISO 834 standard temperature-time curve.

1.8 Chemical compounds used in intumescent coatings

In Wladyka-przybylak and Kozlowski[28], examples of chemicals used as acid source, carbon source, blowing agent and binders are provided. These are reproduced with additional information in Tables 1-1 to 1-4. Some aspects of variations in the various groups are described in the following. The binder takes part in the char formation and ensures a uniform foam structure of the final product[29]. Effects of different binders are investigated by Wang and Yang[29, 30] and Duquesne et al.[30], where it was found that addition of some self cross-linking polymers to the binder improves the thermal insulation properties of the intumescent coating system. Examples of binders are seen in Table 1.1.

Table 1.1. Components used as binders in intumescent coatings.

Binders
Mixed binder of epoxy emulsion and self-cross linked silicone acrylate[29]
Substituted styrene/aceylate/metacrylate[30]
Phenol-formaldehyde[28]
Urea-formaldehyde[28]
Dicyandiamide-formaldehyde[28]
Polyurethane[28]
Chlorinated rubber resins[28]
Latexes of vinyl chloride-vinylinene chloride copolymers[28]
Polyvinyl acetate latex[28]
Polyacrylates[28]
Silicates[28]
Bisphenol A - epoxy acrylate oligomer[31]
Epoxy resin (diglycidyl ether of bisphenol A) and Phenolic resin (resole type) cured by amine (triethylene tetraamine)[32]

It was reported that charring agents (carbon sources) such as pentaerythritol, mannitol or sorbitol are frequently used as additives. However, problems with exudation, water solubility, incompatibility with the polymer matrix, and reduced mechanical strength of the polymer matrix have been found for these additives[33]. Examples of compounds used as carbon sources are seen in Table 1.2.

Table 1.2. Components used as carbon source in intumescent coatings.

Carbon source
Maltose[14]
Arabinose[14]
Erythritol[14]
Pentaerythritol[14]
Pentaerythritol - dimer[14]
Pentaerythritol - trimer[14]
Arabitol[14]
Sorbitol[14]
Inositol[14]
Resorcinol[14]
Starches[14]

The chemical composition and the ratio between the additives are of great importance to the performance of the intumescent coating and the decomposition of the compounds should take place at appropriate temperatures to follow the sequence of the intumescent process[1]. Therefore, the decomposition temperatures of acid sources and blowing agents are shown in the Tables 1-3 and 1-4, respectively.

Table 1.3. Components used as acid sources in intumescent coatings. Decomposition temperatures are also shown where available.

Acid sources /dehydrating agents	Decomposition temperature [°C]
Monoammonium phosphate[28]	147[28]
Diammonium phosphate [28]	87-147[28]
Ammonium polyphosphate[28]	215[28]
Melamine phosphate[28]	~300[28]
Guanyl Urea phosphate[28]	191[28]
Urea phosphate[28]	130[28]
Diammonium phosphate[28]	400[28]
Ammonium tetraborate[28]	-

Table 1.4. Components used as blowing agent. Decomposition temperature and gasses produced during decomposition are also provided[14].

Name	Decomposition temperature in the coating [°C]	Gases produced
Dicyandiamide[14, 28]	~210[14, 28]	NH_3, CO_2, H_2O[14, 28]
Melamine[14, 28]	250[14, 28]	NH_3, CO_2, H_2O[14, 28]
Guanidine[14, 28]	160[14], 190[28]	NH_3, CO_2, H_2O[14, 28]
Glycine[14, 28]	~233[14, 28]	NH_3, CO_2, H_2O[14, 28]
Urea[14, 28]	~130[14, 28]	NH_3, CO_2, H_2O[14, 28]
Chlorinated paraffin (Degree of chlorination 70 % Cl)[14, 28]	190[14] 160-350[28]	HCl, CO_2, H_2O[14, 28]

1.9 Gasses released from intumescent coatings

As described in earlier sections, gasses are released in intumescent coatings during degradation of the blowing agent. In addition, gasses from char degradation reactions may also be produced. Examples of these gasses are seen in Table 1.5. A special concern is the release of toxic gasses, especially from organic intumescent coatings[34]. It is mentioned that phosphorous compounds can

be used with fewer problems because their gas release is less toxic and corrosive[31] than other fire retardants. This is important because the use of halogenated fire retardants is a concern that has led to more focus on intumescent coatings[35]. It is also known that polymeric materials release toxic gasses during combustion[36, 37]. An article mentions that suppliers, due to large smoke generation, generally do not recommend the use of epoxy based coatings for interior spaces[38]. In an older study[39], a discussion of the corrosivity of smoke is given. Here it was found that there is no direct correlation between the content of halogens and the corrosivity of the smoke produced during a fire. In addition to the primary purpose of intumescent coatings, which is to maintain structural stability during a fire, corrosive gasses released during the fire may also cause a problem to the structural stability. This is because investigations and cleaning procedures may have to be performed following the fire and thus it should preferably remain stable[39].

Table 1.5. Volatile products from intumescent coatings. The method of analysis in each case is also shown.

Gas	Analysis method
CO_2[31]	TG-FTIR
CO[31]	TG-FTIR
H_2O[31]	TG-FTIR
CH_4[31]	TG-FTIR
Alkane[31]	TG-FTIR
Aldehyde[31]	TG-FTIR
Carboxylic acid[31]	TG-FTIR
Alkene[31]	TG-FTIR
Aromatic compounds[31]	TG-FTIR
Phenol[31]	TG-FTIR
NH_3[27]	-
NO_2[35]	TGA
SO_2[35]	TGA
HCl[35]	TGA

1.10 Additives in intumescent coatings

In the recent review of intumescent coatings by Weil[2], a thorough description of additives used in intumescent coatings is given. An overview of the additives and comments to their performance are available in Table 1.6. The table is included in the literature survey to exemplify how addition of various chemicals can change the performance of an intumescent coating.

Table 1.6. Selected additives for intumescent coatings. Taken from Weil[2].

Additive	Type of coating	Comment
Zeolites 4A (Na A zeolite)[40]	Classical APP/Pentaerythritol	Formation and stabilization of phosphorous carbonaceous structure leading to improved shield which reduce fuel feeding to the flame.
Polyamide-6[40]	APP/ethylene-vinyl acetate system	Interaction between polyamide-6 and APP by formation of a heat protective shield
Water soluble sodium silicate borax, alumina trihydrate and kaolin[41]		Formation of vitreous thermal barrier
Boric acid[42]	Epoxy, APP, triaryl phosphate, THEIC, silica, perlite and ceramic fibers	Commercialized for hydrocarbon fires
Boric acid[27]	APP-epoxy based	Increased thermal protection, highest expansion, better adhesion and mechanical resistance
Zinc oxide and borate[43]	APP/melamine, flexible epoxy mastics	Improved thermal protection
Refractory fibers (Alumina and silica based fibers)[44]		Improve the high temperature performance and long duration protection.
Alumina silica (fiber Fiberfrax® HS-70C) alumina fiber (Zicar ALBF-1)[45]		Enhance toughness of residual char

1.11 Temperatures and mechanisms of importance

In the literature on intumescent coatings, many different temperatures are mentioned. These are important because they determine the reactions that occur and the rates of heat and mass transport in the intumescent coating. A drawing with the important heat and mass transfer mechanisms for an intumescent coating exposed to a fire is shown in Figure 1.6. Which of the processes that takes place depend on the precise temperature in the coating at a given position and the composition of the coating.

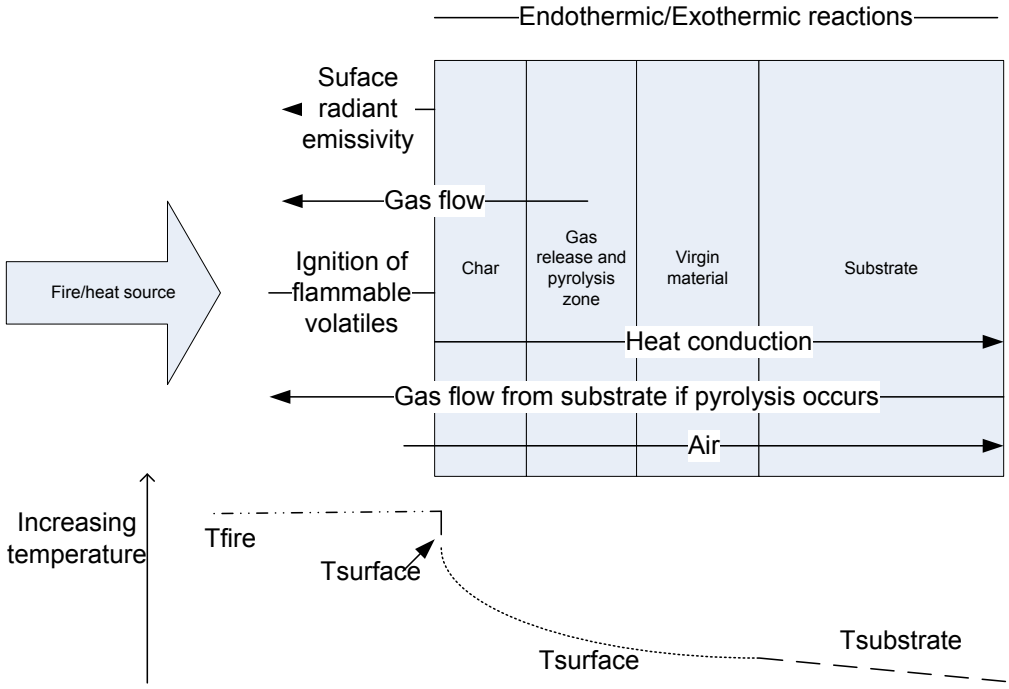

Figure 1.6. Schematic illustration (cross section-view) of activated intumescent coating on steel substrate. The primer coating is not shown. Modified from drawing in Mouritz et al.[46] to illustrate the intumescent process. Temperatures are indicated on the figure for illustrative purposes.

1.12 Substrates and uses of intumescent coatings

In this section a short overview of various uses and substrates for intumescent coatings is summarized. A common kind of protection, which is often mentioned in the literature, is structural

steel. The research into protection of structural steel with intumescent coatings has especially intensified after the collapse of the world trade center[3, 47]. Protection of steel joints is described to be of particular importance to maintain structural stability[47]. Other examples of where intumescent coatings are used would be sealing materials for fire doors, glazing and ventilation[35]. Intumescent coatings are also used on air-crafts and cable holes in fire walls[17]. Another application of intumescent coatings is on ships and submarines where the space is limited and where reduction of mass and volume is important[38, 48]. Protection of metallic substrates in the oil and gas industry is also described[22]. Examples of applications are vessels containing liquefied petroleum[49] or gas pumping units[50]. Protection of such compounds is important because leakages will feed fuel to the fire[51]. Even if the vessel does not break there is a risk that the pressure relief valves on the vessel will fail due to increased temperature[49]. Structural wood, which differ from steel because the substrate in itself is combustible, is also protected using intumescent coatings[18]. Other applications are in space crafts[52], galvanized rolling shutters[53], and textiles[54].

1.13 Application of intumescent coatings to a substrate

When intumescent coatings are applied to steel a distinction between applying the coating on- or off-site is also made. For off -site application, the coating is applied to the substrate before erection of the structure. For on-site application, the coating is applied on the structure after erection. Due to better quality control, the off-site application is becoming more and more attractive[47]. A protective topcoat can be necessary depending on the environment[2]. The problems occurring from lack of a protective topcoat can for instance be seen from a test series on an off-shore oil rig where the intumescent coating suffered from erosion and was discarded[22]. Depending on the substrate and environmental conditions the intumescent coating may also require an anticorrosive primer. One way to determine the corrosivity of the environment can be found in Aggerholm et al.[55] and is reproduced in Table 1.7. In addition to the corrosion from the environment, the possibility of having corrosive compounds included in the intumescent coating itself also exists. This has for instance been seen with a magnesium oxychloride containing coating, which was previously used on an off-shore oil rig where the intumescent coating caused corrosion[22].

A description of the steps on how to successfully apply and maintain an intumescent coating in off-shore applications is given by Roberts[22].

1. Cleaning and priming of the substrate.
2. Coating is applied according to the environmental conditions.
3. Protective top coat is applied to deal with the environmental conditions.
4. Proper treatment of edges. This is to prevent the edges to become corrosion sites.
5. Subsequent inspection for maintenance and repair of damages.

Table 1.7. Corrosion categories. After Aggerholm et al.[55].

Corrosivity category	Environmental impact	Environmental examples
C1	Very low	Indoor in dry rooms (relative humidity <60 %)
C2	Low	Indoor in non-heated and ventilated rooms
C3	Medium	Indoor with high humidity and pollution (production areas). Rural environments far from industrial areas
C4	Heavy	Urban or industrial
C5-I	Very heavy industry	Industrial areas with high relative humidity
C5-M	Very heavy marine	Coastal and offshore areas

As described in section 1.3 fires can be divided into cellulosic and hydrocarbon fires. The intumescent coatings suited for these fires are also referred to as thin (500 – 3800 μm) and thick (2500 – 19000 μm) film coatings, respectively[20]. The application procedure of these two types of coatings is different and will be described in the following paragraphs.

Application of thick film coatings

Figore and Geigger[20] give a detailed and practical guide on considerations regarding intumescent coatings, including application. The thick film intumescent coating generally uses metal, fiberglass, carbon or high temperature mesh reinforcement. They are generally solvent free and are applied using plural-component (heated-inline mixing) airless spray equipment[20].

When the reinforcement is done with metal meshes, these are installed before the coating is applied. After the spray application, the coating is to be stamped into the mesh to destroy voids and ensure the best contact with the metal. The stamping may for instance be done with a trowel[20]. When fabric meshes are used, these are installed at the mid-point of the coating application. First half layer of the coating is sprayed on the substrate. Afterwards the fabric mesh is installed and the coating is smoothened. At the end, the second half of the coating is applied[20]. Figore and Geigger[20] also describe that sometimes control samples need to be prepared and can be kept for later fire tests.

Application of thin film coatings

Thin film coatings are usually applied by an airless spray system that can produce at least 200 bar[20]. It is noted that the thin film coatings should preferably be dried under a moving air flow[20]. This is especially important in humid and cold environments. The coatings can be either solvent or water based. It is stated by Figore and Geigger[20] that some intumescent thin film coatings are able to withstand UL 1709 (jet fires) but this requires up to 8 or 10 layers, and there are long curing times with this application procedure[20]. However, information on which coatings that can be used is not provided.

Apart from the physically drying or chemically curing systems described, UV curable intumescent coatings are also available[31].

1.14 Experimental equipment

In the literature on intumescent and fire retardant coatings, a large number of experimental equipment is used ranging from NMR analysis to simple Bunsen burner tests on the laboratory table. It is beyond the scope of this project to cover all experimental equipment. However, an important point in intumescent coatings development is that coatings are usually evaluated in large scale furnaces, which are expensive and the process time consuming[23]. In the following, three different types of test are described. First, the frequently used cone calorimeter is described. Then follows the commonly used lower oxygen index test. These equipment types are interesting in relation to this project because the effect of gas composition is studied later chapters. Weathering of intumescent coatings is also described.

Cone calorimeter

A standard relating to the use of cone calorimeter, ISO 5660-1, is often described in the literature. The cone calorimeter is a very frequently used experimental setup when testing intumescent coatings although challenges of using the cone calorimeter for intumescent coatings still exist due to the moving front of the intumescent coating and the differences from real fire conditions[12]. A drawing of a cone calorimeter is seen in Figure 1.7.

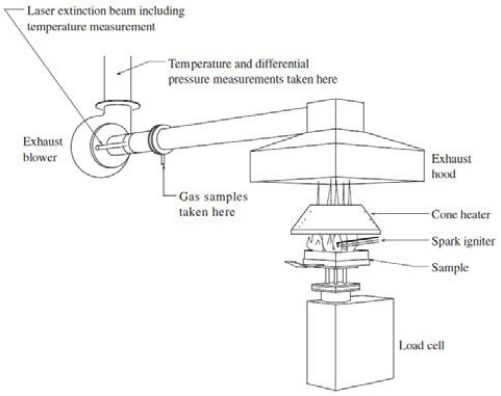

Figure 1.7. Drawing of experimental cone calorimeter[56].

The cone calorimeter consists of a sample holder and an electrically-heated cone heater that emits a constant heat flux. A spark igniter can be used to ignite the sample when the gas release and temperatures allow this[56]. The sample holder typically has dimensions of 10x10x5 cm^3 or less[12]. The samples in the cone calorimeter can be placed both horizontally and vertically. However the horizontal position is the most widely used[12]. The load cell makes it possible to measure the mass loss rate during the experiment[12]. The thickness of the sample is of importance for the ignition and other parameters and samples below 6 mm are considered as thin specimens. This is important because intumescent coatings expand from thin to thick samples during the experiment and may even engulf the heater[12]. Visual inspection is described to be important and should be included in the test evaluation[12, 57]. The heat flux emitted by the cone heater typically varies between 0 and 100 kW/m^2. To simulate developing fires, a heat flux between 20-60 kW/m^2 is usually used and for fully developed fires heat fluxes higher than 50 kW/m^2 can be used. The heat flux from the cone heater is not uniform over the entire sample area[12]. Other parameters, which can be obtained by the cone calorimeter are the time to ignition, the peak heat release, which is the maximum heat release rate, and the total heat evolved[12]. The calorimetry can be performed by oxygen

consumption technique[56]. In relation to product development the cone calorimeter has a scale limit which means that it can only be used to simulate early stage fires and not the fully developed fires due to the sample size. As an example to overcome this and simulate larger fire scenarios a model software called ConeTool has been developed by van Hess et al.[56]. The ConeTool model is used correlate results from a cone calorimeter to a standard test.

Limiting Oxygen Index

Some standards determine the flammability and burning behavior of plastic (UL 94, ISO 4589, ASTM D2863). The ISO 4589 determines the Lower Oxygen Index, which is the lowest oxygen concentration in an O_2/N_2 mixture at which the sample will burn at different temperatures[12, 58] and is especially interesting when studying flame retardants.

Weathering evaluation

Exterior coatings may degrade due to several factors such as ultraviolet radiation or moisture[59]. In the event of fire, the intumescent coating function must be reliable even though it has been attached to the substrate for a long time and potentially has been exposed to a harsh environment. Articles, which investigate the long term resistance to weathering under actual conditions are concerned with off-shore installations[20, 22] or the use of intumescent coatings on gas pumping units[50]. Other examples of research describing the effect of accelerated weathering tests and the thermal conductivity are given by Wang et al.[60] and Almeras and Le Bras et al.[61]. A reduced performance was observed and explained by degradation of ammonium polyphosphate during weathering[61].

1.15 Performance parameters of intumescent coatings

The importance of different performance parameters depends on the intended use of the intumescent coating. One parameter, which is of particular importance, is the thermal insulation between the heat source and the substrate[3, 22, 62, 63]. To describe the thermal insulation property of a char, a thermal conductivity divided by the length of the expanded char can be used[3]. Initial film thickness is also a parameter which is of importance due to cost of application[64].

In the following, a description of methods for determining the thermal char conductivity, the expansion rate, and the surface temperature is provided.

Thermal conductivity estimation methods for intumescent chars

The values available in the literature for thermal conductivity of chars are not collected here because they depend on coating composition, time, temperature, and position. However, as a rule of thumb, thermal conductivities typically vary from 0.05 to 1 $W \cdot m^{-1} \cdot K^{-1}$ in the temperature range of room temperature to 1100 ^{o}C.

The thermal conductivity of the char formed is a key parameter in any evaluation of intumescent coating behavior. Several methods for determining the parameter are described in the literature. Based on image analysis and pore size distribution, Staggs[3] has presented numerical estimates of the effective thermal conductivity of chars produced in a furnace. The numerically calculated thermal conductivities showed good agreement with measurements in a hot disk apparatus. These numerical estimates of the thermal conductivity are also pointed out by Gardelle et al.[65] as an exception to other studies, because thermal conductivities at high temperatures up to 1473 ^{o}C are presented. In another paper from 2010[66], Staggs calculated the steel plate temperature in a furnace by using thermal conductivities from a hot disk method of a fully expanded char. The thermal conductivity of this coating is calculated up to 1200 ^{o}C using the pore size distribution. The hot disk method, which is frequently used, makes it possible to determine the thermal conductivity as a function of temperature[65, 67]. However, the heating conditions in the hot disk method differ from those in a real fire.

Braun et al.[68] have proposed that the thermal conductivity is dependent on both time and temperature. Their thermal conductivity was calculated through finite difference simulations from the back side temperature of steel plates exposed to heat fluxes from a cone calorimeter. In a later study, authors from the same research group as Braun[68] compared thermal conductivities found from the steel temperature simulations in a cone calorimeter and a small scale furnace[69]. It was observed that there were correlations between the thermal conductivities obtained under the cone calorimeter and in the furnace. However, clear limitations, especially at temperatures above 500 ^{o}C were present between the cone calorimeter and a small scale test furnace. In a recent study, Gomez-Mares et al.[70] studied the thermal conductivity of the char by first heating it and after cooling inserted it into a transient plane source (hot disk). At high temperatures (above about 400 ^{o}C), radiation in the char pore volume is important and an effective thermal conductivity, which takes into account both conduction and radiation, is used. To describe the

effect of intra-pore radiation, an expression derived by Di Blasi and Branca[71] specifically developed for intumescent coatings is available

$$k_{char}(T) = \frac{k_{skeletal}(T) \cdot k_{gas}(T)}{(1-\varepsilon) \cdot k_{gas}(T) + k_{skeletal}(T) \cdot \varepsilon} + 13.5 \cdot \sigma \cdot T^3 \cdot \frac{d_b}{\varepsilon \cdot \epsilon} \quad (1\text{-}2)$$

where σ is the Stefan-Boltzmann constant, d_b is the pore diameter, and ϵ is the emissivity of the coating. $k_{skeletal}$ is the skeletal thermal conductivity of the char, d_b is the pore diameter, and ε is the porosity. The temperature must be inserted in K. Although the emissivity can be included in the expressions for the thermal conductivity, most values are based on estimates and few measurements are available. Thermal conductivity of chars is readdressed in Chapter 4 of this thesis.

External radiation

Another aspect of radiation is the external, radiation, from the surroundings (e.g. furnace or cone calorimeter) to the surface of the coating. A study to determine the relative importance of heat transfer from a 1 m^3 gas fired furnace following the BS476 fire is described by Staggs and Phylaktou[72]. It is noted that the BS476 essentially follows the same heating rate as the frequently used ISO 834 fire curve[73]. Staggs and Phylaktou[72] used low and high emissivity coatings (not intumescent) on steel substrates in the furnace and a cone calorimeter to distinguish between radiative and convective heat transfer. The conclusion was that the convective heat transfer is dominant in the furnace. The test lasted for 23 minutes, and the effect of radiation increases with time.

Methods for measuring expansion and contraction of chars

In studies of intumescent coatings, the heat transfer resistance (thermal conductivity divided by the length of the char) is an essential parameter[3]. Therefore, the swelling of the intumescent coating is an important process to follow. In addition to the swelling, some studies also report a negative expansion at higher temperatures. Different models and experimental investigations are available for measuring the transient expansion. If possible, the most straight forward method is to take pictures of the chars as they grow and then measure the height on these pictures at different times. This method has for instance been applied by Gardelle et al.[62] and Staggs[66, 67] in radiative heaters. Another approach to get dynamic expansion data is to place thermocouples

inside the expanding char and follow the temperature profile, which has been done by Mamleev et al.[74] and Bourbigot et al.[63]. Horacek[64] measured the expansion using a thermo mechanical analyzer and the study showed that the intumescent coating starts contracting at higher temperatures after a maximum expansion. A reading from the data in Horacek[64] shows a contraction from about 10% to complete collapse of the char. Although it is not the case for all coatings, the temperature dependent contraction was also found by Koo[45] using a push rod dilatometer. By comparing two fire protective coatings, Koo also found that the better performing of the two coatings had larger expansion and no contraction with increased temperature[2, 45]. Regarding contraction of the samples, our work has shown that contraction of the intumescent char is dependent on the initial coating thickness for samples exposed to fast heating[75]. Finally, the most direct way to measure the expansion is after heating using a ruler[76] or a texture analyzer as will be described in chapter 5[75].

Surface temperature measurements

The surface temperature of the expanding coating cannot be measured using a physical thermocouple because the surface is moving and often it is too fragile to handle the load from a thermocouple[77]. An optical pyrometer is also reported to be unsuitable in the fire environment. This is because the exposure will make the results difficult to interpret due to the influence of the walls and sample. An alternative method, which is investigated by Omrane et al.[77], is thermo graphic phosphor thermometry. The latter is performed by adding a thin layer (<100 µm) of a phosphorous compound to the surface. The choice of phosphorous compound depends on the temperature range. Due to the thin layer of phosphorous it is assumed that the surface temperature of the intumescent coating is the same as for the phosphorous compound. As the experiment proceeds a laser is used to excite the phosphorous compounds and the temperature can be measured. The method can be used for temperatures up to about 1600 ^{o}C. For more details and other combustion applications of this technique a thorough review is in press and can be found according in Alden et al.[78]. An important note from Omrane et al.[77] is that they have not found other reliable measurements of the surface temperature in intumescent coatings. One method could be the use of an optical pyrometer[74] although the surface emissivity may not be known.

1.16 Mathematical modeling of intumescent coatings

Another issue related to intumescent coatings is mathematical modeling. This topic will be addressed in Chapter 4. However, recent review articles describing the present state of modeling can be found in Weil[2], Griffin[62], and Shi and Chew[79].

1.17 Conclusions

Intumescent fire protective coatings, which were first patented in 1938, are often regarded as a subtopic of fire retardancy. The coatings provide fire protection for many different types of substrates and applications. Numerous additives and compounds are used in the coating formulations as demonstrated in this chapter.

Intumescent coatings are divided into two types. One is related to hydrocarbon fires which may take place in the oil and gas industry. The other relate to cellulosic fires which may take place in buildings. Very different requirements for fire tests used in third party approval of the two coating types exist. However, it was seen that in the early stages of the temperature-time curves up to about 500 ^{o}C the heating rates are similar. In this project intumescent coatings for cellulosic fires are investigated.

Another important aspect is the weathering resistance of the intumescent coating and the interaction with other coating layers.

The frequently used test method of the cone calorimeter was described and challenges of using the equipment in relation to intumescent coatings were found. Different methods for obtaining important parameters, such as thermal conductivity and expansion rate were described. These sections were included in the literature study to illustrate how results for intumescent coatings may be obtained from many different sources.

In the remaining part of the thesis, four studies are presented. In Chapter 2, a novel test method for fast screening of primers for intumescent coatings is presented and failure mechanisms of the primers are discussed. Chapter 3 presents a model of intumescent coatings validated against data series from a pilot-scale gas-fired furnace. Expansion rate, steel temperature and temperatures inside the char are used for the model validation. Chapter 4 and 5 are both concerned with development of a fast screening method using “shock heating” for a cellulosic intumescent

coating. A special case where the cellulosic coating is exposed to fast heating to high temperatures in different gas compositions and different film thicknesses is investigated. The evaluation is concerned with mechanical stability of the char and expansion/contraction. Finally, conclusions are drawn and suggestions for further work provided.

1.18 References

[1] H. Vandersall, Intumescent coating systems, their development and chemistry, Journal of Fire and Flammability 9 (2) 97-140 (1971).

[2] E.D. Weil, Fire-Protective and Flame-Retardant Coatings-A State-of-the-Art Review, J. Fire Sci. 3 (29) 259-296 (2011).

[3] J.E.J. Staggs, Thermal conductivity estimates of intumescent chars by direct numerical simulation, Fire Saf. J. 4 (45) 228-237 (2010).

[4] N. Amir, F. Ahmad, P. Megat-Yusoff, Study on the Fibre Reinforced Epoxy-based Intumescent Coating Formulations and their Char Characteristics, J. Appl. Sci. (Pakistan) 10 (11) 1678-1687 (2011).

[5] http://www.slideshare.net/GauravMeshram/executive-summaryintumescent-coatings accessed 260214.

[6] Z.W. Wicks, F.N. Jones, P.S. Pappas, D.A. Wicks, Organic coatings: science and technology, Wiley-Interscience, 2007, ISBN 9780470079072.

[7] S. Kiil, Quantification of simultaneous solvent evaporation and chemical curing in thermoset coatings, Journal of coatings technology and research 7 (5) 569-586 (2010).

[8] P.A. Sørensen, S. Kiil, K. Dam-Johansen, C.E. Weinell, Anticorrosive coatings: a review, J. Coat. Technol. Res. 2 (6) 135-176 (2009).

[9] W. Scholz, J. Bieleman, W. Heilen, U. Ferner, G. Lüers, Additives for Surface Modification, Wiley-VCH Verlag GmbH, 2000, 9783527613304.

[10] Ullmann's Encyclopedia online, WILEY-V C H VERLAG GMBH, 2000, ISBN 15214095.

[11] S. Bourbigot, S. Duquesne, Fire retardant polymers: recent developments and opportunities, J.Mater.Chem. 22 (17) 2283-2300 (2007).

[12] B. Schartel, T. Hull, Development of fire-retarded materials—Interpretation of cone calorimeter data, Fire Mater. 5 (31) 327-354 (2007).

[13] C.A. Wilkie, A.B. Morgan, Fire retardancy of polymeric materials, CRC, 2009, ISBN 9781420083996.

[14] J.W. Lyons, The chemistry and uses of fire retardants, RE Krieger Pub. Co.(Malabar, Fla.), 1970, ISBN 0471557404.

[15] S. Liang, N.M. Neisius, S. Gaan, Recent developments in flame retardant polymeric coatings, Progress in Organic Coatings 11 (76) 1642-1665 (2013).

[16] G. Bertelli, G. Camino, E. Marchetti, L. Costa, E. Casorati, R. Locatelli, Parameters affecting fire retardant effectiveness in intumescent systems, Polym. Degrad. Stab. 2-4 (25) 277-292 (1989).

[17] K.M. Butler, Physical modeling of intumescent fire retardant polymers, in: ACS Symposium Series, ACS Publications, 1997, pp. 214-230, ISBN 9780841235168.

[18] T.T. Lie, C.E. American Society of, Structural fire protection, New York,N.Y., 1992, ISBN 0872628884.

[19] M. Jimenez, S. Duquesne, S. Bourbigot, Kinetic analysis of the thermal degradation of an epoxy-based intumescent coating, Polym. Degrad. Stab. 3 (94) 404-409 (2009).

[20] T. Figore, P.P. Greigger, Intumescent coatings for fire protection: What specifiers and applicators need to know, J. Prot. Coat. Linings 6 (22) 40-47 (2005).

[21] M. Jimenez, S. Duquesne, S. Bourbigot, Multiscale experimental approach for developing high-performance intumescent coatings, Ind Eng Chem Res 13 (45) 4500-4508 (2006).

[22] T. Roberts, L. Shirvill, K. Waterton, I. Buckland, Fire resistance of passive fire protection coatings after long-term weathering, Process Saf. Environ. Prot. 1 (88) 1-19 (2010).

[23] M. Jimenez, S. Duquesne, S. Bourbigot, High-throughput fire testing for intumescent coatings, Ind Eng Chem Res 22 (45) 7475-7481 (2006).

[24] T.L. Graham, G.M. Makhviladze, J.P. Roberts, On the theory of flashover development, Fire Saf. J. 3 (25) 229-259 (1995).

[25] T. Harmathy, M. Sultan, Correlation between the severities of the ASTM E119 and ISO 834 fire exposures, Fire Saf. J. 2-3 (13) 163-168 (1988).

[26] European Organisation for Technical Approvals (EOTA), ETAG 018 Guideline for European Technical Approval of Fire Protective Products Part2: Reactive Coatings for Fire Protection of Steel Elements; European Organization for technical approvals, Brussels 1-35 (2006).

[27] M. Jimenez, S. Duquesne, S. Bourbigot, Characterization of the performance of an intumescent fire protective coating, Surface and Coatings Technology 3-4 (201) 979-987 (2006).

[28] M. Wladyka-Przybylak, R. Kozlowski, The Thermal Characteristics of Different Intumescent Coatings, Fire Mater. 33 (23) 33-43 (1999).

[29] G. Wang, J. Yang, Influences of binder on fire protection and anticorrosion properties of intumescent fire resistive coating for steel structure, Surface and Coatings Technology 8 (204) 1186-1192 (2010).

[30] S. Duquesne, S. Magnet, C. Jama, R. Delobel, Intumescent paints: fire protective coatings for metallic substrates, Surface and Coatings Technology (180) 302-307 (2004).

[31] L. Chen, L. Song, P. Lv, G. Jie, Q. Tai, W. Xing, Y. Hu, A new intumescent flame retardant containing phosphorus and nitrogen: Preparation, thermal properties and application to UV curable coating, Progress in Organic Coatings 1 (70) 59-66 (2011).

[32] J. Laza, C. Julian, E. Larrauri, M. Rodriguez, L. Leon, Thermal scanning rheometer analysis of curing kinetic of an epoxy resin: 2. An amine as curing agent, Polymer 1 (40) 35-45 (1999).

[33] S. Bourbigot, M. Le Bras, S. Duquesne, M. Rochery, Recent advances for intumescent polymers, Macromolecular Materials and Engineering 6 (289) 499-511 (2004).

[34] Z. Wang, E. Han, W. Ke, An investigation into fire protection and water resistance of intumescent nano-coatings, Surface and Coatings Technology 3-4 (201) 1528-1535 (2006).

[35] C. Branca, C. Di Blasi, H. Horacek, Analysis of the combustion kinetics and thermal behavior of an intumescent system, Ind Eng Chem Res 9 (41) 2107-2114 (2002).

[36] S. Watt, J. Staggs, A. McIntosh, J. Brindley, A theoretical explanation of the influence of char formation on the ignition of polymers, Fire Saf. J. 5 (36) 421-436 (2001).

[37] S.M. Neininger, J. Staggs, A. Horrocks, N. Hill, A study of the global kinetics of thermal degradation of a fibre-intumescent mixture, Polym. Degrad. Stab. 2 (77) 187-194 (2002).

[38] U. Sorathia, T. Gracik, J. Ness, A. Durkin, F. Williams, M. Hunstad, F. Berry, Evaluation of intumescent coatings for shipboard fire protection, J. Fire Sci. 6 (21) 423-450 (2003).

[39] M.M. Hirschler, Discussion of smoke corrosivity test methods: analysis of existing tests and of their results, Fire Mater. 5 (17) 231-247 (1993).

[40] M. Le Bras, G. Camino, S. Bourbigot, R. Delobel, Fire retardancy of polymers: the use of intumescence, Cambridge: The Royal Sociey of Chemistry, 1998, ISBN 9781855738041.

[41] F. Dimanshteyn, U.S. patent 5,035,951 (1991).

[42] J. Hanafin, U.S. Patent 6096812 (2000).

[43] Nugent, R., Ward, T., Greigger, P. Seiner, J., U.S. patent 5108832 (1992).

[44] Gottfried, S. (to No Fire Technology, Inc), U.S. Patent 5723515 (1998).

[45] J.H. Koo, Thermal characteristics comparison of two fire resistant materials, J. Fire Sci. 3 (15) 203-221 (1997).

[46] A. Mouritz, S. Feih, E. Kandare, Z. Mathys, A. Gibson, P. Des Jardin, S. Case, B. Lattimer, Review of fire structural modelling of polymer composites, Composites Part A: Applied Science and Manufacturing 12 (40) 1800-1814 (2009).

[47] X. Dai, Y. Wang, C. Bailey, Effects of partial fire protection on temperature developments in steel joints protected by intumescent coating, Fire Saf. J. 3 (44) 376-386 (2009).

[48] R.J. Asaro, B. Lattimer, C. Mealy, G. Steele, Thermo-physical performance of a fire protective coating for naval ship structures, Composites Part A: Applied Science and Manufacturing 1 (40) 11-18 (2009).

[49] B. Droste, Fire protection of LPG tanks with thin sublimation and intumescent coatings, Fire Technol. 3 (28) 257-269 (1992).

[50] G. Shaidurova, I. Vasil'ev, Y.S. Shevyakov, N. Ul'yanova, A. Ivanova, Comprehensive assessment of durability of fireproof materials under gas-pumping equipment operation conditions, Chemical and Petroleum Engineering 9 (45) 562-565 (2009).

[51] Y.N. Shebeko, I. Bolodian, V. Filippov, V.Y. Navzenya, A. Kostyuhin, P. Tokarev, E. Zamishevski, A study of the behaviour of a protected vessel containing LPG during pool fire engulfment, J. Hazard. Mater. 1-3 (77) 43-56 (2000).

[52] D. Cagliostro, S. Riccitiello, K. Clark, A. Shimizu, Intumescent coating modeling, J. Fire & Flammability 4 (6) 205-222 (1975).

[53] Y.J. Chuang, Y.H. Chuang, C.Y. Lin, Fire tests to study heat insulation scenario of galvanized rolling shutters sprayed with intumescent coatings, Mater Des 7 (30) 2576-2583 (2009).

[54] A.R. Horrocks, Developments in flame retardants for heat and fire resistant textiles--the role of char formation and intumescence, Polym. Degrad. Stab. 2-3 (54) 143-154 (1996).

[55] P.A. Sørensen, S. Kiil, K. Dam-Johansen, C.E. Weinell, Anticorrosive coatings: a review, Journal of Coatings Technology and Research 2 (6) 135-176 (2009).

[56] P. van Hees, P. Andersson, M. Hjohlman, N. Wenne, M.A. Hassan, Use of the Cone Calorimeter and ConeTools software for development of innovative intumescing graphite systems, Fire Mater. 7 (34) 367-384 (2010).

[57] B. Schartel, M. Bartholmai, U. Knoll, Some comments on the use of cone calorimeter data, Polym. Degrad. Stab. 3 (88) 540-547 (2005).

[58] Y.V. Gnedin, R. Gitina, S. Shulyndin, G. Kartashov, S. Povikov, Investigation of phosphorus-containing foam-forming systems as combustion retardants for polypropylene, Polymer science USSR 3 (33) 544-550 (1991).

[59] S. Kiil, Model-based analysis of photoinitiated coating degradation under artificial exposure conditions, Journal of Coatings Technology and Research 4 (9) 375-398 (2012).

[60] L. Wang, Y. Wang, J. Yuan, G. Li, Thermal conductivity of intumescent coating char after accelerated aging, Fire Mater. 6 (37) 440-456 (2013).

[61] X. Almeras, M. Le Bras, P. Hornsby, S. Bourbigot, G. Marosi, P. Anna, R. Delobel, Artificial weathering and recycling effect on intumescent polypropylene-based blends, J. Fire Sci. 2 (22) 143-161 (2004).

[62] G. Griffin, The Modeling of Heat Transfer across Intumescent Polymer Coatings, J. Fire Sci. 3 (28) 249-277 (2010).

[63] S. Bourbigot, S. Duquesne, J.M. Leroy, Modeling of heat transfer of a polypropylene-based intumescent system during combustion, J. Fire Sci. 1 (17) 42 (1999).

[64] H. Horacek, Reactions of stoichiometric intumescent paints, J Appl Polym Sci 3 (113) 1745-1756 (2009).

[65] B. Gardelle, S. Duquesne, V. Rerat, S. Bourbigot, Thermal degradation and fire performance of intumescent silicone-based coatings, Polym. Adv. Technol. 1 (24) 62-69 (2012).

[66] J. Staggs, Numerical characterization of the thermal performance of static porous insulation layers on steel substrates in furnace tests, J. Fire Sci. 2 (29) 177-192 (2011).

[67] B. Gardelle, S. Duquesne, P. Vandereecken, S. Bourbigot, Characterization of the carbonization process of expandable graphite/silicone formulations in a simulated fire, Polym. Degrad. Stab. 5 (98) 1052-1063 (2013).

[68] M. Bartholmai, R. Schriever, B. Schartel, Influence of external heat flux and coating thickness on the thermal insulation properties of two different intumescent coatings using cone calorimeter and numerical analysis, Fire Mater. 4 (27) 151-162 (2003).

[69] M. Bartholmai, B. Schartel, Assessing the performance of intumescent coatings using bench-scaled cone calorimeter and finite difference simulations, Fire Mater. 3 (31) 187-205 (2007).

[70] M. Gomez-Mares, A. Tugnoli, G. Landucci, F. Barontini, V. Cozzani, Behavior of intumescent epoxy resins in fireproofing applications, J. Anal. Appl. Pyrolysis (97) 99-108 (2012).

[71] C. Di Blasi, C. Branca, Mathematical model for the nonsteady decomposition of intumescent coatings, AICHE J. 10 (47) 2359-2370 (2001).

[72] J.E.J. Staggs, H.N. Phylaktou, The effects of emissivity on the performance of steel in furnace tests, Fire Saf. J. 1 (43) 1-10 (2008).

[73] W. Hung, W. Chow, Review on the requirements on fire resisting construction, International Journal on Engineering Performance-Based Fire Codes 3 (4) 68-83 (2002).

[74] V.S. Mamleev, E.A. Bekturov, K.M. Gibov, Dynamics of intumescence of fire-retardant polymeric materials, J Appl Polym Sci 8 (70) 1523-1542 (1998).

[75] K.P. Nørgaard, K. Dam-Johansen, P. Català, S. Kiil, Investigation of char strength and expansion properties of an intumescent coating exposed to rapid heating rates, Prog. Org. Coat. 12 (76) 1851-1857 (2013).

[76] L.L. Wang, Y.C. Wang, J.F. Yuan, G.Q. Li, Thermal conductivity of intumescent coating char after accelerated aging, Fire Mater. 6 (37) 440-456 (2013).

[77] A. Omrane, Y.C. Wang, U. Goransson, G. Holmstedt, M. Alden, Intumescent coating surface temperature measurement in a cone calorimeter using laser-induced phosphorescence, Fire Saf. J. 1 (42) 68-74 (2007).

[78] M. Aldén, A. Omrane, M. Richter, G. Särner, Thermographic phosphors for thermometry: A survey of combustion applications, Progress in Energy and Combustion Science 4 (37) 422-461 (2011).

[79] L. Shi, M.Y.L. Chew, A review of fire processes modeling of combustible materials under external heat flux, Fuel (106) 30-50 (2013).

Chapter 2 - Laboratory and gas-fired furnace performance tests of epoxy primers for intumescent coatings

This chapter was published with the title “Laboratory and gas-fired furnace performance tests of epoxy primers for intumescent coatings” in Progress in Organic Coatings, February 2014, http://dxdoi.org/10.1016/j.porgcoat.2013.10.018. (authors Kristian Petersen Nørgaard, Kim Dam-Johansen Pere Català and Søren Kiil).

2.1 Abstract

Protection of steel structures, using so-called intumescent coatings, is an efficient and space saving way to prolong the time before a building, with load bearing steel constructions, collapses in the event of a fire. In addition to the intumescent coating, application of a primer may be required, either to ensure adhesion of the intumescent coating to the steel or to provide corrosion resistance. It is essential to document the performance of the intumescent coating together with the primer to ensure the overall quality of coating system. In the present work, two epoxy primers were used to investigate the potential failure mechanism of a primer applied prior to an intumescent coating. The analysis was carried out using; 1) gas-fired test furnace, 2) a specially designed electrically heated oven, and 3) thermo gravimetric analysis. When tested below an acrylic intumescent coating, exposed to a gas-fired furnace following the ISO 834 fire curve (a so-called cellulosic fire), one of the primers selected performed well and the other poorly. From tests in the electrically heated oven, it was found that both primers were sensitive to the film thickness employed and the presence of oxygen. At oxygen-rich conditions, higher primer thicknesses gave weaker performance. In addition, a color change from red to black was observed in nitrogen, while the color remained red in the oxygen-nitrogen mixture. In summary, the results suggest that an adequate choice of primer, primer thickness, and intumescent coating is essential for a good performance of an intumescent coating system.

2.2 Explanatory notes

Gas-fired furnace	-	Gas-fired furnace for testing steel panels according to ISO 834 fire curve.
Horizontal oven	-	Electrically heated oven with variation in the gas composition.
Primer A	-	Solvent based polyhydroxyether epoxy/polyamide. The primer is a shopprimer pigmented with zinc aluminum phosphate.
Primer B	-	Solvent based bisphenol-A epichlorydrin/phenalkamine. The primer is pigmented with zinc phosphate and micaceous iron oxide.
Reduced oxygen	-	Mixture of 10 % oxygen and 90 % nitrogen.
SEM	-	Scanning Electron Microscope.
TGA	-	Thermo Gravimetric Analysis.

2.3 Introduction

In the event of fire, or merely temperatures in the range of 400 to 550 °C, the load bearing ability of steel is reduced significantly and this has implications for buildings based on steel parts[1, 2]. An efficient way to protect the building structure and prolong the time before the problematic steel temperature is reached is by intumescent coatings. At elevated temperatures, the latter swells to a thermally insulating char with a thermal conductivity from 0.1 to 1 $W \cdot m^{-1} \cdot K^{-1}$, depending on coating composition and temperature[2-4]. For the intumescent coatings suited for so-called cellulosic fires, the coatings are applied at thicknesses up to 1.5 mm[5]. An important target in ongoing intumescent research is to reduce the required dry film thickness[6].

Intumescent coatings are comprised of five basic compound groups: blowing agent, acid- and carbon sources, a binder, and pigments. All compounds are important for the char formation process[5, 7]. The interaction between these compounds is complex, and various reaction sequences are reported in the literature. Bourbigot et al.[8] stated that the intumescent process consists of six steps, the first being the temperature-triggered release of an inorganic acid, which esterify with the carbon source. Following this, the binder melts, and the ester dehydrates and forms a carbon-inorganic residue. Furthermore, gasses are simultaneously released, blowing the melted structure into a foam, and finally gelation and solidification occurs. However, in addition to these reaction

mechanisms, intumescent coatings are also subject to interaction with other coating layers, such as an underlying primer. The latter ensures good adhesion to the metal substrate and provides anticorrosive properties[9]. Primer detachment from the substrate will cause irreversible damage to the intumescent coating performance, yet very few scientific studies on primers in intumescent coating systems are available. A study of a zinc primer, protected by an intumescent coating consisting of expandable graphite, ammonium polyphosphate, melamine, boric acid, bisphenol-A epoxy resin, and ACR hardener polyamide was presented by Ullah et al.[10]. Effects of variations in the intumescent coating formulation on steel-primer-intumescent coating performance was studied by heating in a muffle furnace (a type of furnace where the heating source is separated from the furnace room) to 500 ^{o}C and following the development by analysis of Scanning Electron Microscope (SEM) pictures before and after heating. The investigation showed that with an optimal intumescent coating formulation, i.e. weight percentages of ammonium polyphosphate and boric acid of 25 and 15%, respectively, the strongest structure of the coating-primer-metal after heating was obtained. An example of a SEM picture of a coating-primer-metal interface before and after heating is provided in Figure 2.1. Subsequent exposure, it can be seen that the primer and intumescent coating are still attached to the substrate and primer, respectively, although minor cracks are present.

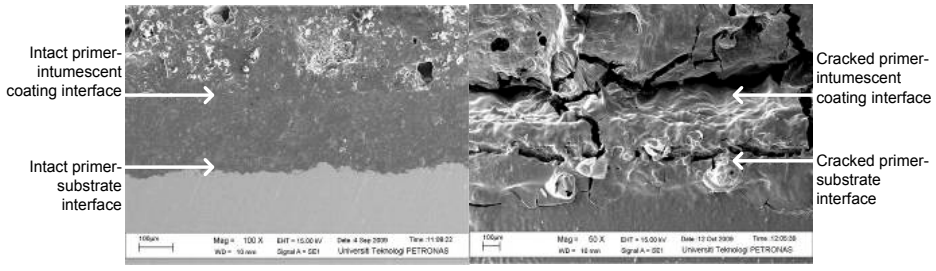

Figure 2.1. SEM picture of a metal-primer-coating interface. The picture to the left shows the sample before heating and the figure to the right the sample after heating to 500 ^{o}C. After Ullah[10] *with explanatory notes added.*

In the ETAG 018 approval guideline for intumescent coating testing, the importance of a primer is emphasized. When an intumescent coating is approved, it should be specified, which primers can be used in combination with the coating[11]. In addition, due to the expensive and time consuming approval requirements of intumescent coating systems, fast screening tests for intumescent

coating systems are of interest. Jimenez et al.[12, 13] correlated the following input parameters, 1) the insulating properties of the intumescent coatings below a radiant heater, 2) mass loss, 3) char expansion, and 4) rheology of heated intumescent coatings, to the output parameter, fire test performance in a gas-fired furnace. Another aspect of a potential fast screening test is the mechanical stability of intumescent chars using shock heating, which is investigated in our earlier work[14] (this topic will be addressed in Chapter 4 and 5 of this thesis). In the present work, the focus is on testing of the primer below the intumescent coating. An empirical correlation relating results of gas-fired furnace tests of a primer-intumescent coating system to the primer thickness and gaseous environment (oxygen content) below an intumescent coating is developed. An important reason to study the effects of oxygen content is that in a well-tuned test furnace chamber, the oxygen concentration will be around 4 mol%[15]. At other conditions, the oxygen concentration may vary significantly from well ventilated conditions below a radiant heater to very low concentrations in an impinging flame[15]. In addition to the variation in the oxygen content of the gas phase, the oxygen concentration close to the primer may vary even more because of the intumescent char present between the fire and the primer. The motivation to study primer thickness is that the performance of many anticorrosive coatings (e.g. barrier coatings) requires a high thickness to work well[9].

2.4 Brief overview of intumescent mechanisms

In this paragraph, a brief overview of the intumescent chemistry, comprised of seven steps, is given. The steps occur as the temperature increases and the exact sequence will be dependent on the chemical coating composition. Common intumescent coating compounds are: ammonium polyphosphate, melamine, pentaerythritol, melamine, SiO_2, and TiO_2.

1. At coating temperatures between 150 – 215 ^oC, an inorganic acid is released from a salt[8, 16]. For instance, the acid source (e.g. ammonium polyphosphate, $(NH_4PO_3)_n$) can thermally degrade into NH_3, water and acidic phosphoric groups[17]. Based on information in Fan et al.[18] and Bourbigot et al. [19] an example of the degradation with release of NH_3 is shown in reaction (2-1).

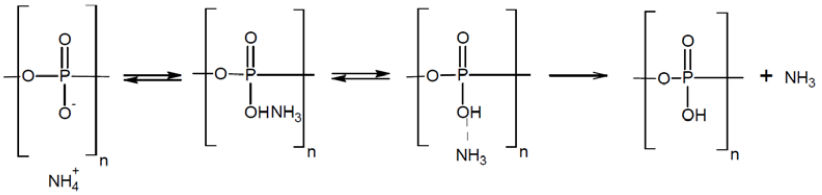

(2-1)

The repeating unit, n, in the ammonium polyphosphate may take a value of 700 up to more than 1000[20, 21].

2. At coating temperatures slightly higher than those of the acid formation, the acid and hydroxyl groups on the carbon source react and form a phosphoric ester[8, 22]. The formation of the phosphoric ester can happen according to esterification or phosphorylation (alcoholysis)[21, 23, 24], which can lead to many different structures[23]. An example of the esterification between a hydroxyl group of pentaerythritol (carbon source) and an acidic phosphoric group on the decomposed acid source, based on Kandola and Horrocks[23], is seen in reaction (2-2).

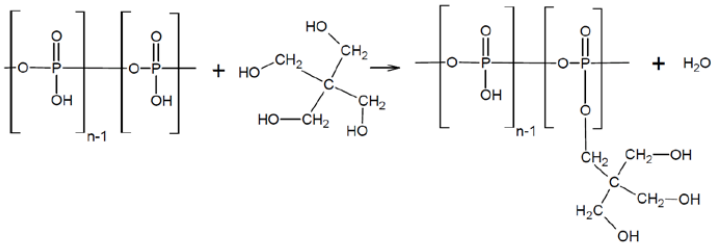

(2-2)

The reaction can be catalyzed by amines or amides[16]. It is not clear if, in general, all repeating units on the phosphoric acid group react with a pentaerythritol hydroxyl group. The coating used to develop the reactions, in Kandola and Horrocks[23], consists of a commercial mixture of ammonium polyphosphate, melamine, and pentaerythritol (MPC1000) mixed with pulverized flame retardant nonwoven viscose fabric fibers. The molar ratio of ammonium polyphosphate (repeating units) and pentaerythritol molecules in the coating, can be calculated to 0.56. Considering functional groups, the ratio is 0.56/4 = 0.14. This means that there is a substantial stoichiometric excess of pentaerythitol hydroxyl groups and a high crosslink density is not expected.

3. At coating temperatures somewhere between the temperature of step 1 and during the esterification (step 2), the binder partly melts[16].

4. At temperatures from 280 to 350 °C, decomposition of the ester and subsequent reactions result in a carbon-inorganic residue[8]. The inorganic reactant could for instance be SiO_2[22, 25, 26] or TiO_2[27].
5. Meanwhile, the blowing agent (e.g. melamine) decomposes and emits gases such as NH_3, CO_2, water, and NO_2[28, 29]. The gasses released from the blowing agent, the acid source, and pyrolysis of the binder and carbon source, are trapped in the melted binder and make the coating swells[8, 26].
6. At higher coating temperatures, solidification, through cross-linking of the melted compounds, takes place and a solid char is formed[16]. The solid char could for instance be comprised of titanium pyrophosphate (TiP_2O_7) which is formed through reaction of TiO_2 with the acidic groups from the decomposed acid source[27, 30, 31]. Various reactions for the formation of titanium pyrophosphate from phosphoric acidic groups are proposed in the literature. An exact reaction for the phosphoric acid ester shown in reaction (2-2) was not found. However, reaction (2-3) shows the formation of TiP_2O_7 from phosphoric acid[30].

$$TiO_2 + 2\ H_3PO_4 \rightarrow TiP_2O_7 + 3\ H_2O \qquad (2\text{-}3)$$

In reactions (2-4) and (2-5), a two-step reaction mechanism, based on Horacek[6], is proposed.

$$C_{10}H_{10}O_6P_2 \rightarrow 2\ HPO_3 + 2\ CH_4 + 8\ C \qquad (2\text{-}4)$$

$$2\ HPO_3 + TiO_2 \rightarrow TiP_2O_7 + H_2O \qquad (2\text{-}5)$$

The starting material for the reactions is $C_{10}H_{10}O_6P_2$ which is a degradation product of the phosphoric acid ester $C_{10}H_{16}O_9P_2$, formed by the release of water. Reaction (2-4) shows decomposition of ($C_{10}H_{10}O_6P_2$) to polyphosphoric acid $(HPO_3)_n$, methane and carbon. Reaction (2-5) shows the formation of titanium pyrophosphate from a reaction between polyphosphoric acid and TiO_2. Reactions (2-4) and (2-5) are reported to take place at 600 °C[6].

7. At even higher coating temperatures, thermal decomposition and/or oxidation of the char takes place[8, 32]. The degradation could for instance be oxidation of the carbon.

2.5 Strategy of investigation

In this study, the simple model system shown in Figure 2.2 is taken to represent an intumescent coating system. It is assumed that the intumescent coating provides a barrier against oxygen and heat and that the temperature of the primer is the same as the steel. Other gasses formed from the intumescent coating are not considered.

Two primers, primer A and B, applied below an acrylic intumescent coating are tested in a gas-fired furnace. Primer A has previously shown good adhesion and primer B detachment at a steel temperature of about 300 ^{o}C. Photo of the intumescent char and char cross section after heating are used to visualize the importance of testing the primers in the presence of oxygen and homogeneous temperatures.

To investigate differences between the two primers, samples of primers on steel, without intumescent coating on top, are heated in a horizontal tube oven. To experimentally simulate the protective mechanisms of the intumescent coating, a temperature increase up to 500 ^{o}C, under a flow of either atmospheric air or nitrogen, is used.

Compatibility between the primers and intumescent coating is also tested using Thermo Gravimetric Analysis (TGA), where the mass loss of the two primers and intumescent coating is measured. The TGA experiments are performed in “reduced oxygen” (10% oxygen + 90% nitrogen)[15] and in 100 % nitrogen.

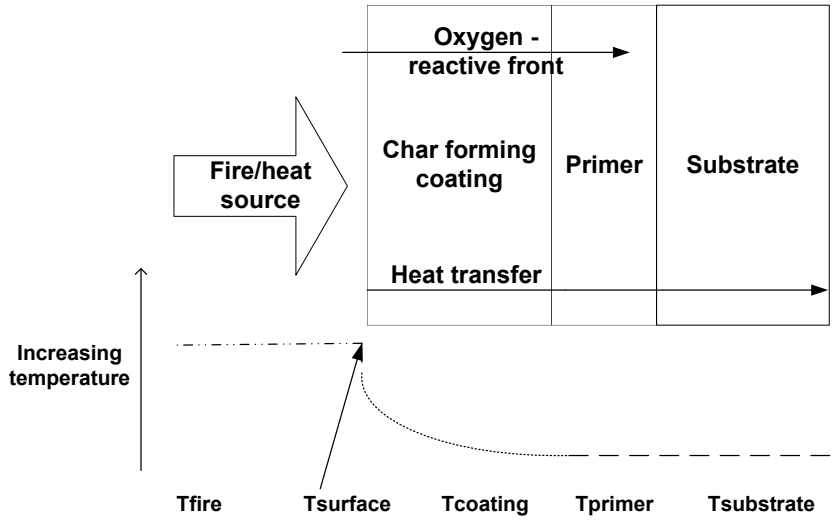

Figure 2.2. Schematic illustration (cross-section view) of an intumescent coating system exposed to a fire. The idealized system consists of a protective coating/char layer, a primer, and a metal substrate. A simplified temperature profile is illustrated.

2.6 Experimental procedures

Materials

Two commercial primers and a generic solvent-borne acrylic intumescent coating are used in the study. Primer A is a polyhydroxyether epoxy/polyamide with zinc aluminum phosphate pigment and primer B, a shop primer, is bisphenol-A epichlorydrin/phenalkamine primer with zinc phosphate and micaceous iron oxide pigments. The micaceous iron oxide is used to provide color and the zinc pigments are used in sacrificial coatings to provide anodic protection[9].

Preparation of primer samples for the horizontal oven

For heating in the horizontal oven, samples consisting of only primer and metal were used. The primer samples were applied to 0.3 mm thick steel sheets, using a drawdown CoatMaster 509 MC from Erichsen testing equipment. Prior to application of the primers, the metal substrates were first washed with xylene and then demineralized water. After curing for 1 week, the samples were cut into squares of 1x1 cm^2. The cutting was performed with a large metal sheet cutter (Cidan, type MS-F 13/3,0). To limit shattering of the solid coating to a minimum during cutting, a 0.3 mm

sheet of metal was placed on top of the sample. To ensure good adhesion before heating, any loose coating was scratched away with metal tweezers. After cutting the steel sheets, the dry film thicknesses were measured at 5 positions on each sample using an Elcometer 355 Top.

Heating of primer samples in horizontal oven

A horizontal tube oven, from Entech, seen in Figure 2.3, was used for heating. The oven has a ceramic pipe inside for insertion of the samples and was heated under flows of 100 NL/min nitrogen (AGA purity grade 5) or dry atmospheric air. The gas flow enters at one end of the ceramic pipe and exits after having passed the samples. The latter were heated to 500 °C at a heating rate of 10 °C/min and then remained at this temperature for 30 min before cooling took place. The oven has previously been used to study the influence of gas composition on expansion and mechanical properties of an intumescent coating[33] (this will be addressed in Chapter 5). The oven is equipped with a water cooled chamber, which makes it possible to insert and remove the sample up to a temperature of 1200 °C under a selected gas composition. However, in this work it was decided to use a slower heating rate to resemble steel temperatures in a gas-fired furnace.

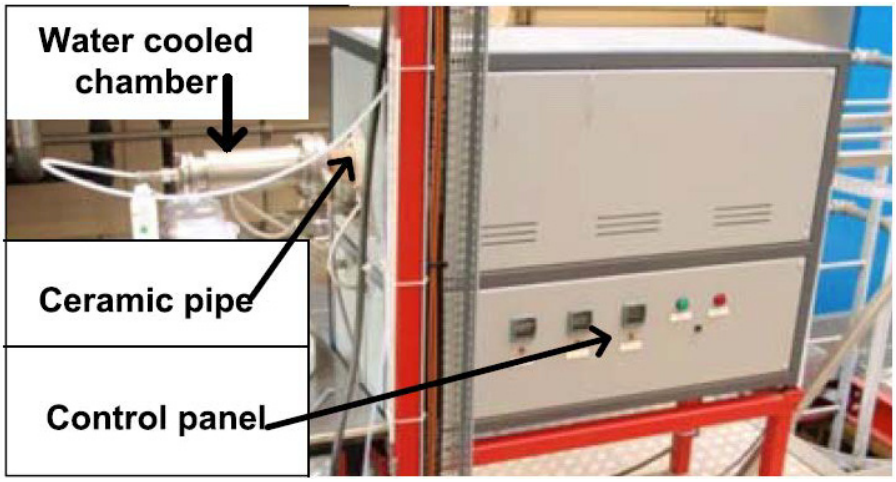

Figure 2.3. Left: Horizontal tube oven. To the left the gas inlet to the water cooled chamber is seen and to the right the oven and control panels are seen.

When heating, 12 samples were placed on a steel sheet in the bottom of the sledge seen in Figure 2.4. The length and width of the sledge is 130 mm and 30 mm, respectively. The 12 samples

consist of six samples of primer A and six samples of primer B, placed in two rows parallel to the gas flow. For each primer three thicknesses were chosen. These are referred to as thin, medium and thick.

Due to the heating of 12 samples at once, a potential concern is that the exposure to oxygen and temperature varies at different positions in the sledge. To account for this, two samples of each primer at each thickness were used. The samples were placed as shown in Figure 2.4. This ensures that the position in the sledge along the gas flow direction does not affect the result.

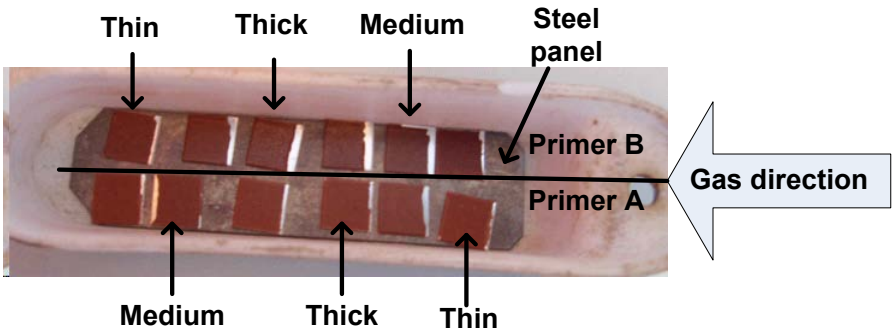

Figure 2.4. Picture of samples in sledge before heating in horizontal oven. Primer B is placed in the top row and primer A in the bottom row. Samples are placed in a way that allows analysis of the effect of position.

Test of intumescent-primer system in gas-fired furnace

Tests using steel plates coated with both primer and intumescent coating in a gas-fired test furnace were performed. The furnace consists of a rectangular channel with inner length, height, and width of 2.5 m, 0.65 m and 0.4 m, respectively. Primer coated steel panels of dimensions 200x300x6 mm^3 were employed. The intumescent coating was sprayed on to the primer at a dry film thickness of 1 mm using airless spray equipment. The thickness of primer A for the gas-fired furnace tests was 25 µm and the thickness of primer B was 113-119 µm. These film thicknesses were chosen in accordance with the product sheets which specify the "indicated dry film thicknesses" for primer A and B, to be 15 and 100 µm, respectively.

Two tests with each primer were carried out. Two 1.5 mm K-type thermocouples were used at the center of the back side of the steel which were placed in a vertical position. The gas fired furnace

is heated by a pre-mixed flame with a constant air to natural gas volume ratio of 10:1. Assuming stoichiometric combustion of methane, as shown in reaction (2-6), and 21% oxygen in the air, the oxygen concentration in the furnace is 1%. However, this value may change if the combustion was incomplete or the natural gas contained higher hydrocarbons or inert gasses, such as nitrogen.

$$CH_4 + 2O_2 \rightarrow CO_2 + 2H_2O \quad (2\text{-}6)$$

A single K-type thermocouple inside the furnace is used to control the temperature to follow the ISO 834 as set point.

Thermo gravimetric analysis with primer or intumescent coating

Samples for TGA were prepared as free films with an Erichsen CoatMaster 509 MC. Each film consisted of one coating, being either primer A, primer B or the intumescent coating. The substrate was overhead transparencies produced by Folex. The coatings were cured in a fume cupboard for at least 3 weeks. Powders of the cured primers and the coating were ground in a metal mortar to obtain fine powders. The mass loss was investigated in a Netzsch Jupiter F1 STA, using alumina crucibles of 7 mm in diameter. For all TGA experiments, a total gas flow of 100 NmL/min was used. It is noted that the flow is one thousandth of the flow used in the horizontal tube oven. Sample masses were between 5-6 mg and 2 runs of each sample were made. The gas compositions were either pure nitrogen or 10% oxygen in nitrogen (reduced oxygen). The oxygen and nitrogen were supplied from AGA and of purity grade 5. The heating rate was 10 ^{o}C/min and the final temperature was 500 ^{o}C.

2.7 Results

In the following, the experimental results are described. To outline the importance of testing primers at well-defined conditions with and without coatings, a practical case from the gas-fired furnace is first discussed.

Practical importance of testing at well-defined conditions

The intuitive way to test the compatibility between a primer and an intumescent coating is to apply them as a system to a steel substrate, and test them in a fire. Such tests were carried out in the gas-fired furnace. An example of the char and a cross section of the char after heating the steel plate to 550 ^{o}C are seen in Figure 2.5. However, a limitation to these tests is that a failure can

only be assigned to the combined system, and the factors affecting the individual compounds may be difficult to identify. One important limitation in particular, is that it is difficult to determine if the primer has been exposed to oxygen or not. The reasons for this are described in the following.

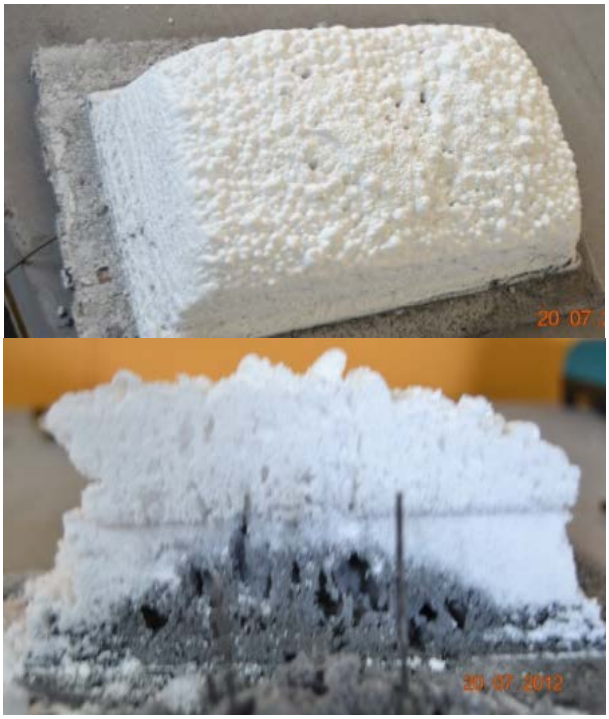

Figure 2.5. Top: Photo of intact and cooled intumescent char. Bottom: Cross section of the char. The char was tested on a steel plate. The maximum height of the char is approximately 75 mm in the middle.

In our previous work[33] (addressed in Chapter 5) with the same intumescent coating as used in this study, it was shown that after heating to 1100 ^{o}C in the horizontal oven, samples in nitrogen were black and in atmospheric air white. To test the color of the intumescent coatings at a lower temperature, free films of intumescent coating was heated to 500 ^{o}C, in nitrogen and atmospheric air, respectively, using the horizontal oven. These tests showed that at 500 ^{o}C, the samples were black in both gasses. Therefore, up to 500 ^{o}C the color does not reveal if the char has been exposed to oxygen or not. On the contrary, it can be known for sure that the white parts have been oxidized. This is further supported by Griffin et al.[15], who found that degradation of the char,

for three different intumescent coatings, is first significantly affected by the oxygen content at a temperature of 540 ^{o}C or higher.

Looking at the char cross section shown in Figure 2.5, it is seen that the color close to the steel plate is not the same in all places, although the majority is grey, which means that some parts (at the sides) have been exposed to oxygen, whereas other parts are more uncertain. Thus, from this combined test, it cannot be seen if the primer has been tested in the presence of oxygen or not, but only if the combined system works well. Therefore, as the results in the coming paragraphs will show, the presence of oxygen should be used to ensure tests in a worst case scenario. It is noted that a combined test provides useful information of the system and compatibility between the coatings. Combined tests are also necessary to perform weathering tests of the system.

Gas-fired furnace tests of primer with intumescent coating

In Figure 2.6, the steel temperatures from tests of primer covered with intumescent coating in the gas-fired furnace are shown. Time-temperature curves which follow the ISO834 fire curve as set point are also shown. The fire curves of the experiments are overlapping. From the steel temperatures of the samples coated with primer B with intumescent coating, it is seen that in both tests primer B detached after 22 min (corresponding to the steep temperature increase at a steel temperature of 300 ^{o}C). From the steel temperatures and evaluation after the tests, it could be seen that primer A with intumescent coating did not detach.

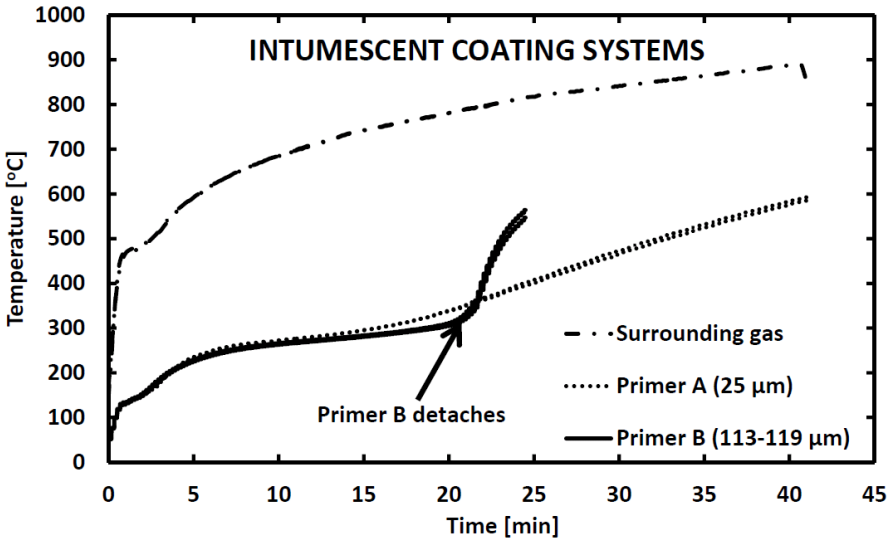

Figure 2.6. Backside steel temperature of steel plate covered with intumescent coating above the primers in the gas-fired furnace. The detachment of primer B after 22 min is seen as the steep temperature increase. The gas temperature measured is also shown. Two runs with each primer are shown, but almost completely overlap. The dry film thicknesses of the primers are provided in the legend.

Primer characterization after heating in horizontal oven

Photos of the primers without intumescent coating after heating in atmospheric air and nitrogen to 500 °C are shown in Figure 2.7 and Figure 2.8, respectively. In the figures samples with increasing thickness from top to bottom are shown. Two samples at each film thickness are shown. In nitrogen it was observed that for both primers, the color changed from red to black after heating, and only in one case, with primer A, was a small detachment from the substrate observed. In air, i.e. in presence of oxygen, the color of the primer remained red. The color change of the primers, from red to black in nitrogen, may be due to reduction of the red iron(III)oxide pigment (Fe_2O_3) to the black iron(II)oxide ($Fe_{0.95}O$)[34], or formation of char on the surface. In Figure 2.7, it can visually be observed that for both primers, the damage of the primer increases with increasing thickness (top to bottom). In all cases, primer A shows a better performance than primer B. It can also be seen in Figure 2.7 that the medium and thick primer B samples were almost entirely removed from the substrate.

It is noted that the thinnest samples of primer B are thicker than the thinnest samples of primer A. When attempting to prepare thinner samples with primer B, the wetting of the steel plate was too poor, with parts of the steel being visual, and therefore these samples were not included in the investigation.

	Thickness [µm]	Primer A	Primer B	Thickness [µm]
Thin	16.2±1.9	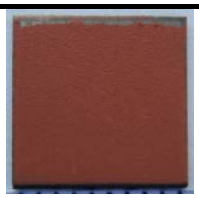		23.0±1.6
	14.8±2.6	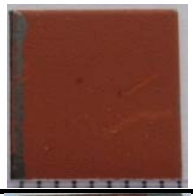	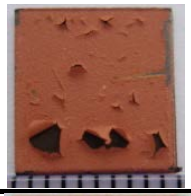	25.3±2.9
Medium	35.1±4.7			34.6±6.5
	34.6±5.2		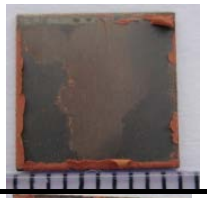	32.5±2.6
Thick	57.6±5.8			61.6±8.2
	61.1±6.0		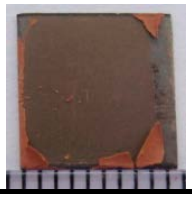	60.5±3.7

Figure 2.7. Primers after heating to 500 °C in atmospheric air in the horizontal oven. Average and standard deviation of thicknesses measured five times before heating in the horizontal oven are shown. For primer B almost complete detachment is seen for all coating thicknesses investigated.

	Thickness [µm]	Primer A	Primer B	Thickness [µm]
Thin	20.8±1.8	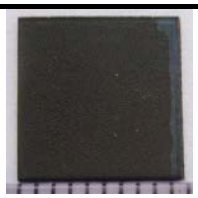		30.4±3.6
	21.8±3.5		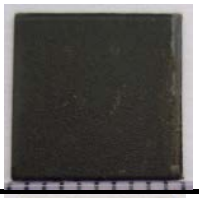	26.3±3.4
Medium	39.5±4.3		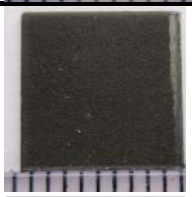	39.7±4.4
	43.9±7.1	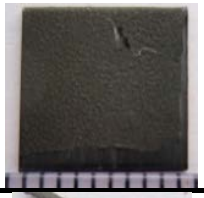	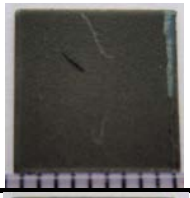	41.3±6.3
Thick	60.8±7.6			60.2±7.6
	68.9±6.6	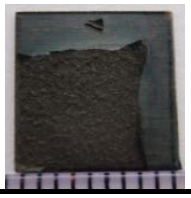	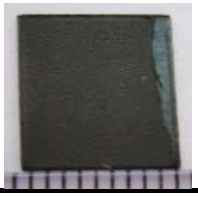	62.5±5.5

Figure 2.8. Primers after heating to 500 °C in nitrogen in the horizontal oven. Average and standard deviation of thicknesses measured five times before heating in the horizontal oven are shown. No coating detachment is observed for any of the coatings except the thick samples of primer A.

Mass loss of primer

The mass loss of the two primers and the coating in the presence of reduced oxygen and nitrogen are shown in Figure 2.9. The graphs show two tests of each sample, indicating good repeatability. It is interesting to notice that even though the absolute values of the mass losses are different for the two primers and the coating, the behavior of the primers and the coating are similar, except for primer B in oxygen. Considering that the failure of primer B happened at a steel temperature of 300 ^{o}C, it is noticed that except for primer B in oxygen, all the three remaining primer curves run in parallel to the coating curve from 300 ^{o}C. Also, the change in slope in the range from 450 - 500 ^{o}C is observed in all tests except for primer B in reduced oxygen. However, considering that the primer failure was found in both coatings, in the presence of oxygen, the differences in mass loss behavior are probably not causing the failure. The changed behavior of primer B indicates that this primer is more sensitive to the presence of oxygen than primer A. This could be one reason for primer B performing worse than primer A at similar thicknesses.

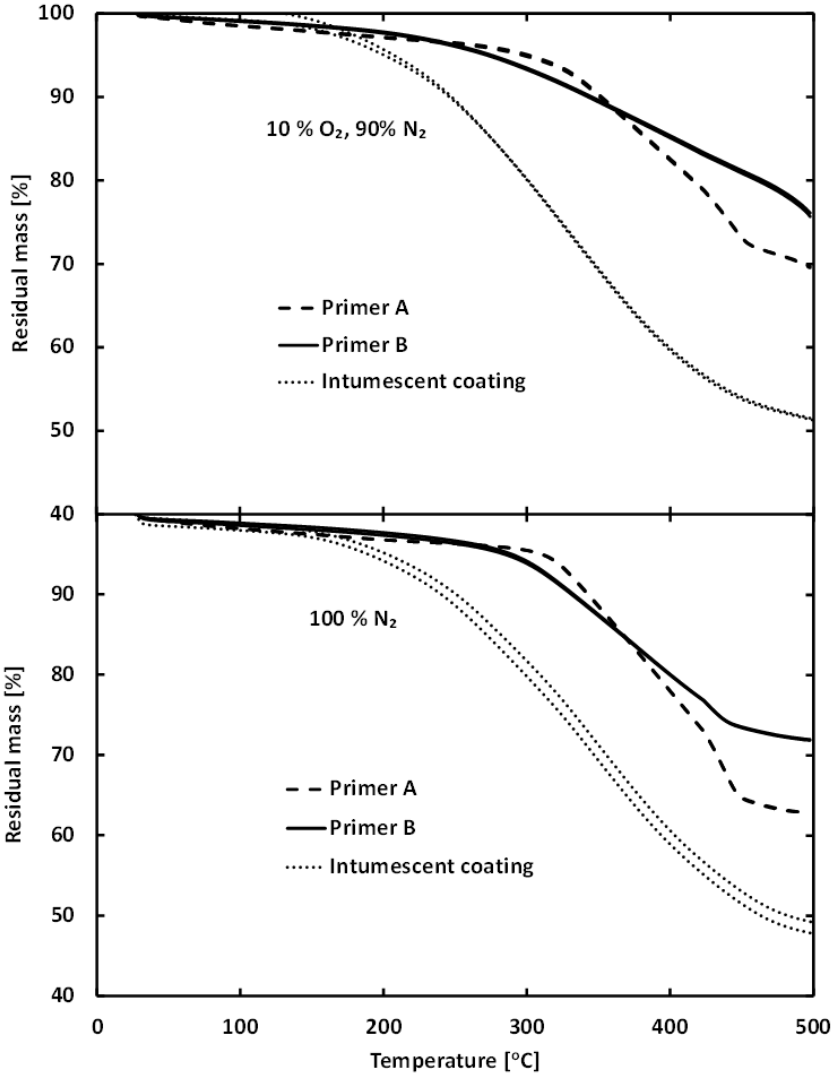

Figure 2.9. Mass loss curves (TGA) for the two primers and intumescent coating (all individual one-coat layer). The top plot shows mass loss under reduced oxygen and the bottom plot mass loss in nitrogen. For each sample, two data series are shown, verifying a good repeatability.

2.8 Discussion

It is evident, from the results presented above that the oxygen concentration and coating thickness of the primer are both influential on the primer performance in the intumescent coating system. Although the exact mechanism behind this is not completely understood, three different failure mechanisms can be proposed:

1) Prior to conducting the tests in the horizontal tube oven, it was suspected that incompatibility between primer B and the intumescent coating caused the failure. This seemed a reasonable expectation, based on the gas-fired furnace tests and TGA experiments. However, it was found that primer A also failed when its film thickness was increased. Therefore, it does not seem plausible that the failure can be explained by the changed mass loss behavior observed for primer B in oxygen. However, it is possible that the different behavior of primer B in the presence of oxygen is part of the explanation for the poorer performance of primer B relative to A. It does not seem likely that the intumescent coating is causing the primer failure in the gas-fired furnace.
2) A second possibility could be that differences in the thermal expansion coefficients and temperature gradients, across the system of the intumescent coating, primer and metal caused the system to fail. However, this does not seem probable because the failure did not happen in nitrogen, were the same temperature gradients and thermal expansions, as in the presence of oxygen would be expected.
3) A third explanation could be that the volume of gasses produced by the oxidation process is larger than those from the inert conditions (pyrolysis). This would lead to an increased pressure inside the coating, and in the anticipated melted primer binder, this would form larger bubbles. With higher thicknesses the total amount of gas would increase, and the distance this gas would have to travel to the surface would increase. Due to the longer distance to the surface, this would mean that more gas is accumulated inside the primer. It is expected that the bubbles would be larger, and hence more fragile. This is in parallel to the bubble formation in the intumescent coating, where a too low melt viscosity of the binder gives larger bubbles and a fragile char[16].

An important finding in this study is that testing of a given primer in controlled conditions, simulating the protective mechanisms of the intumescent coating, is important. Furthermore, apart from oxygen and heat shielding, other interactions with the intumescent coating may be less important, although the results are not evidence that this is always the case. Although the exact explanation for the observations has not been found, a clear conclusion is that for primer A, the thickness should not exceed 30 μm and primer B should not be used in the presence of oxygen, which may, for obvious reasons, be difficult to attain. If high thicknesses cannot be avoided, e.g. due to a highly corrosive environment, where anticorrosive barrier coatings are desired, the intumescent coating should be formulated to provide as effective a shield against oxygen as possible. It is also noted that the method provides a fast screening test for selecting primers and primer thicknesses for an intumescent coating system, irrespectively of the exact intumescent coating formulating.

Although it has not been verified, a final remark regarding testing the combined intumescent-primer-steel system in a gas-fired furnace is to use the color change observed in nitrogen and oxygen to verify the representativeness of a given test. This could be done removing the intumescent char and observe if the primer color is red or black. If the primer has turned black it has not been in any longer contact with oxygen. This may lead to a false negative result, relative to a real case scenario, where oxygen may indeed come in close contact with the primer via coating damages or unpredictable fire developments.

2.9 Conclusions

In this study, the performance of two epoxy primers for an acrylic intumescent coating was investigated at three different primer thicknesses, and comparison of samples heated in an electrically heated oven, a gas-fired furnace, and a thermo gravimetric analyzer. The protective mechanism of the intumescent coating against oxygen penetration is experimentally simulated in the electrically heated oven, with controlled gas and temperature conditions. Based on the experiments, it was found that with increasing film thickness, and in the presence of oxygen both primers showed a weaker performance.

Although it is not completely verified, it is very likely that the behavior of an epoxy primer in oxygen, at maximum thickness to be used for anticorrosive purposes, after heating to 500 ^{o}C will provide a strong indication of the primer performance under an intumescent coating, and thus the method can be used as a fast screening test, for different primer compositions and thicknesses. In terms of practical applicability, the results suggest that testing of a primer below an intumescent coating should not be limited to considerations of temperature, but also include oxygen contact. Thermogravimetric mass loss behavior could not be used to identify the failure mechanism.

2.10 References

[1] M. Jimenez, S. Duquesne, S. Bourbigot, Intumescent fire protective coating: Toward a better understanding of their mechanism of action, Thermochimica Acta 1–2 (449) 16-26 (2006).

[2] J.E.J. Staggs, Thermal conductivity estimates of intumescent chars by direct numerical simulation, Fire Saf. J. 4 (45) 228-237 (2010).

[3] L. Wang, Y. Wang, J. Yuan, G. Li, Thermal conductivity of intumescent coating char after accelerated aging, Fire Mater. 6 (37) 440-456 (2013).

[4] M. Gomez-Mares, A. Tugnoli, G. Landucci, F. Barontini, V. Cozzani, Behavior of intumescent epoxy resins in fireproofing applications, J. Anal. Appl. Pyrolysis (97) 99-108 (2012).

[5] E.D. Weil, Fire-Protective and Flame-Retardant Coatings-A State-of-the-Art Review, J. Fire Sci. 3 (29) 259-296 (2011).

[6] H. Horacek, Reactions of stoichiometric intumescent paints, J Appl Polym Sci 3 (113) 1745-1756 (2009).

[7] H. Vandersall, Intumescent coating systems, their development and chemistry, Journal of Fire and Flammability 9 (2) 97-140 (1971).

[8] S. Bourbigot, S. Duquesne, Fire retardant polymers: recent developments and opportunities, J.Mater.Chem. 22 (17) 2283-2300 (2007).

[9] P.A. Sørensen, S. Kiil, K. Dam-Johansen, C.E. Weinell, Anticorrosive coatings: a review, Journal of Coatings Technology and Research 2 (6) 135-176 (2009).

[10] S. Ullah, F. Ahmad, P. Megat-Yusoff, N.H.B. Azmi, A Study of Bonding Mechanism of Expandable Graphite Based Intumescent Coating on Steel Substrate, J. Appl. Sci. (Pakistan) 9 (11) 1630-1635 (2011).

[11] European Organisation for Technical Approvals (EOTA), ETAG 018 Guideline for European Technical Approval of Fire Protective Products Part 2: Reactive Coatings for Fire Protection of Steel Elements; European Oranization for Technical Approvals, Brussels. 1-35 (June 2006).

[12] M. Jimenez, S. Duquesne, S. Bourbigot, Multiscale experimental approach for developing high-performance intumescent coatings, Ind Eng Chem Res 13 (45) 4500-4508 (2006).

[13] M. Jimenez, S. Duquesne, S. Bourbigot, High-throughput fire testing for intumescent coatings, Ind Eng Chem Res 22 (45) 7475-7481 (2006).

[14] K.P. Nørgaard, K. Dam-Johansen, P. Català, S. Kiil, Investigation of char strength and expansion properties of an intumescent coating exposed to rapid heating rates, Prog. Org. Coat. 12 (76) 1851-1857 (2013).

[15] G.J. Griffin, A.D. Bicknell, T.J. Brown, Studies on the effect of atmospheric oxygen content on the thermal resistance of intumescent, fire-retardant coatings, J. Fire Sci. 4 (23) 303-328 (2005).

[16] K.M. Butler, Physical modeling of intumescent fire retardant polymers, in: ACS Symposium Series, ACS Publications, 1997, pp. 214-230, ISBN 9780841235168.

[17] G. Camino, L. Costa, L. Trossarelli, Study of the mechanism of intumescence in fire retardant polymers: Part V--Mechanism of formation of gaseous products in the thermal degradation of ammonium polyphosphate, Polym. Degrad. Stab. 3 (12) 203-211 (1985).

[18] F. Fan, Z. Xia, Q. Li, Z. Li, Effects of inorganic fillers on the shear viscosity and fire retardant performance of waterborne intumescent coatings, Progress in Organic Coatings 5 (76) 844-851 (2013).

[19] S. Bourbigot, M. Le Bras, R. Delobel, P. Bréant, J. Trémillon, Carbonization mechanisms resulting from intumescence-part II. Association with an ethylene terpolymer and the ammonium polyphosphate-pentaerythritol fire retardant system, Carbon 3 (33) 283-294 (1995).

[20] M. Jimenez, S. Duquesne, S. Bourbigot, Characterization of the performance of an intumescent fire protective coating, Surface and Coatings Technology 3-4 (201) 979-987 (2006).

[21] G. Camino, L. Costa, L. Trossarelli, F. Costanzi, G. Landoni, Study of the mechanism of intumescence in fire retardant polymers: Part IV—Evidence of ester formation in ammonium polyphosphate-pentaerythritol mixtures, Polym. Degrad. Stab. 1 (8) 13-22 (1984).

[22] M. Wladyka-Przybylak, R. Kozlowski, The Thermal Characteristics of Different Intumescent Coatings, Fire Mater. 33 (23) 33-43 (1999).

[23] B.K. Kandola, A.R. Horrocks, Complex char formation in flame-retarded fibre-intumescent combinations--II. Thermal analytical studies, Polym. Degrad. Stab. 2-3 (54) 289-303 (1996).

[24] Z. Lei, Y. Cao, F. Xie, H. Ren, Study on surface modification and flame retardants properties of ammonium polyphosphate for polypropylene, J Appl Polym Sci 1 (124) 781-788 (2012).

[25] A.M. Pereyra, G. Canosa, C.A. Giudice, Nanostructured Protective Coating Systems, Fireproof and Environmentally Friendly, Suitable for the Protection of Metallic Substrates, Ind Eng Chem Res 6 (49) 2740-2746 (2010).

[26] Z. Wang, E. Han, W. Ke, An investigation into fire protection and water resistance of intumescent nano-coatings, Surface and Coatings Technology 3-4 (201) 1528-1535 (2006).

[27] S. Duquesne, P. Bachelet, S. Bellayer, S. Bourbigot, W. Mertens, Influence of inorganic fillers on the fire protection of intumescent coatings, J. Fire Sci. 3 (31) 258-275 (2013).

[28] C. Branca, C. Di Blasi, H. Horacek, Analysis of the combustion kinetics and thermal behavior of an intumescent system, Ind Eng Chem Res 9 (41) 2107-2114 (2002).

[29] Z. Han, A. Fina, G. Malucelli, G. Camino, Testing fire protective properties of intumescent coatings by in-line temperature measurements on a cone calorimeter, Progress in Organic Coatings 4 (69) 475-480 (2010).

[30] B. Friederich, A. Laachachi, M. Ferriol, M. Cochez, R. Sonnier, V. Toniazzo, D. Ruch, Investigation of fire-resistance mechanisms of the ternary system (APP/MPP/TiO2) in PMMA, Polym. Degrad. Stab. 11 (97) 2154-2161 (2012).

[31] J. Gu, G. Zhang, S. Dong, Q. Zhang, J. Kong, Study on preparation and fire-retardant mechanism analysis of intumescent flame-retardant coatings, Surface and Coatings Technology 18 (201) 7835-7841 (2007).

[32] G. Griffin, The Modeling of Heat Transfer across Intumescent Polymer Coatings, J. Fire Sci. 3 (28) 249-277 (2010).

[33] K.P. Nørgaard, K. Dam-Johansen, P. Català, S. Kiil, Testing of intumescent coatings under fast heating, European Coatings Journal (June Issue) 34-39 (2012).

[34] G. Rayner-Canham, Descriptive inorganic chemistry, 2nd ed., W.H. Freeman, New York,N.Y., 2000, ISBN 0716735539.

Chapter 3 - Mathematical modeling of intumescent coating behavior in a pilot-scale gas-fired furnace

This chapter is intended for publication and will be submitted to a relevant journal in March 2014 with the title “Mathematical modeling of intumescent coating behavior in a pilot-scale gas-fired furnace” (authors Kristian Petersen Nørgaard, Kim Dam-Johansen Pere Català and Søren Kiil).

3.1 Abstract

In the event of a fire, intumescent fire protective coatings expand and form a thermally insulating char that protects the underlying substrate from heat and subsequent structural failure. The intumescence includes several rate phenomena, which have been investigated and quantified in the literature for several decades. However, various challenges still exist. The most important one concerns mathematical model validation under realistic exposure conditions and/or time scales. Another is the simplification of advanced models to overcome, the often seen, lack of a complete set of input and adjustable model parameters for a given coating, thereby providing models for industrial applications. In this work, these two challenges are addressed. Three experimental series, with an intumescent coating inside a 0.65 m^3 gas-fired furnace, heating up according to so-called cellulosic fire conditions, were conducted and a very good repeatability was evident. The experiments were run for almost three hours, reaching a final gas temperature of about 1100 °C. Measurements include transient temperature developments inside the expanding char, at the steel substrate, and in the mineral wool insulation placed behind the substrate. A mathematical model, describing the intumescent coating behavior and temperatures in the furnace using a single overall reaction was developed and validated against experimental data. By including a decomposition front movement through the char, a good qualitative agreement was obtained. After further

validation against experiments with other coating formulations, it has potential to become a practical engineering tool.

3.2 Nomenclature

carbonaceous char	non oxidized part of char
char	all expanded coating
$C_{p,ste}$	heat capacity of steel, $J \cdot kg^{-1} \cdot K^{-1}$
d_b	pore diameter of the char, m
$d_{\epsilon,carb,char}$	pore diameter of the carbonaceous char divided by emissivity, m
$d_{\epsilon,residue}$	pore diameter of the oxidized residue divided by emissivity, m
E_a	activation energy, $J \cdot mol^{-1}$
h	heat transfer coefficient, $W \cdot m^{-2} \cdot K^{-1}$
k	thermal conductivity, $W \cdot m^{-1} \cdot K^{-1}$
$k_{carb,char}$	thermal conductivity of carbonaceous (non-oxidized) char, $W \cdot m^{-1} \cdot K^{-1}$
k_{gas}	thermal conductivity of gas, $W \cdot m^{-1} \cdot K^{-1}$
k_{ins}	thermal conductivity of backside insulation, $W \cdot m^{-1} \cdot K^{-1}$
k_r	first order rate constant, s^{-1}
$k_{residue}$	thermal conductivity of oxidized residue, $W \cdot m^{-1} \cdot K^{-1}$
$k_{skeletal}$	thermal conductivity of solid in char, $W \cdot m^{-1} \cdot K^{-1}$
k_0	pre-exponential factor, s^{-1}
k_{300}	thermal conductivity of solid at 300 K, $W \cdot m^{-1} \cdot K^{-1}$
l	position, m

l_{char}	position of char surface, m
l_{ins}	position of interface between insulation and steel substrate, m
l_{ste}	position of interface between steel substrate and char, m
l_0	position at backside of insulation, m
M	parameter describing the nucleii growth mechanism, s^{-N}
N	discrete parameter describing the nucleii growth mechanism, -
R	gas constant, $J \cdot mol^{-1} \cdot K^{-1}$
residue	residue after oxidation of char
T	temperature, K
t	time, s
Th#	thermocouple, # refers to distance to steel substrate in cm
Th_{set}	thermocouple measuring the gas temperature
$T_{backside}$	temperature at backside of insulation, K
T_{gas}	gas temperature, K
$T_{gas,measured}$	measured gas temperature, K
T_{ste}	temperature of isothermal steel substrate, K
T_{sur}	surface temperature, K
$t_{63\%}$	time for decomposition front to reach 63% conversion, s
X	solids conversion, -

Greek letters

β	empirical constant in temperature dependency of thermal conductivity, -

δ_{ins}	thickness of backside insulation, m
δ_{char}	thickness of char, m
$\delta_{char,final}$	final thickness of char, m
δ_{front}	thickness of decomposed zone, m
δ_{ste}	thickness of steel substrate, m
δ_0	initial intumescent coating thickness, m
ε	porosity, -
ε_0	initial coating porosity, -
ϵ	emissivity, -
ρ_{ste}	density of steel, $kg \cdot m^{-3}$
σ	Stefan-Boltzmann constant, $5.6703 \cdot 10^{-8}\ W \cdot m^{-2} \cdot K^{-4}$

3.3 Introduction

If a fire takes on, intumescent fire protective coatings undergo a complex reaction sequence, which results in a thick, thermally insulating char on top of the substrate (e.g. steel). The char prolongs the time before a steel structure reaches a critical temperature and collapses[1-3]. In general, intumescent coatings expand according to a series of steps, which begins with melting and degradation of the polymer matrix, followed by decomposition of gas releasing compounds and char formation, and finally, at high temperatures, char degradation[4]. A detailed description of the chemistry and physics of the various steps in the intumescent char formation process can be found in earlier work[5].

An important challenge in intumescent coatings development is the requirements for expensive and time consuming third party approval tests, which must take place prior to a new coating being marketed. To improve fire safety, mapping the influence of furnace process parameters, and optimize coatings for approval tests, a fundamental understanding of the underlying intumescent process mechanisms is of great interest. To provide such understanding, mathematical models are useful and many modeling activities have taken place as described in three important review articles[2, 4, 6]. In short, the mathematical models developed are typically validated against experimental data obtained in well-controlled, small-scale laboratory equipment (e.g. cone calorimeters), where conditions, e.g. gas flows or heating rates, can differ substantially from those present in real fire conditions. In addition, the models developed are often of a very high complexity (partial differential equations), requiring a large number of input and adjustable parameters, e.g. melt viscosities of the binder phase and a set of rate constants, which may be tedious and/or time consuming to measure or validate for new coating systems or process conditions. While the advanced models can certainly help to map the phenomena involved, their practical use may be somewhat limited.

The aim of the present work was to obtain several experimental data series for an intumescent coating exposed in a pilot-scale, natural gas-fired furnace. Additionally, a mathematical model, containing the most important rate phenomena only, is developed. The model can simulate transient developments in char and steel temperatures, as well as expansion-time curves of an intumescent coating. Model simulations are compared to the pilot-scale furnace measurements and suggestions provided for how to use the model in daily work with coating optimization and process development.

3.4 Validation methods for previous models of intumescent coatings

A number of models on intumescent coatings are available in the literature and have been reviewed by several authors[2, 4, 6]. The models range from classical mathematical models[2, 4, 7], considering factors such as heat conduction, expansion and gas production, to more empirical models[8-10], in which a set of experimental data, obtained in laboratory-scale equipment, are used to rank performance of different coating formulations for full-scale tests. In 2010, Griffin[6] identified five main limitations to the current models before these can be applied to real world situations. The limitations are: 1) models are only in 1D, 2) complete data for a particular coating system is not available, 3) effects of radiation and turbulent gasses, present in large scale furnace tests and difficult to mimic in small-scale laboratory equipment, are not included in current models, 4) the use of an expansion factor based on the post heated char thickness is often used, and 5) studies on the effect of variations in oxygen content are limited. It is noted by Griffin that multidimensional models are of particular interest when simulating the behavior of coatings applied to complex geometries used in many types of constructions. Shi and Chew[4] identified a lack of models dealing with the mechanical behavior of intumescent coatings under external loads (not specified further) and also a need for modeling of toxic gasses produced in the coating during a fire. Furthermore, modeling of expansion of intumescent coatings is complicated by the often seen irregular expansion behavior [4]. Shi and Chew[4] provide a table of input parameters taken into account in different models of intumescent coatings. Parameters related to heat conduction, pyrolysis, transport of gas volatiles, coating/char volume change, internal gas pressure, water evaporation, gas permeability, porosity of the char, and mechanical behaviors are often included in the complex models.

In Table 3.1, some details of the most recent models in the literature have been listed with respect to the experimental methods used for the validation of the models and the experimental times used in the experiments. Note that several of the models presented in the table focus on modeling of laminates, ablative coatings, or composites and not traditional intumescent coatings. Further details regarding the models can be found in Shi and Chew[4]. The table shows that validation of the models done with laboratory equipment and over relatively short experimental times. Other relevant models can be found regarding intumescent coatings[11-13]. The articles by Mamleev et al.[13] and Bourbigot et al.[14] are interesting in that they used thermocouples, drilled through a steel substrate, to measure the temperature inside an expanding intumescent coating, placed below a gas burner or in the so-called lower oxygen index test. In the work by Mamleev et al.[13], the temperatures were measured for 60 minutes and validation of the model performed using measurements at different positions inside the char. The modeling focused mostly on the viscosity of the coating during the intumescent process and included phenomena such as foam drainage and char shrinkage. However, as noted by Griffin[6], the model shows poor agreement between experimental and modeled temperatures. In summary, there is a strong need for pilot-scale furnace experiments under realistic conditions.

Table 3.1. Recent mathematical models of intumescent coatings with year of publication and equipment and time span used when validating the models. Other details can be found in Shi and Chew[4].

Model	Year	Equipment used for validation	Time of experiment [min]
Stoliarov et al.[31]	2010	Cone calorimeter (steel temperature)	10
Griffin[6]	2010	Cone calorimeter (steel temperature), mass loss (TGA), expansion, surface temperature	33
Lautenberger and Fernandez-Pello[10]	2009	TGA and cone calorimeter (data from Griffin 2005[7, 32])	33
Farkas et al.[33]	2008	Simulated gas flux from mass loss cone calorimeter	17
Bai et al.[34, 35]	2008	Experiments of deflection of beams	N/A
Feih et al.[36]	2007	External heat load under cone calorimeter, steel temperature	50
Trelles and Lattimer[37]	2007	Temperatures and mass losses measured in a mass loss calorimeter	~4
Bahramian et al.[38]	2006	Back side temperature of steel protected by ablative composite. Exposed to oxyacetylene flame.	0.3

3.5 Experimental procedures

Materials and sample preparation

A generic solvent-borne acrylic intumescent coating, intended for protection against so-called cellulosic fires, has been used for this study. Besides binder and solvent the coating contains the usual intumescent compounds, i.e. blowing agent (e.g. melamine), carbon source (e.g. pentaerythritol), acid source (e.g. ammonium polyphosphate), and pigments (e.g. TiO_2). The coating was sprayed on to C16 steel substrate of dimensions 200x300x6 mm^3. Prior to spraying of the intumescent coating, the steel substrate was coated with a commercial epoxy primer. The re-coating interval was at least 1 month, and the coating was sprayed onto the large face of the steel

substrate using an airless spray with a tip 419. The dry coating thicknesses aimed at were approximately 1.2 and 2 mm, but some variation, due to the spray application and deformation during drying of the coating, cannot be avoided. The substrates were allowed to dry for at least two weeks. After drying, and just before the fire tests, coating thicknesses were measured using an Elcometer 456 TOP F1. Depending on the coating thickness, appropriate probes, either in the range of 0-1500 or 0-5000 µm, were applied for the readings. The thicknesses for the two 1200 µm experiments were measured in 9 different places on the individual substrates and found to be 1199±46 and 1171±47 µm and for the 2000 µm cases 1969±67 and 1948±99 µm. Experiments with uncoated steel were also performed.

Gas-fired furnace

A photo of the custom-build furnace, with important inner dimensions, is seen in Figure 3.1. The steel substrate with intumescent coating was placed in a vertical position inside a frame in the wall of the gas-fired furnace, opposite to the viewing port and parallel to the gas flow. On the back side of the steel substrate, 8 cm of Superwool® mineral insulation is present. The temperature of the furnace is controlled by a thermocouple in front of the steel substrate and follows the ISO834 temperature-time curve, valid for cellulosic intumescent coatings. The gas to air ratio was 1:10 and the natural gas consumption approximately 13 m^3 per hour at STP, thereby corresponding to a linear approximate velocity of 0.6 m/s, falling in the laminar regime.

Three types of experiments are used for the investigation and each experiment was run twice:

1. Steel substrate with coating thicknesses of approximately 1200 µm. Thermocouples are drilled through the steel substrate and positioned in steps of 1 cm above the coating.

2. Steel substrate with coating thicknesses of approximately 2000 µm. Thermocouples arranged as described under 1.
3. Uncoated steel substrates also with thermocouples placed as described above. These experiments were used as reference to help evaluating expansion rates by comparing results for coated and uncoated steel substrates and thermocouples drilled through the steel plate. The heat transfer coefficient of the furnace was also determined from these experiments (more on this later).

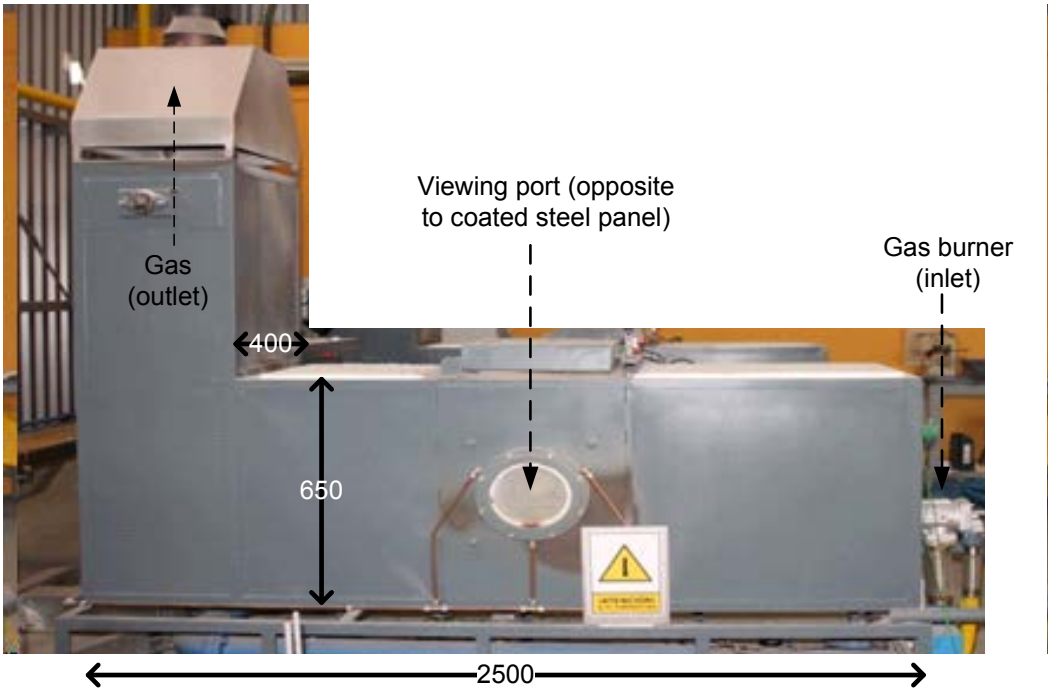

Figure 3.1. Photo of furnace with dimensions in mm. The coated steel substrate (cannot be seen) is inserted in a vertical position opposite to the viewing port. Arrows indicate inner dimensions.

The heating conditions and furnace differ, but it is noted that the thermocouple methodologies of Mamleev et al.[13] and Bourbigot et al.[14] have been important inspirations for the experiments of this work.

Thermocouples and expansion measurements in gas fired furnace

A drawing of the experimental system in one dimension is seen in Figure 3.2, where temperatures measured (denoted Th#) are indicated. In addition to the thermocouples shown, some thermocouples were placed at a greater distance from the coating, to measure the gas temperature. However, due to the response time of the thermocouples, these cannot not give a reliable gas temperature reading in the beginning of the experiments, where the temperature gradients are very steep. The set point temperature (Th_{set}) is measured by a thermocouple in a shielding ceramic cover. K-type thermocouples, with a junction diameter of 1.5 mm were used to measure the temperatures. The high junction diameter was selected for better endurance at the high temperatures in the furnace[15] and new thermocouples were used for each test run. The thermocouples were either drilled 3 mm into the backside of the steel substrate or drilled through the steel substrate and positioned for every centimeter. A thermocouple was also used to measure the temperatures inside the backside insulation, 6 cm behind the steel substrate. The char expansion rate was measured by observing when the temperatures of the thermocouples, drilled through the steel substrate began to deviate strongly from the temperatures measured with the uncoated steel substrates. The steel substrate is only coated on one side and heat can potentially flow to the steel substrate from the sides. To avoid this, a stone frame which, as shown in Figure 3.2, partly covers the steel substrate was inserted. It is noted that the experiments, for reasons of understanding the behavior, were run for longer times than would normally be the case in a test series. Experiments were halted when the steel substrate temperature reached 550 ^{o}C.

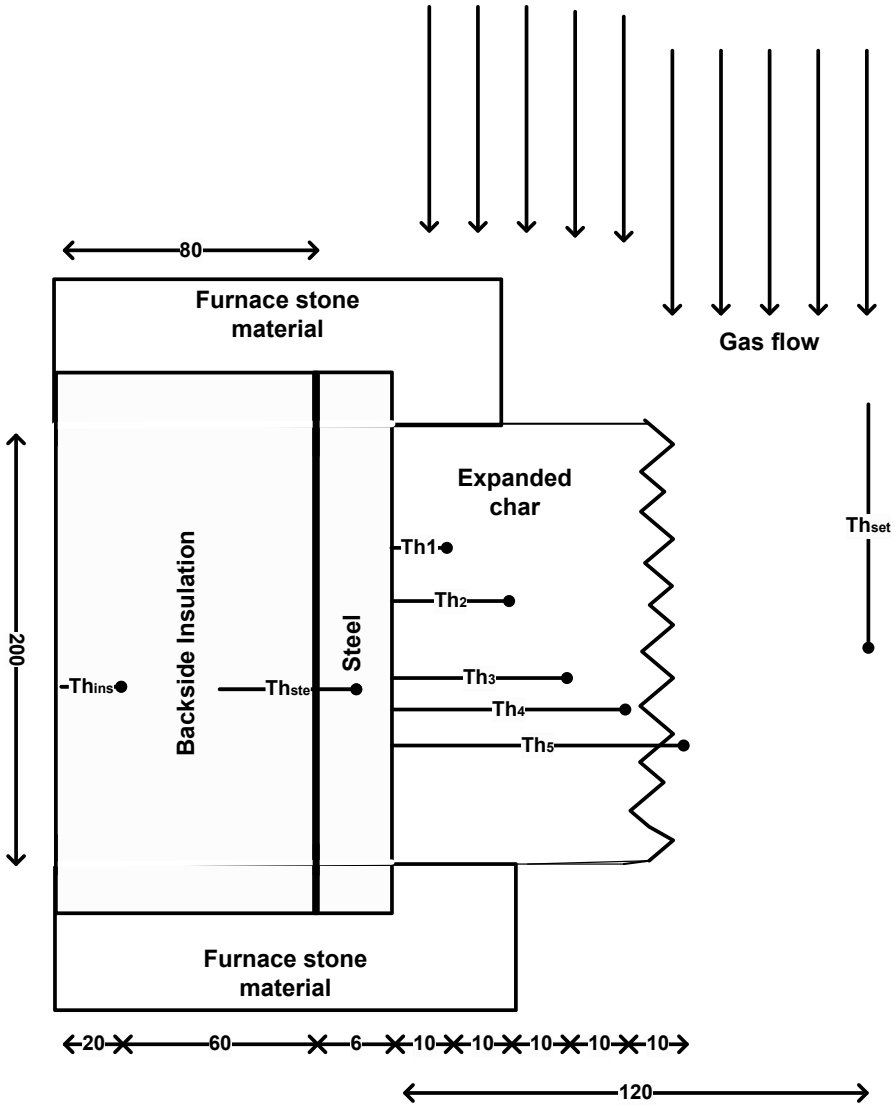

Figure 3.2. A principal drawing of the experimental system inside the furnace (seen from above). On the drawing, the temperatures measured are indicated. Dimensions are all provided in mm. "Th" refers to thermocouples, where the subscripts "ins", is the insulation, "ste" is the steel, "set" is the set point thermocouples and "Th1-5" are thermocouples at positions from 1 to 5 cm above the steel substrate. Furnace stone material is placed around the steel substrate.

3.6 Mathematical modeling

A mathematical model describing the behavior of an intumescent coating exposed to heating in a pilot-scale furnace is now presented. A schematic drawing showing the physical system, with indications of temperatures and thicknesses used for the model derivation, is provided in Figure 3.3. A single overall reaction is included to describe the char expansion. This reaction represents all phenomena in the expansion process including acid formation, char formation, decomposition of the blowing agent, and melting of the binder. Char degradation and oxidation, setting in at high temperatures, are described by a separate reaction mechanism.

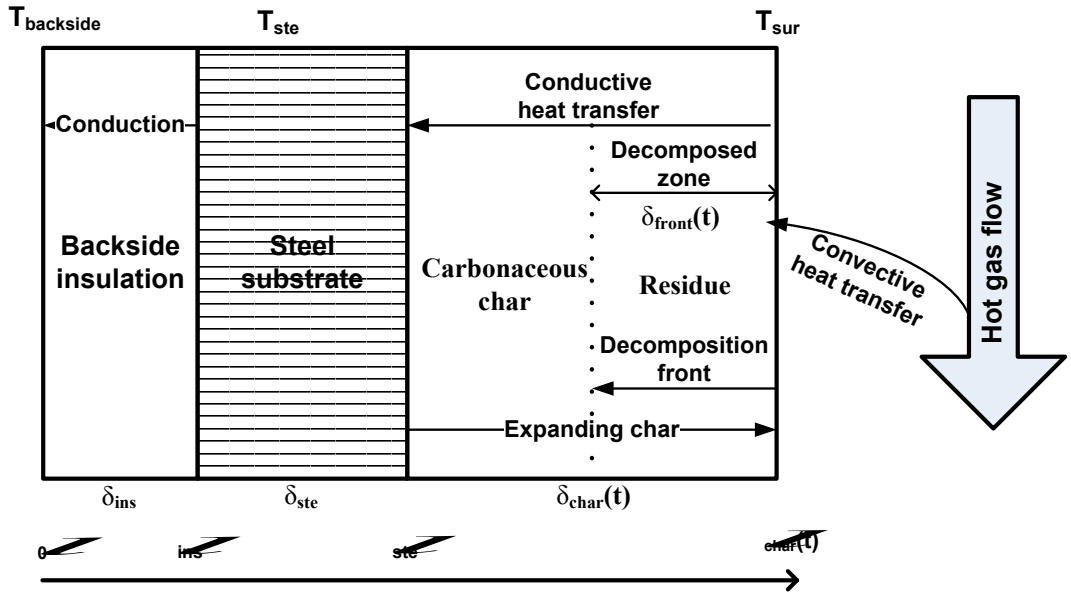

Figure 3.3. Schematic illustration of the model system, showing the main mechanisms included in the model. Not to scale. Positional variables are shown below the figure and temperatures above. δ_{ins}, δ_{ste}, and δ_{char} represent the thickness of the backside insulation, the steel substrate and the char, respectively. δ_{front} represents the thickness of the decomposed zone. The vertical dotted line shows the interface between carbon containing char and inorganic residue.

Assumptions underlying the model development

- The intumescent coating contains blowing agent, binder, acid source, carbon source and pigments.
- Slab geometry only is considered.
- Heat transfer takes place in one dimension only.
- Heat transfer from gas to char surface is governed by convection only. Radiation from walls and gas to the coating is neglected.
- The heat transfer coefficient can be determined from experiments with uncoated steel.
- The steel substrate and backside insulation are chemically inert at all temperatures.
- Shrinkage of the expanded char is neglected.
- The expansion of the char layer can be described by a single chemical reaction, first order in the solids concentration.
- The rate of reaction for the expansion is evaluated at the temperature of the steel substrate (i.e. the expansion develops from the position of the original non-expanded coating).
- The chemical reaction of the solid coating is irreversible.
- Convective heat transfer inside the char pores is neglected.
- The char is considered intact at all times (i.e. no cracks in the surface).
- The gas pressure inside the char is equal to ambient pressure, and the thermal conductivity of the gas only depends on temperature.
- The steel substrate is isothermal at all times.
- Heat effects from the char expansion reaction are neglected.

- During intumescence the entire coating is transformed into char (i.e. a single solids conversion value, X, is used and when X=1 full expansion is established).
- The porosity and density of the char formed attain constant temperature-independent values.
- A front moves through the char according to a decomposition reaction followed by oxidation at temperatures of 600 ^{o}C. This front is referred to as the "decomposition front".
- Behind the decomposition front, the only solid present is TiP_2O_7.
- The thermal char properties on each side of the decomposition front can be slightly different (more on this later).

When describing the model development, three terms for the expanded coatings are used. "Char" refers to the expanded coating irrespectively of the thickness of the decomposed zone. "Residue" refers to oxidized char (present only in the decomposed zone) and "carbonaceous char" refers to char where carbon has not been oxidized. This is shown in Figure 3.3 and the separation between residue and carbonaceous char is defined by the decomposition front position.

Char expansion

The current char thickness, δ_{char}, is described using the solids conversion, X, and the maximum expansion, $\delta_{\text{char,final}}$, (measured after cooling of the expanded char)

$$\delta_{\text{char}} = \text{X} \cdot \delta_{\text{char,final}} + \delta_0 \tag{3-1}$$

where δ_0 is the initial intumescent coating thickness.

The solids conversion is described by the following first order reaction

$$\frac{d\text{X}}{d\text{t}} = \text{k}_\text{r}(\text{T}) \cdot (1\text{-X}) \tag{3-2}$$

where $k_r(T)$ is a rate constant.

The initial condition is

$$X(t = 0) = 0 \tag{3-3}$$

Energy balance

An energy balance of the steel plate, modeled as a thermal resistor network gives

$$\rho_{ste} \cdot C_{p,ste}(T) \cdot \delta_{ste} \frac{\partial T_{ste}}{\partial t} = \frac{1}{\frac{1}{h} + \frac{\delta_{front}(t)}{k_{residue}(T)} + \frac{\delta_{char}(t) - \delta_{front}(t)}{k_{carb,char}(T)}} \left(T_{gas} - T_{ste}\right) - \frac{k_{ins}(T)}{\delta_{ins}} \left(T_{ste} - T_{backside}\right) \tag{3-4}$$

where ρ_{ste} is the density of steel, $C_{p,ste}$ is the heat capacity of steel, δ_{ste} is the thickness of the steel plate, h is the heat transfer coefficient, δ_{front} is the thickness of the decomposed zone, $k_{residue}$ is the thermal conductivity of the oxidized residue, and $k_{carb,char}$ is the thermal conductivity of the carbonaceous char. T is temperature and t is time. The thicknesses and temperatures are illustrated in Figure 3.3.

The initial condition is

$$T(l, t=0) = T_{ste,0} \tag{3-5}$$

The gas temperature, T_{gas}, of the furnace is a model input parameter and $T_{backside}$ is assumed constant at 25 °C.

Decomposition front

Based on the experimental results, which are presented in a later paragraph, a decomposition front moving through the char is included in the model. The front movement is initiated at a temperature of 600 °C and the mechanism is assumed to be solid decomposition followed by

oxidation. The decomposition reaction is assumed to be the first step of titanium pyrophosphate formation where the phosphorous ester decomposes to polyphosphoric acid, methane and carbon[5, 16]

$$C_{10}H_{10}O_6P_2\ (s) \rightarrow 2\ HPO_3\ (s\ or\ l) + 2\ CH_4\ (g) + 8\ C\ (s) \tag{3-6}$$

In the second step, units of polyphosphoric acid, react with TiO_2 and form the white solid titanium pyrophosphate[5, 16]

$$2\ HPO_3\ (s\ or\ l) + TiO_2\ (s) \rightarrow TiP_2O_7\ (s) + H_2O\ (g) \tag{3-7}$$

Meanwhile, oxidation of methane and carbon occurs

$$CH_4\ (g) + 4\ C\ (s) + 6\ O_2\ (g) \rightarrow 5\ CO_2\ (g) + 2\ H_2O\ (g) \tag{3-8}$$

The reaction shown in (3-6) is a solid decomposition where a solid transforms into gaseous and solid product(s). Such reactions are known to proceed according to a growth of nucleii where the product phases are formed at reactive points in the original solid phase[17]. The solid decomposition is assumed to follow an S-shaped (sigmoidal) conversion-time behavior as described by Levenspiel[18]. The kinetics for such reactions is described by e.g. Avrami[19]

$$\delta_{\mathrm{front}}(t) = \delta_{\mathrm{char}}(t) \cdot \left(1 - \exp\left(-M \cdot t^{-N}\right)\right) \tag{3-9}$$

the initial condition is

$$\delta_{\mathrm{front}}(t = 0) = 0 \tag{3-10}$$

where N is a discrete integer describing the mechanism of nucleii formation. N is dependent on whether the nucleii are all present from the start or formed at a steady rate. N also describes if the

nucleii formation happens in 1, 2 or 3 dimensions[18]. The front growth equation (3-9), presented above, has been used to describe several reaction rate phenomena e.g. crystallization, adsorption, solid-gas reactions, and catalysis[17, 20]. From (3-9) it is seen that at the time where $\delta_{\mathrm{front}}(\mathrm{t})$ is 63% of $\delta_{\mathrm{char}}(\mathrm{t})$, the following relation between M and N is valid

$$\mathrm{M} = (\mathrm{t}_{63\%})^{-\mathrm{N}} \tag{3-11}$$

where $t_{63\%}$ is the time in seconds to achieve 63% decomposition of the char. The unit of M depends on the value of N. In summary, two kinetic parameters, N and $t_{63\%}$, need to be estimated in order to use the kinetics in the overall intumescent coating model. It is assumed here that nucleii are formed at a steady rate (in three dimensions at the microscopic level) and therefore N = 4.

Due to variations in the coating formulation, it is noted that the reactions occurring in the experiments of this work may differ from those presented above. Also other phenomena could influence the decomposition front movement, e.g. mass transfer of gaseous species and a temperature dependency of the decomposition rate. Therefore, the expression in (3-9) could have several rate phenomena lumped into one equation in a similar manner as (3-2) which describes the char expansion. This also means that detailed mass balances for eqs. (3-6)-(3-8) have not been included in the model, the entire mechanism is represented by eq. (3-9) and the imposed changes in thermal conductivities.

External heat transfer coefficient

The heat transfer coefficient, h, is determined from experiments as a function of temperature using the uncoated steel plate experiment and by setting up a heat balance for the steel plate

$$h \cdot \left(T_{gas} - T_{sur}\right) = \rho_{ste} \cdot \delta_{ste} \cdot C_{p,ste}(T) \cdot \left.\frac{\partial T_{ste}}{\partial t}\right|_{t} \quad (3\text{-}12)$$

where T_{sur} is the surface temperature. The steel plate is assumed isothermal and thus $T_{sur} = T_{ste}$. The heat transfer to the backside insulation is neglected in the calculations.

Solution procedures

The new engineering model only contains ordinary (as opposed to partial) differential equations. The solution of the model was carried out using the ordinary differential equation solver ODE45 in MatLab. The adjustable parameters were varied manually to match simulations and experimental data of T_{ins}, $T_{ste,}$ the temperatures inside the char, and the char expansion. Due to the uncertainty of the experimental data, no attempt to get very accurate values of the adjustable parameters, using a minimization routine, was carried out. Temperatures inside the char layer were found using interpolation between the surface-, decomposition front- and steel temperatures and assuming the heat flux through the char is constant at a given point in time at all positions. This is the same as a thermal resistor network described in Mills[21]. The temperature in the backside insulation was found by assuming a linear temperature profile between $T_{backside}$ and T_{ste}. The data matching was done based on both the 1200 and 2000 µm. When determining $\frac{\partial T_{ste}}{\partial t}$ for the heat transfer coefficient in (3-12) a 9th order polynomial is fitted to the experimental results

3.7 Estimation of model parameters

A summary of the input parameters for the model is given in Table 3.2, and here follows a description of the input parameters.

Table 3.2. List of input parameters to simulations. Reference to an equation number is provided where the parameter is calculated using an equation or correlation.

Parameter	Value	Unit	Reference/note
ρ_{ste} – Density of steel	7858	$kg \cdot m^{-3}$	Incropera and De Witt[23]
k_{ins} – Thermal conductivity of backside insulation	Eq. (3-13)	$W^{-1} \cdot m^{-1} \cdot K^{-1}$	From supplier product sheet[22]
$C_{p,ste}$ – Heat capacity of the steel	Eq. (3-14)	$J \cdot K^{-1} \cdot kg^{-1}$	Incropera and De Witt[23]
h – heat transfer number	34	$W^{-1} \cdot m^{-2}$	Average value based on measurements (see Figure 3.9)

Thermal properties of backside insulation (superwool® plus)

The thermal conductivity of the backside insulation material is described by

$$k_{ins}(T) = 0.0348 \cdot e^{0.00201 \cdot T} \quad (3\text{-}13)$$

The correlation was derived from data in the supplier product sheet where the thermal conductivity is provided for every 200 °C[22]. T must be inserted in °C.

Properties of the steel

An expression for the heat capacity of C16 steel is derived from data in Incropera and De Witt[23]

$$C_{p,ste}(T) = 2.364 \cdot 10^{-6} \cdot T^3 - 1.758 \cdot 10^{-3} \cdot T^2 + 0.783 \cdot T + 420.209 \quad (3\text{-}14)$$

where T must be inserted in °C and $C_{p,ste}$ is given in the unit $J \cdot kg^{-1} \cdot K^{-1}$.

The density of steel is set to constant values defined at room temperature[23].

Effective thermal conductivity of char layers

For the effective thermal conductivity of the carbonaceous char, $k_{carb,char}$, and the residue, $k_{residue}$, an expression specifically developed for intumescent chars by Di Blasi and Branca[24] is used. The

expression includes contributions from both radiation in the pores and conduction in the gas and solid phase

$$k(T) = \frac{k_{skeletal}(T) \cdot k_{gas}(T)}{(1-\varepsilon) \cdot k_{gas}(T) + k_{skeletal}(T) \cdot \varepsilon} + 13.5 \cdot \sigma \cdot (T)^3 \cdot \frac{d_b}{\varepsilon \cdot \epsilon} \quad (3\text{-}15)$$

where σ is the Stefan-Boltzmann constant, d_b is the pore diameter, and ϵ is the emissivity of the coating. $k_{skeletal}$ and k_{gas} are the thermal conductivity of the solid char and gas, respectively. ε is the porosity of the char. The pore diameter, d_b, is assumed independent of temperature. The temperature must be inserted in eq. (1-2) in K. The temperature dependencies are based on the arithmetic mean of either the carbonaceous char layer or the residue layer.

Thermal conductivity of gas phase

The thermal conductivity of the gas inside the char, k_{gas}, is described by the expression provided by Di Blasi and Branca[24]

$$k_{gas}(T) = 4.815 \cdot 10^{-4} \cdot T^{0.717} \quad (3\text{-}16)$$

where T must be entered in K, and k_{gas} is in $W \cdot K^{-1} \cdot m^{-1}$.

Porosity of char layer

The porosity, ε, of the char is crudely estimated by a simple relation of proportionality

$$\varepsilon = 1 - \frac{\delta_0 \cdot (1-\varepsilon_0)}{\delta_{char,final}} \quad (3\text{-}17)$$

where ε_0 is the initial porosity of the coating. It is noted that equation (3-17), due to lack of a reliable number, neglects the effect of solids being converted to gas during the intumescence process.

3.8 Adjustable parameters

In addition to the input parameters described in the previous paragraph, the simulations are based on seven adjustable parameters. A summary of these and their values after matching of experiments and simulations is given in Table 3.3. The parameters are described in the following and a separate section with discussion and validation of the adjustable parameter values from the data matching is provided in a later paragraph.

Table 3.3. Values of adjustable parameters used in the mathematical model. Values for both the 1200 and 2000 µm simulations are shown.

Parameter	Value 1200 µm	Value 2000 µm	Unit
*Parameters affecting thermal conductivity**			
$d_{\epsilon,carb,char}$ – pore diameter divided by emissivity of carbonaceous char	250	190	µm
$d_{\epsilon,residue}$ – pore diameter divided by emissivity of carbonaceous char	300	225	µm
β - empirical constant in temperature dependency of thermal conductivity	1	1	-
k_{300} – Thermal conductivity of solid at 300 K	0.345	0.345	$W \cdot m^{-1} \cdot K^{-1}$
Parameters affecting char expansion			
E_a - Activation energy	34000	34000	$J \cdot mol^{-1}$
k_0 - Pre-exponential factor	15	10	s^{-1}
Parameters affecting decomposition front			
$t_{63\%}$ - Time to 63% conversion	5580	6300	s

**The sensitivity analysis performed shows that the parameters related to thermal conductivity are of little influence on the results.*

Rate constant for char expansion

The rate constant, k_r, describing the char expansion is given by an Arrhenius expression

$$k_r(T) = k_0 \cdot \exp\left(\frac{-E_a}{R \cdot T}\right) \tag{3-18}$$

where k_0 is the pre-exponential factor, E_a is the activation energy and R is the gas constant. Both k_0 and E_a are adjustable parameters in the model.

Pore diameter and emissivity

The pore diameter divided by emissivity, describes the effect of intra-char radiation in the effective thermal conductivity shown in (1-2). The ratio between these, d_ϵ, is defined as

$$d_\epsilon = \frac{d_b}{\epsilon} \tag{3-19}$$

where d_ϵ in the carbonaceous char and the residue layer are referred to as $d_{\epsilon,carb,char}$ and $d_{\epsilon,residue}$, respectively. Both these parameters are adjustable in the model.

Skeletal thermal conductivity

To estimate the skeletal thermal conductivity, $k_{skeletal}$, of the solid in the porous char, an expression derived by Palankovski[25] for the temperature dependence of the thermal conductivity of solids is used

$$k_{skeletal}(T) = k_{300} \cdot \left(\frac{T}{300}\right)^{\beta} \tag{3-20}$$

where k_{300} is the thermal conductivity at 300 K, and β is an empirical parameter. The values are assumed to be the same in the carbonaceous char and the residue. Both β and k_{300} are adjustable parameters in the model.

Parameter affecting the decomposition front

The parameter describing the movement of the decomposition front, $t_{63\%}$, is an adjustable parameter in the model. A change in $t_{63\%}$ will displace the onset of the decomposition front movement.

3.9 Results and discussion

In this section, the experimental results obtained are first explained and discussed with respect to repeatability. Then follow simulations and model validation. Finally, a sensitivity analysis and parameter study of the model and evaluation of assumptions are discussed.

Experimental series and repeatability

Several experimental series were conducted in the pilot-scale furnace and repetitions included to evaluate the uncertainty. To provide a visual impression of the char formed, a photo taken after 3 hours of heating and subsequent cooling to room temperature is seen in Figure 3.4. The intumescent coating has expanded from about 1 mm to about 4.5 cm. The expansion was fairly uniform in the large middle zone of the coated substrate, whereas somewhat lower expansion was observed near the edges of the char. The inside of the char was completely white, the color originating from TiO_2 and titanium pyrophosphate formed during the intumescence[5].

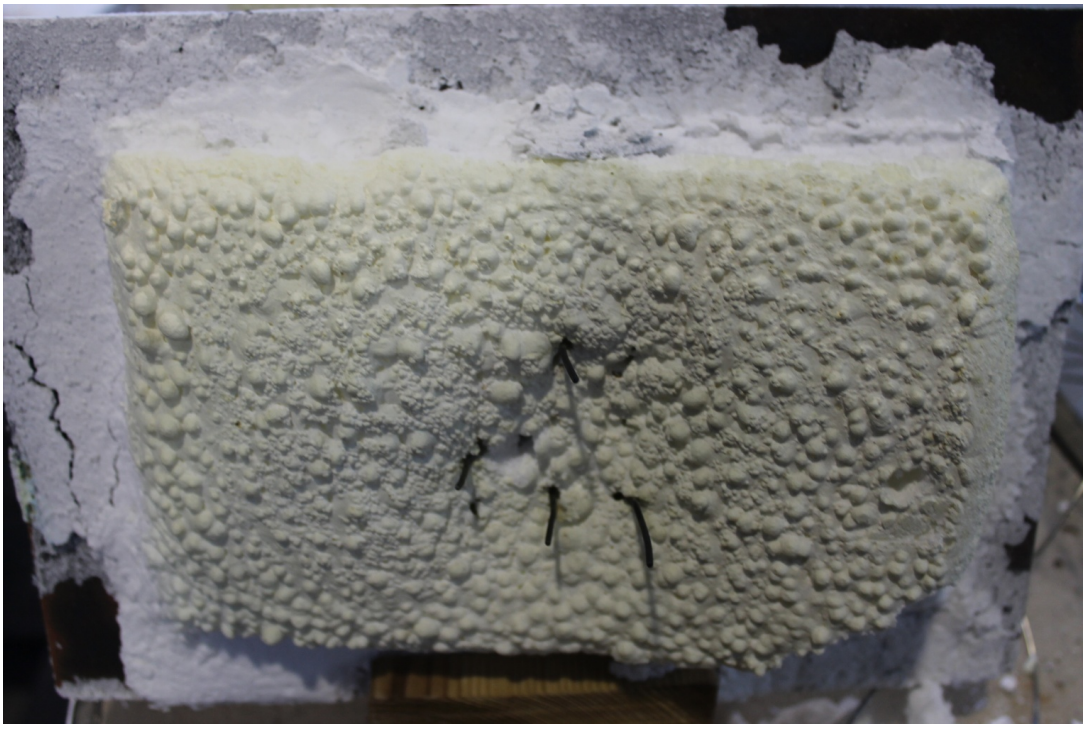

Figure 3.4. Photo of expanded char after 3 hours of heating in the furnace. The five uncovered metal thermocouples, placed above the char, can be seen close to the center of the char surface. The thermocouples already covered cannot be seen.

A thin (about 1 mm) layer of a yellow material had formed on the outer surface of the char. The chemical nature of this top layer was not identified, but it appeared in all the experiments and probably originates from an incipient chemical conversion of the, presumably inorganic, white char at high temperatures. Another important observation in Figure 3.4 is the rough morphology of the outer surface, which is most likely formed when gas bubbles, released by the blowing agent, reaches the char surface, but not overcoming the surface tension of the molten char phase.

To aid the subsequent model discussion, temperature-time curves measured in the furnace are shown in Figure 3.5 with indication of four characteristic time periods, termed P1-P4 (shown as an example for the thermocouple initially placed 1 cm above the coated steel substrate). The four curves represent the following:

- P1 is the time period prior to a thermocouple being covered by the expanding char.
- P2 is the time period during which a falling temperature is observed.
- P3 is the time period with a close to constant temperature increase.
- P4 is the time period during which the temperature increases at a lower rate.

During P4, the steel reaches the critical temperature of about 500 °C. The backside insulation temperature (measured at a position 6 cm behind the steel substrate) is also shown.

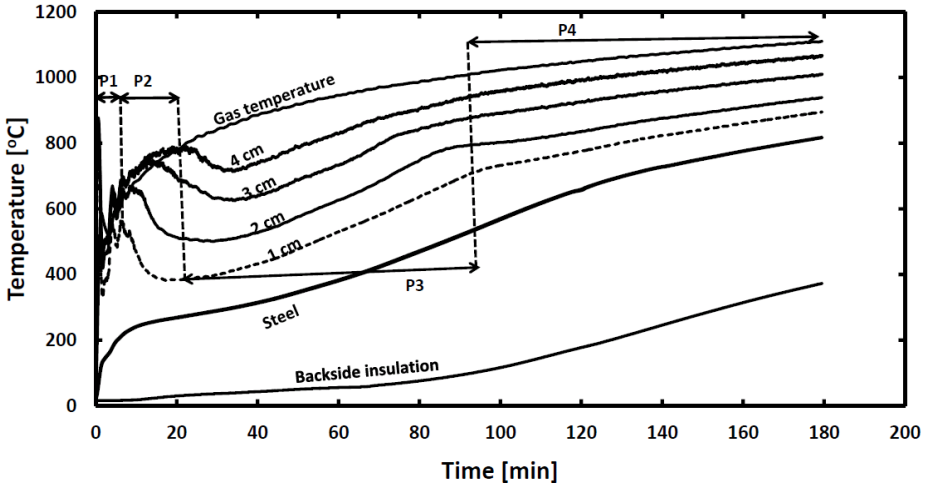

Figure 3.5. Measured temperatures for an experiment with a 1200 µm thick intumescent coating. For the thermocouple placed 1 cm above the steel substrate, the temperature-time curve is divided into four time periods, termed P1-4. Temperatures of the gas, the backside insulation, the steel substrate and various positions above the steel substrate are also shown.

In Figures 3.6 and 3.7, repetitions of the two furnace experiments employing an initial coating thickness of 1200 µm and 2000 µm, respectively, are compared. An excellent agreement is evident for all temperatures, except at positions farthest away from the steel substrate (3 and 4 cm), where the arrival, to the immobilized thermocouples, of the expanding char (and subsequent development of an irregular surface) is bound to be more uncertain. For the experiments with a 2000 µm coating, the repeatability at 3 cm, is, however, also quite good. The backside insulation temperature shows quite some variation between the experiments. This can be attributed to practical challenges of keeping the thermocouple immobilized at the right position when closing the furnace opening prior to initiation of an experiment. Consequently, this temperature reading is less reliable than the other measurements.

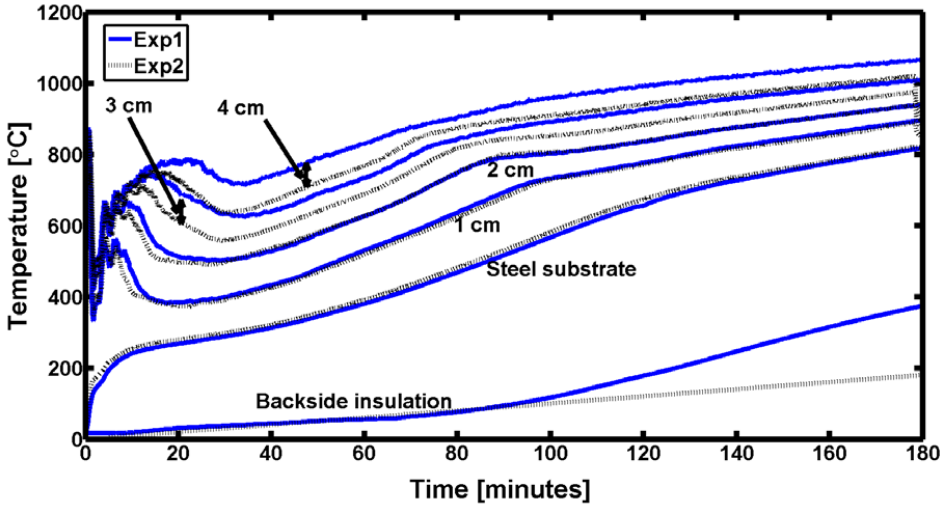

Figure 3.6. Example of the repeatability of experiments conducted in the furnace. The figure shows a comparison of temperatures for the two experiments (referred to as exp1 and 2) employing a coating thickness of 1200 µm.

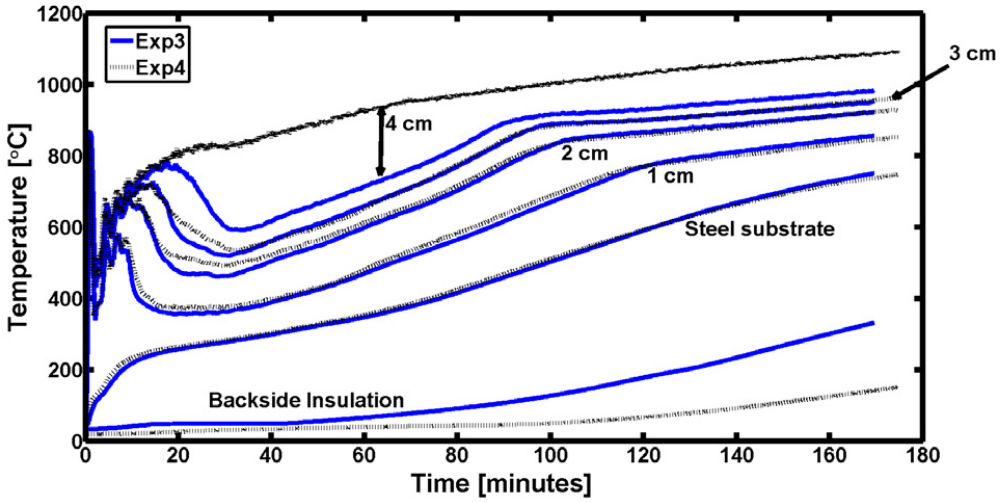

Figure 3.7. Example of the repeatability of experiments conducted in the furnace. The figure shows a comparison of temperatures for the two experiments (referred to as exp3 and 4) employing a coating thickness of 2000 µm.

In Figure 3.8, all indirect char expansion measurements, conducted using the thermocouples in the furnace, are shown. A reasonably good repeatability can be seen, especially at short times of experimentation. The rate and extent of expansion are fairly similar for the two initial coating thicknesses. Shi and Chew[4] pointed out the repeatability of expansion measurements as being particular challenging. Note, that the entire expansion takes place in the first 20-30 minutes of the experiments. The final thickness measured after 3 hours and cooling to room temperature was about 4.5 cm at the center where the thermocouples are placed. One experiment showed an expansion of about 5.5 cm. It is noted that these measurements, at room temperature, due to the irregular surfaces, are subject to some uncertainty.

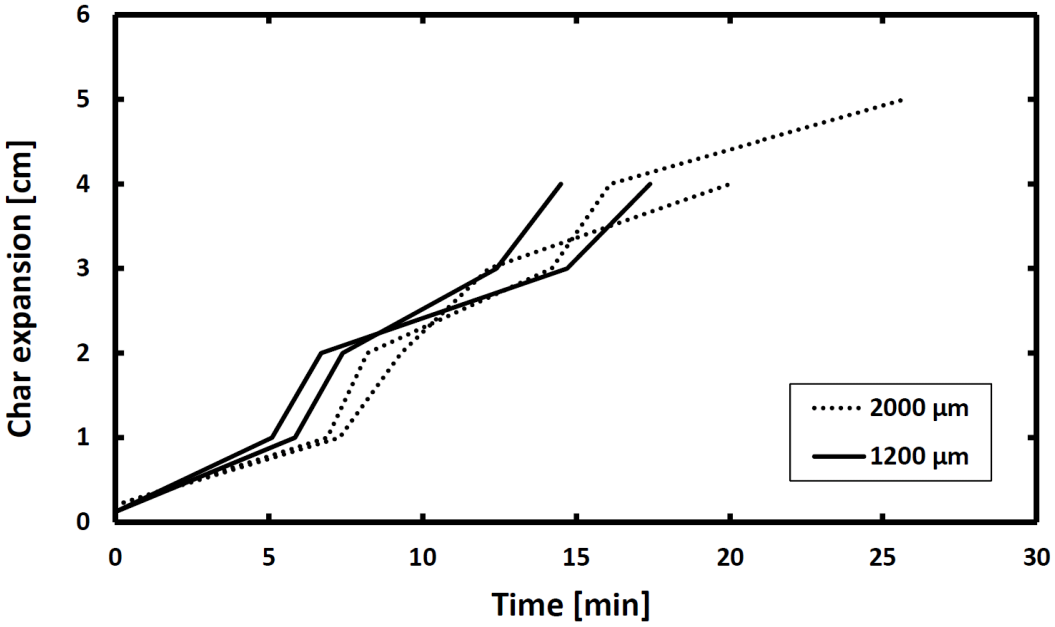

Figure 3.8. Measured values of char thickness as a function of time for two initial coating thicknesses. In total, four independent measurement series are shown, two for each coating thickness. Measurements were only possible at discrete points in time (i.e. when the individual thermocouples were covered by the expanding char layer).

Model simulations

As mentioned in an earlier paragraph, it is of practical importance to develop engineering models of a low degree of complexity. Simulations with the model derived earlier are now presented in the following.

A plot of the heat transfer coefficient calculated for two hours is seen in Figure 3.9. In the first minute the value drops from 500 $W \cdot m^{-2} \cdot K^{-1}$ and afterwards it becomes stable with an average value of 34 $W \cdot m^{-2} \cdot K^{-1}$. This value is used in the following simulations. The high value in the

beginning of the experiment is due to the rapid increase of the gas temperature and the oscillations seen in Figure 3.9 are due to the polynomial data fitting.

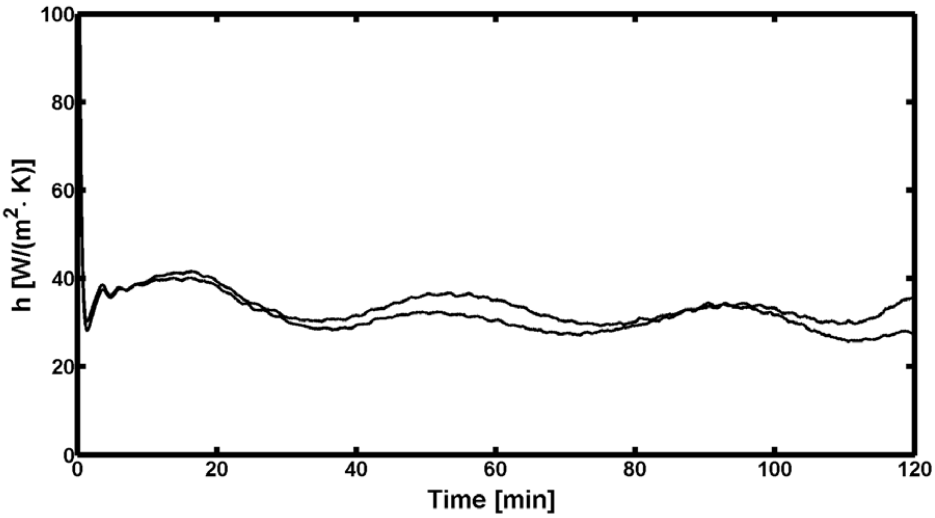

Figure 3.9. Heat transfer coefficient determined for two hours in experiments with uncoated steel. Each line represents an experiment. The initial value of h is 500 $W \cdot m^{-2} \cdot K^{-1}$ but the y-axis is scaled to ease the reading throughout the experiment.

In Figures 3.10 and 3.11, simulations are compared to the experimental data series for an initial coating thickness of 1200 µm. Adjustable parameters used in the simulations for the char expansion (k_0 and E_a), for the temperature-time development ($d_{\epsilon,carb,char}$, $d_{\epsilon,residue}$, β, k_{300}), and the decomposition front movement ($t_{63\%}$), are provided in Table 3.3. There is a very good agreement between simulations and experimental char expansion data. For the temperature curves, a good qualitative agreement, capturing most of the behavior, is evident, in particular for the steel substrate and at the positions 1 and 2 cm. However, in the upper parts of the char layer, at positions 3 and 4 cm, the time to coverage of the thermocouples are very uncertain and this is

reflected in the poor agreement. Additionally, the temperature difference between simulated and experimental results after coverage of the thermocouples is due to the uncertainty in expansion measurements and simulated steel temperature. There is also some deviation for the temperature inside the back side insulation material, but, due to the large uncertainty of this particular measurement, this is of less importance.

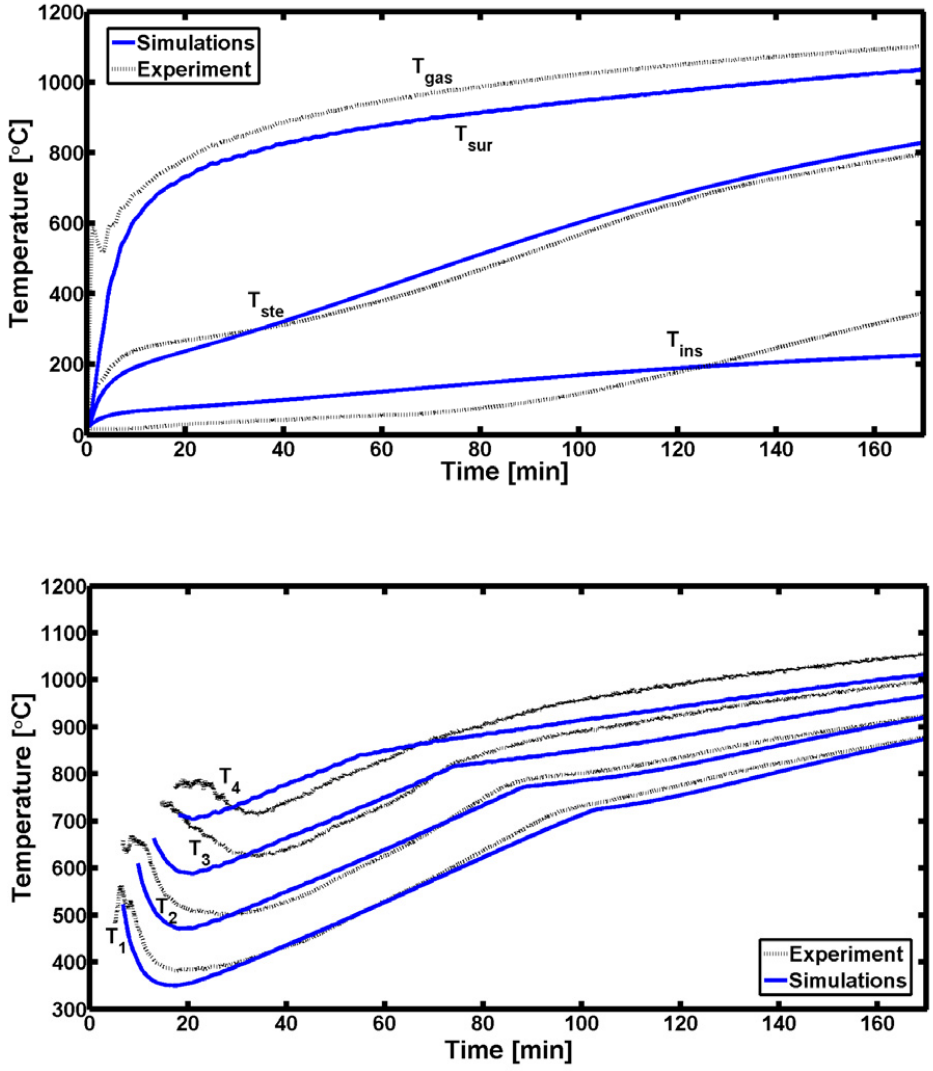

Figure 3.10. Simulated and experimental temperatures for an experiment with a coating thickness of 1200 µm. (TOP) Backside insulation temperature, steel temperature, calculated surface temperature, and measured gas temperature. (BOTTOM) Temperatures inside the char layer.

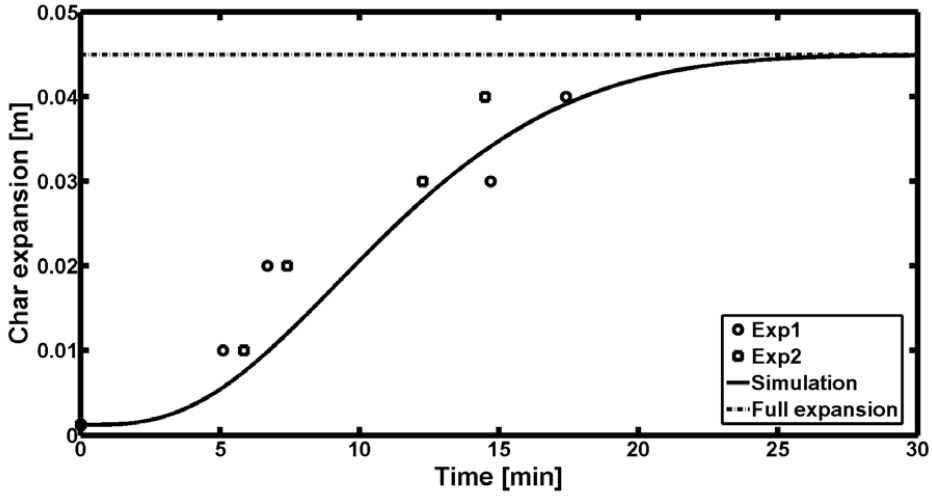

Figure 3.11. Experimental and simulated expansion-time behavior for a coating of thickness 1200 µm. Exp1 and 2 refers to repetitions of the same experiment.

In Figures 3.12 and 3.13, simulations and experimental data for an experiment with initial coating thickness of 2000 µm are shown. The adjustable parameters are provided in Table 3.3. Similarly to the experiments with a 1200 µm coating, the best fits are obtained close to the steel plate where the experimental repeatability was also the best. The moving decomposition front starts about 20 minutes later than in the 1200 µm experiments. In summary, it is possible to get a reasonably good description of the coating behavior using a single overall reaction for the char expansion coupled with a simple expression for a decomposition front and an energy balance of the steel substrate.

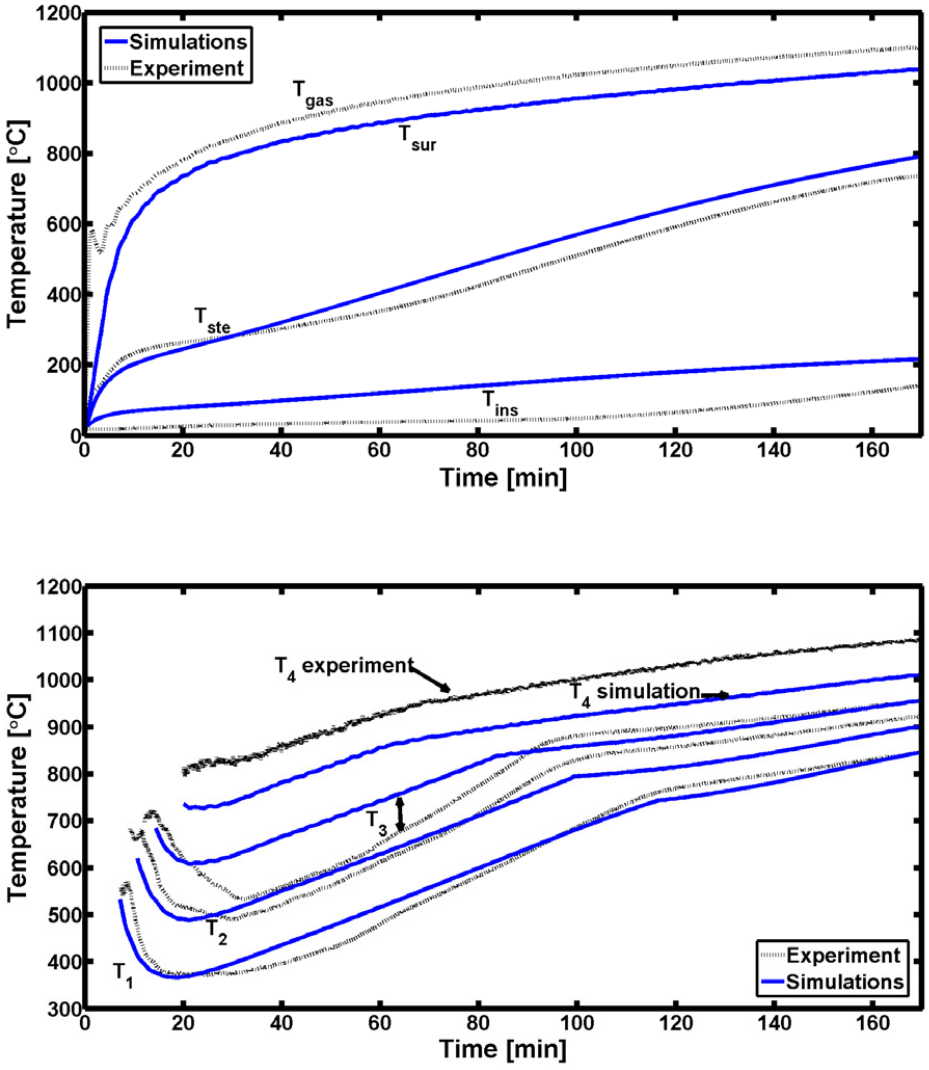

Figure 3.12. Simulated and experimental temperatures for an experiment with a coating thickness of 2000 µm. (TOP) Backside insulation temperature, steel temperature, calculated surface temperature, and measured gas temperature. (BOTTOM) Temperatures inside the char layer.

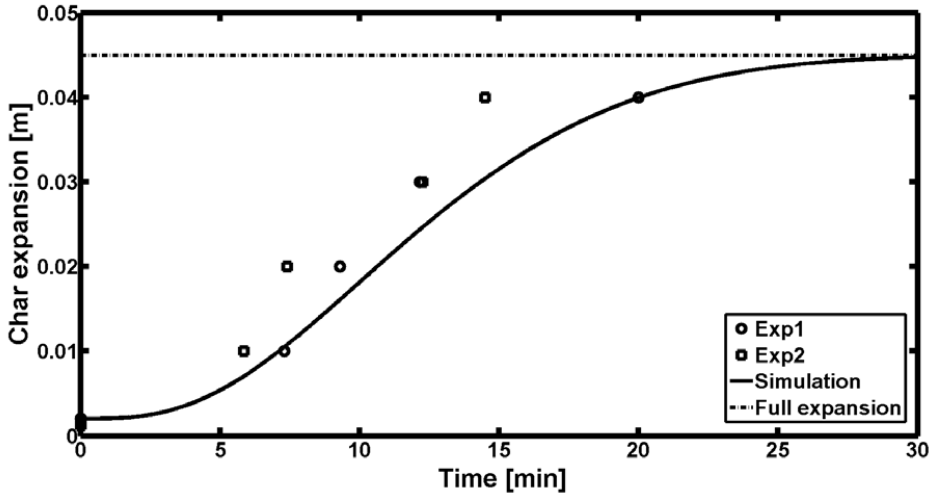

Figure 3.13. Experimental and simulated expansion-time behavior for a coating of thickness 2000 µm. Exp3 and 4 refers to repetitions of the same experiment.

The simulated thickness of the decomposed zone can be observed from Figures 3.10 and 3.12. As an example it is seen from Figure 3.10 that after 55 minutes the decomposition front has moved 0.5 cm away from the surface and after 105 minutes it has moved 3.5 cm away from the surface.

It is noted that the model excludes the heat of reaction(s) and the slope change due to the decomposition front movement only shows up in the simulations because of different thermal conductivity properties in the carbonaceous char and the residue (on each side of the front). The properties used in the simulations are close to those of air due to the high porosity of the char. During the model development, heat of carbon oxidation was also included. However in the given case this did not lead to significant changes in the temperatures inside the char and the simulations are not described in detail in this work. However, the finding is rather surprising and a few remarks on the topic are given in the following. In an earlier study[5] the oxygen content in the

furnace was calculated to be 1 vol% from a stoichiometric mole balance. Additionally, it was observed visually (cross-section view) from the experiments in the present work that the decomposition front had moved through the entire char after the 3 hours. By implementing an oxygen diffusion-controlled oxidation front[18] it was found that the carbon fraction in the carbonaceous char could maximum be 3 wt.%. This is the maximum mass fraction that would allow the front to move through the char in 3 hours. The heat generated from combustion of this carbon content accounts for 6 % of the total energy transferred to the system. In the simulations, the effect of this energy addition over the 3 hours of experiments becomes insignificant because the increased temperature leads to reduced heat transfer from the gas into the expanded coating. Therefore it can be concluded that the heat of reaction does not have a significant influence on the steel temperature in the experiments.

As a final note, the model use as input the post heated char expansion, which was one of the main critiques of current models pointed out by Griffin [6]. However, several data points, sampled during the experiments at different values of time, were used to validate the char expansion rate, thereby not relying on the post heated expansion only.

3.10 Sensitivity analysis of model simulations

A sensitivity analysis of the model with respect to the adjustable parameters was performed under the conditions of Figure 3.10 with a 1200 µm experiment (termed base case). The parameters E_a, k_0, $d_{\epsilon,carb,char}$, $d_{\epsilon,residue}$, β, k_{300}, and $t_{63\%}$ were reduced to 80% of the values given in Table 3.3. The simulation results of the steel temperature and the temperature 1 cm above the steel plate are seen in Figure 3.14. The parameter $t_{63\%}$ affects the time of the onset of the characteristic slope

change and the main effect is seen in the simulations of the temperature 1 cm above the steel plate. From the simulations the effect of the four parameters describing the thermal conductivity is small. This is because these parameters describe the thermal conductivity of the solid and the heat transfer due to radiation. At low temperatures the main contribution to the thermal conductivity is from the gas inside the char. As well the high porosity of the char makes the contribution of heat transfer through the solid insignificant. Therefore the simulations suggest that the radiation part may be removed from the expression of the thermal conductivity, which has also previously been used in models of intumescent coatings[24]. In addition this shows that the slope change between P3 and P4 is mainly due to the different temperatures on each side of the moving front which causes different values of $k_{residue}$ and $k_{carb,char}$.

The parameters affecting expansion are seen to have a large influence on the temperatures.

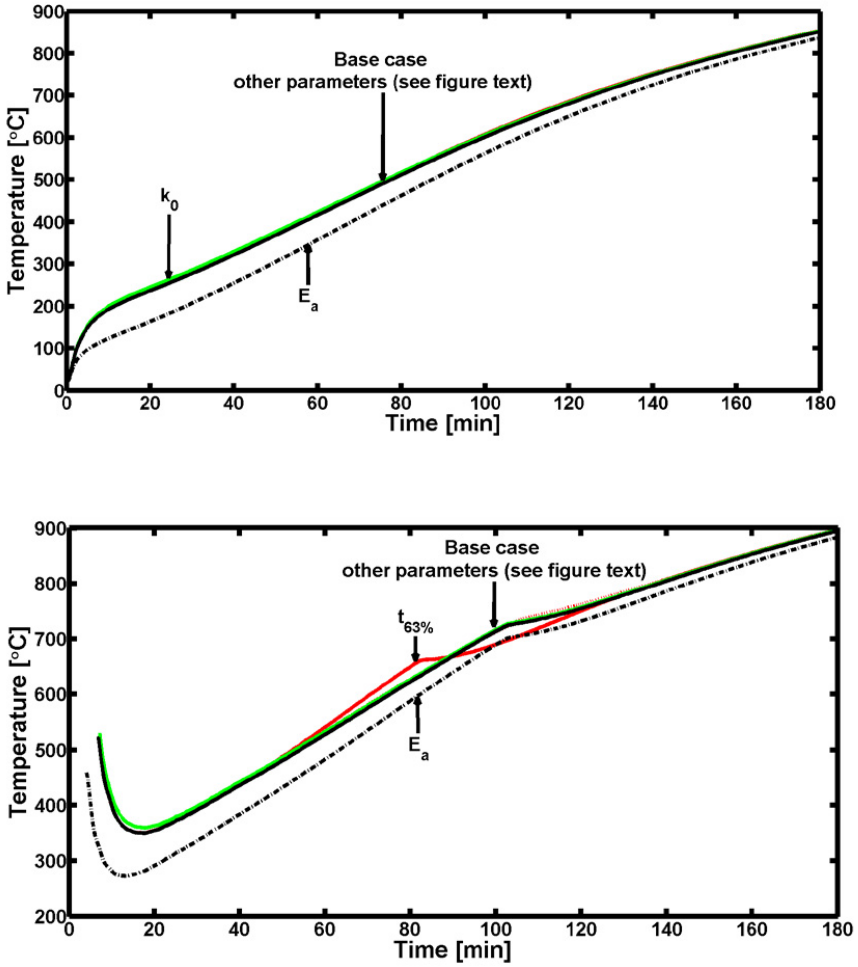

Figure 3.14. Simulated changes by varying the adjustable parameters, E_a, k_0, $d_{\epsilon,carb,char}$, $d_{\epsilon,residue}$, β, k_{300}, and $t_{63\%}$. The values are reduced to 80% of the value given in Table 3.3. (TOP) Simulation of steel temperature. (BOTTOM) Simulation of temperatures 1 cm above the steel plate. For the steel temperature only the effect of changing E_a and k_0 are clearly observed in the graphs. For the temperature inside the $t_{63\%}$ and E_a are the most clearly observable parameters. Changes form the other parameters are below 20 °C. β and k_{300} does not affect the temperatures noticeably.

3.11 Parameter study

The validated model was also used to study the influence of selected process parameters, namely the thickness of the steel and the gas temperature. These parameters were increased by 10 % and Figure 3.15 shows the effect on the steel temperature and the temperature 1 cm inside the char. The changes in these two parameters show increasing effect over time, and for a time period of approximately 15 minutes the effect is almost non-existent. This is because the expansion is affected by the temperatures and a reduced gas temperature leads to a slower expansion which then increases the heat transfer to the steel. The same effects are observed 1 cm inside the char.

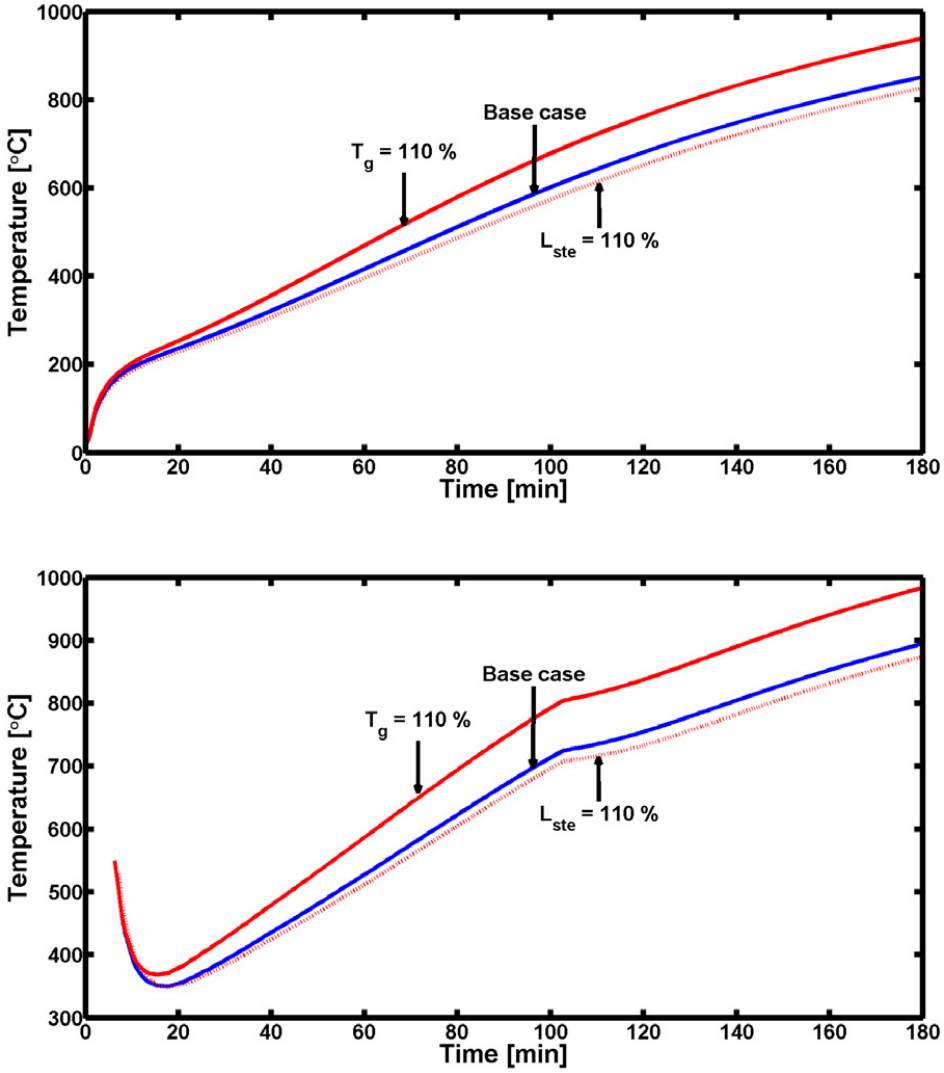

Figure 3.15. Parameter study where the mass of steel and gas temperature have been. The base case simulation with parameters from Table 3.3 is also shown. (TOP) Simulations of the steel temperature. (BOTTOM) simulations of temperatures 1 cm above the steel plate.

3.12 Evaluation of adjustable parameters

An advantage of the model presented in this work is that it requires only two adjustable input parameters related to the char expansion (E_a and k_0), four for char insulation properties ($d_{\epsilon,carb,char}$, $d_{\epsilon,residue}$, β, k_{300}), and one related to the decomposition front ($t_{63\%}$). However, the evaluation showed that the two parameters related to the skeletal thermal conductivity (β, k_{300}) do not influence the results significantly. Therefore in principle five adjustable parameters can be used. In the following, a discussion of the adjustable parameters used in the model is provided and values are compared with data from literature sources. A summary of the adjustable model parameters is provided in Table 3.3.

Arrhenius parameters for expansion reaction

The fitted value of the pre-exponential factor, k_0, is 10 and 15 s^{-1}, and is considered realistic. Pre-exponential factors for expansion reactions can vary significantly, for instance in the study by Caglostro et al.[26], values in the range from five to $6.9 \cdot 10^5$ s^{-1} were found, and Griffin[6] reported values of 71 to $1.7 \cdot 10^5$ s^{-1} for the melting and intumescence reactions, which were used to describe the expansion process.

The activation energies used in the studies by Caglostro et al.[26] are between 53 and 93 kJ · mol^{-1}. Similarly, Griffin found values for the melting and intumescence reaction to be in the range of 39 to 95 kJ · mol^{-1}, which are close to the 34 kJ · mol^{-1} used in this study.

Char insulation properties

In this work a temperature dependency of the thermal conductivity of char developed by Di Blasi and Branca[24] especially for intumescent coatings has been used. It consists of a part describing the conduction and a part describing the radiative heat transfer. However, the value of the radiation

part is relatively small and at temperatures below 500 °C, the thermal conductivity of the char is almost identical to that of air. This can be seen from Figure 3.16 where values from literature are compared to the values used in this work. The difference between the reported values may originate from both the method of investigation and the coating formulations used.

Decomposition front

Although the exact value of $t_{63\%}$ describing the decomposition front is difficult to validate, a short discussion of the mechanism is given in the following. The parameters are fitted according to Avrami[19] kinetics which are similar to Prout-Tompkins models[18, 27]. This model has been used for the study of biomass degradation[28]. The mechanism also explains why the front starts moving at a late stage in the experiments because the phosphorous ester has to decompose before oxidation occurs. Additionally, some earlier research supports that oxygen diffusion is not the limiting mechanism of the oxidation. This can be seen from the following deduction. In our earlier research on primers for intumescent coatings it was shown experimentally that the primer is exposed to oxygen after 22 minutes in the furnace. This corresponds to a steel temperature of 300 °C[5] and is significantly earlier than the decomposition front reaches the steel plate in the experiments used for model validation. Additionally, Griffin et al.[7] determined that the thermo gravimetric behavior of intumescent coatings is independent of oxygen content in the gas at temperatures up to 540 °C. This is similar to the 600 °C where reaction (3-6) (decomposition of the phosphorous ester) is reported to initiate. Examination of Figures 6 and 7 shows that the change between P3 and P4 does not take place at temperatures below 550 °C. Based on the temperatures described in this paragraph it is therefore concluded that oxygen is present at the steel plate and at a lower temperature than the one at which the decomposition front initiates. Therefore diffusion of

oxygen is not the rate limiting mechanism and the front does not move before decomposition of the phosphorous ester has occurred.

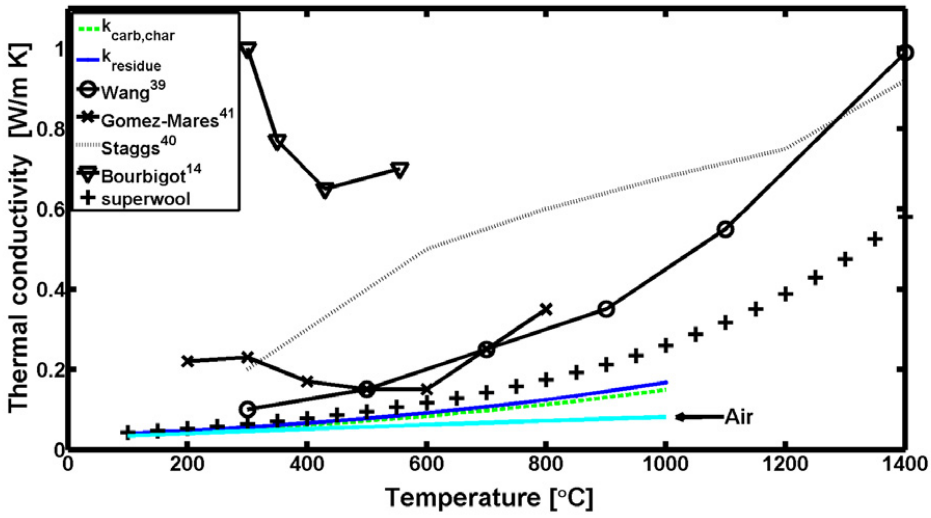

Figure 3.16. Thermal conductivity of chars as a function of temperature. Data from literature are presented for comparison. Wang et al.[39] (non-disclosed coating system) is based on image analysis of the char and validated against steel temperatures in a furnace. Bourbigot et al.[14] (polypropylene system) determined on pre-heated samples, values obtained from modeling. Staggs[40] (non-disclosed coating system) determined thermal conductivity from image analysis of char and thermal resistor network. Gomez-Mares et al.[41] (epoxy system) used muffle furnace and hot disk. Thermal conductivity of the backside superwool insulation and the value of this work are also included. The thermal conductivity of air is also shown. The simulated value of this work refers to the arithmetic average temperature of the steel and char surface temperature.

3.13 Validation of model assumptions

A number of assumptions are underlying the model development. The most important of these are discussed here.

Shrinkage of the char was assumed to be negligible. Although this assumption cannot be completely verified none of the covered thermocouples were later uncovered. Therefore, any degree of shrinkage would be very low.

It was assumed that the char expansion can be described by a single first order reaction. This is obviously not correct as the expansion is the combination of at least three chemical reactions[5], but the assumption was included to keep the number of adjustable parameters low. Results presented show that the expansion can be properly described this way, but the effects of formulation variables are only expressed indirectly.

Convection inside the pores in the char is neglected. This is supported by Kantorovich and Bar-Ziv's review on heat transfer in porous chars, in which it is mentioned that for pores less than 1 cm in porous chars, heat transfer due to convection can usually be neglected[29].

The char was considered intact at all times and effects of surface cracks neglected. This was verified by inspecting the chars after heating. Also, damages in the char, for instance due to primer failure, can easily be observed from the temperature profiles, as shown in our earlier work[5].

Another assumption is that the radiation from the furnace walls is neglected. Although this cannot be completely verified, work by Staggs[30] on steel beams coated with high and low (non-intumescent) emissivity coatings in a furnace show that the heat transfer contribution of radiation is small.

3.14 Conclusions

A mathematical model, describing the behavior of an intumescent coating on a steel substrate exposed to heating in a cellulosic type fire, was developed. The most relevant phenomena, char

formation, expansion and oxidation, and subsequent transient developments in char, steel substrate, and backside insulation temperatures were included. Experimental data series obtained in a pilot-scale, gas-fired furnace were used for model validation. A good qualitative agreement between simulations and experiments was found using two adjustable parameters for the char expansion, four for the temperature-time behavior and one for the decomposition front movement. The four adjustable parameters for the char insulation properties describing, radiation and conduction through solid, are of little influence on the results. This suggests that the main influencing parameter in the given coating is heat transfer through the gas phase. However in other coatings with lower porosity the other parameters may be more significant. An important outcome of the investigation is a documentation of the necessity to measure temperatures inside the expanding char layer when validating mathematical models. If only the steel substrate temperature and the char expansion are measured, it is rather easy to get a good quantitative match of simulations and experimental data. Supplementing with intra-char temperatures provide a much more challenging set of data, useful for mapping of important mechanisms. A limitation of the present model is that specific details on the coating formulation are not directly expressed, only macroscopic properties, such as pore size and degree and rate of expansion, reflect the formulation.

The model developed is sufficiently simple (ordinary differential equations) and relies on a low number of input and adjustable parameters, giving it potential as an engineering tool that can be used for practical pilot-scale evaluation of intumescent coatings. Future work should involve an extension to other coating formulations for cellulosic fires, as well as an adaptation to coatings for hydrocarbon fires with very high heating rates (room temperature to 1100 °C in about 5 min), substantially higher than for cellulosic fires (room temperature to 1100 °C in about three hours).

Furthermore, the proposed decomposition-oxidation mechanism needs to be chemically confirmed.

References

[1] Bourbigot S, Le Bras M, Duquesne S, et al. Recent advances for intumescent polymers. *Macromolecular Materials and Engineering* 2004; 289: 499-511.

[2] Weil ED. Fire-Protective and Flame-Retardant Coatings-A State-of-the-Art Review. *J Fire Sci* 2011; 29: 259-296.

[3] Bourbigot S and Duquesne S. Fire retardant polymers: recent developments and opportunities. *J.Mater.Chem.* 2007; 17: 2283-2300.

[4] Shi L and Chew MYL. A review of fire processes modeling of combustible materials under external heat flux. *Fuel* 2013; 106: 30-50.

[5] Nørgaard KP, Dam-Johansen K, Català P, et al. Laboratory and gas-fired furnace performance tests of epoxy primers for intumescent coatings. *Prog Org coat* 2014; 77: 1577-1584.

[6] Griffin G. The Modeling of Heat Transfer across Intumescent Polymer Coatings. *J Fire Sci* 2010; 28: 249-277.

[7] Griffin GJ, Bicknell AD and Brown TJ. Studies on the effect of atmospheric oxygen content on the thermal resistance of intumescent, fire-retardant coatings. *J Fire Sci* 2005; 23: 303-328.

[8] Jimenez M, Duquesne S and Bourbigot S. Multiscale experimental approach for developing high-performance intumescent coatings. *Ind Eng Chem Res* 2006; 45: 4500-4508.

[9] Jimenez M, Duquesne S and Bourbigot S. High-throughput fire testing for intumescent coatings. *Ind Eng Chem Res* 2006; 45: 7475-7481.

[10] van Hees P, Andersson P, Hjohlman M, et al. Use of the Cone Calorimeter and ConeTools software for development of innovative intumescing graphite systems. *Fire Mater* 2010; 34: 367-384.

[11] Zhang F, Zhang J and Wang Y. Modeling study on the combustion of intumescent fire-retardant polypropylene. *Express Polymer Letters* 2007; 1: 157-165.

[12] Butler KM. Physical modeling of intumescent fire retardant polymers *ACS Symposium Series*, 1997, p.214.

[13] Mamleev VS, Bekturov EA and Gibov KM. Dynamics of intumescence of fire-retardant polymeric materials. *J Appl Polym Sci* 1998; 70: 1523-1542.

[14] Bourbigot S, Duquesne S and Leroy JM. Modeling of heat transfer of a polypropylene-based intumescent system during combustion. *J Fire Sci* 1999; 17: 42.

[15] Nicholas J, White DR and Wiley J. *Traceable temperatures: an introduction to temperature measurement and calibration.* Wiley, 2001.

]16] Horacek H. Reactions of stoichiometric intumescent paints. *J Appl Polym Sci* 2009; 113: 1745-1756.

[17] Khawam A and Flanagan DR. Solid-state kinetic models: Basics and mathematical fundamentals. *J Phys Chem B* 2006; 110: 17315-17328.

[18] Levenspiel O. *The Chemical reactor omnibook.* OSU, 1993.

[19] Avrami M. Kinetics of phase change. II. Transformation-time relations for random distribution of nuclei. *J Chem Phys* 1940; 8: 212-224.

[20] Brown ME. The Prout-Tompkins rate equation in solid-state kinetics. *THERMOCHIMICA ACTA* 1997; 300: 93-106.

[21] Mills AF. *Heat Transfer / International Student Edition.* IRWIN, 1992.

[22] http://ereader.morgantechnicalceramics.com/emags/european_product_databook_080911/print/print.pdf 18.02.2014.

[23] Incropera FP and DeWitt DP. *Introduction to heat transfer.* Wiley, 1990.

[24] Di Blasi C and Branca C. Mathematical model for the nonsteady decomposition of intumescent coatings. *AICHE J* 2001; 47: 2359-2370.

[25] Palankovski V. *Simulation of Heterojuncion Bipolar Transistors*Dissertation Technical University of Wien, 2000.

[26] Cagliostro D, Riccitiello S, Clark K, et al. Intumescent coating modeling. *J Fire & Flammability* 1975; 6: 205-222.

[27] Prout EG and Tompkins FC. The thermal decomposition of potassium permanganate. *Transactions of the Faraday Society* 1944; 40: 488-498.

[28] Garcia Barneto A, Ariza Carmona J, Martin Alfonso JE, et al. Simulation of the thermogravimetry analysis of three non-wood pulps. *Bioresour Technol* 2010; 101: 3220-3229.

[29] Kantorovich II and Bar-Ziv E. Heat transfer within highly porous chars: a review. *Fuel* 1999; 78: 279-299.

[30] Staggs JEJ and Phylaktou HN. The effects of emissivity on the performance of steel in furnace tests. *Fire Saf J* 2008; 43: 1-10.

[31] Stoliarov SI, Crowley S, Walters RN, et al. Prediction of the burning rates of charring polymers. *Combust Flame* 2010; 157: 2024-2034.

[32] Lautenberger C and Fernandez-Pello C. Generalized pyrolysis model for combustible solids. *Fire Saf J* 2009; 44: 819-839.

[33] Farkas E, Meszena Z, Toldy A, et al. Modelling of transport processes in a developing char. *Polym Degrad Stab* 2008; 93: 1205-1213.

[34] Bai Y, Vallée T and Keller T. Modeling of thermal responses for FRP composites under elevated and high temperatures. *Composites Sci Technol* 2008; 68: 47-56.

[35] Bai Y and Keller T. Time dependence of material properties of FRP composites in fire. *J Composite Mater* 2009; 43: 2469.

[36] Feih S, Mathys Z, Gibson A, et al. Modelling the compression strength of polymer laminates in fire. *Composites Part A: Applied Science and Manufacturing* 2007; 38: 2354-2365.

[37] Trelles J and Lattimer BY. Modelling thermal degradation of composite materials. *Fire Mater* 2007; 31: 147-171.

[38] Bahramian AR, Kokabi M, Famili MHN, et al. Ablation and thermal degradation behaviour of a composite based on resol type phenolic resin: Process modeling and experimental. *Polymer* 2006; 47: 3661-3673.

[39] Wang L, Wang Y, Yuan J, et al. Thermal conductivity of intumescent coating char after accelerated aging. *Fire Mater* 2013; 37: 440-456.

[40] Staggs JEJ. Thermal conductivity estimates of intumescent chars by direct numerical simulation. *Fire Saf J* 2010; 45: 228-237.

[41] Gomez-Mares M, Tugnoli A, Landucci G, et al. Behavior of intumescent epoxy resins in fireproofing applications. *J Anal Appl Pyrolysis* 2012; 97: 99-108.

Chapter 4 - Investigation of char strength and expansion properties of an intumescent coating exposed to rapid heating rates

This chapter was published with the title “Investigation of char strength and expansion properties of an intumescent coating exposed to rapid heating rates” in Progress in Organic Coatings 76 (2013) 1851-1857. (authors Kristian Petersen Nørgaard, Kim Dam-Johansen Pere Català and Søren Kiil).

4.1 Nomenclature

W_{90}	-	Work to reach 90 % of the distance into the sample, J
Vertical expansion factor	-	Final height divide by initial dry film thickness, -
W_{Dist}	-	Work divided by the distance (average force), N
W_{1mm}	-	Work to destroy the first 1 mm, J
Work of destruction	-	Accumulated work measured by piston to reach a certain position, J
Subscript		
des	-	Samples stored in desiccator

4.2 Abstract

An efficient and space saving method for passive fire protection is the use of intumescent coatings, which swell when exposed to heat, forming an insulating char layer on top of the virgin coating. Although the temperature curves related to so-called cellulosic fires are often referred to as slow heating curves, special cases where the protective char is mechanically damaged and partly removed can cause extremely fast heating of the coating. This situation, for a solvent based intumescent coating, is simulated using direct insertion of free films into a muffle oven. The char formed is evaluated with respect to the mechanical resistance against compression, degree of

expansion, and residual mass fraction. Experimental results show that when using this type of shock heating, the mechanical resistance of the char against compression cannot meaningfully be correlated to the expansion factor. In addition, char properties, measured at room temperature, were dependent on the preceding storage conditions (in air or in a desiccator). The char was found to have the highest mechanical strength against compression in the outer crust facing the heat source. For thin (147 μm) free coating films, a tendency to contract in the horizontal plane was observed. The experimental approach is relevant for testing of intumescent coatings used in buildings where moving or falling objects may damage the char during a fire.

4.3 Introduction

Intumescent fire protective coatings expand when exposed to a sufficiently high temperature (e.g. in a fire). The expanded coating forms a porous char that thermally insulates the underlying steel substrate and establishes a protective barrier against oxygen. This is important during fires because at temperatures above 500 ^{o}C steel loses its mechanical strength to a degree where collapse of the steel structure may occur with potential loss of lifes or assets. The insulating char prolongs the time, often by more than 2 hours, before this critical temperature is reached. Therefore, research on intumescent coatings is reported to have flourished since the collapse of the World Trade Center in 2001[1]. It is common to distinguish between coatings suitable for fast and slow heating curves, so-called hydrocarbon and cellulosic fires, respectively. However, in special cases, which may arise during a fire, coatings intended for cellulosic fires can be exposed to very fast heating rates. One such case could be that the char is damaged by falling objects, e.g. building elements, at a point in time where the gas temperature is at a high level. This is illustrated in Figure 4.1. The underlying, non-swelled, residual coating is then suddenly exposed to a very rapid heating rate. When a frequently used fire curve, the ISO 834 time-temperature curve, describing cellulosic fires, is assumed valid then the temperature of the gas will be close to 1100 ^{o}C after 2 hours[2].

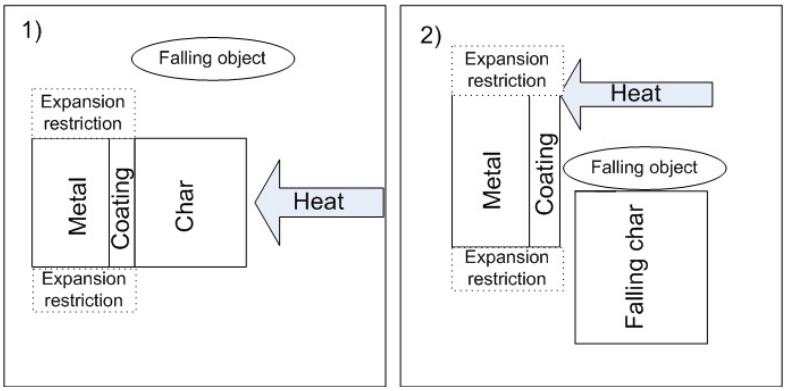

Figure 4.1. Schematic illustration of the special case where the coating/char is damaged due to a falling object. Picture 1 shows the situation before the object hits the char and picture 2 shows how "intact" coating is exposed by the falling object. The coating may be spatially restricted from the sides or have free expansion possibilities as indicated.

Intumescent coatings are often evaluated based on expensive full-scale tests[3]. To predict the performance of coatings for hydrocarbon fires in full-scale tests, a study with the aim of correlating results from laboratory experiments to full-scale tests, was carried out by Jimenez et al.[4]. It was found that one of the essential parameters was the mechanical strength against compression measured after heating to 500 ^{o}C at a heating rate of 10 ^{o}C/min in a thermal scanning rheometer. The mechanical stability was measured by letting the coating expand freely and then compress while recording the resisting force. Other methods to investigate the mechanical strength of intumescent chars are discussed in references[5, 6, 7]. Reshetnikov et al.[5] and Berlin et al.[6] investigated variations in expansion and mechanical stability for different intumescent compounds (e.g. sorbitol and ammonium polyphosphate). In Reshetnikov et. al.[7], various equipments to measure mechanical strength at high temperatures are described. One method finds the minimum force necessary to destroy the char by inserting a rod through the heated sample at temperatures up to 1200 ^{o}C. Another method, in which the gas temperature is 3000 ^{o}C, is used to measure the shear strength of the char. The principle is to spin the sample at a controlled rate (1000 rounds/min), until the char breaks at the weakest point, and then the mass of the detached char can be used to find the shear strength of the char. A complication to the method is that the gas flow (2 m/s) adds to the destructive force, which complicates the investigation of "weak" chars due to the additional destructive force. Both of these high

temperature techniques are reported only to perform well at low expansion factors (1.5 - 2). Another frequently used method is the thermomechanical analysis. This is for example used to test different intumescent formulations on powder form for volume expansion upon heating of a sample[8]. Other aspects of mechanical stability are those related to the coating before heat exposure. Examples are tensile strength (break strength), flexural strength (bending strength) or impact strength, as for example described in Li and Xu.[9]. The above methods related to mechanical stability do not consider the use of shock heating. In this work, the mechanical stability, mass loss, and degree of expansion of chars, produced by shock heating to 1100 ^{o}C, are investigated. The results presented represent a continuation of the preliminary work presented in popular form in Nørgaard et al.[10] (addressed in Chapter 5), where effects of gas composition, residence time, and position in the horizontal plane on mechanical stability of the first 1 mm of the chars were explored. Effects of physical restrictions against sidewards expansion, film thickness, and small changes in the heating rate are also studied in the present work. The investigation is important for intumescent coatings applied where objects may fall down on the coating during a fire and damage the char. Requirements to screening tests may also demand shorter residence times, where no heat up time is required leading to a higher throughput. Therefore, investigation of the char behavior under these conditions is important. Furthermore, restricted expansion is also of interest for coatings used in corners and bends, as well as when cracks occur in the coating. The problem with cracks is mentioned as a short coming to intumescent coatings by Weil[11]. The methods used in the present study should not be confused with previous investigations, where the mechanical properties of the melted phase, (i.e. viscoelastic properties) are investigated as for instance in Le Bras et al.[12].

4.4 Strategy of investigation

The purpose of this paper is to investigate how four potentially important parameters, for a coating exposed to the conditions illustrated in Figure 4.1, affect the char expansion, mass loss, and mechanical resistance against compression. The parameters of interest are: 1) heating rate, simulation of small variations in this parameter, 2) crucible size, to investigate the effect of conditions of free sidewards expansion versus restricted expansion, 3) initial dry film thickness, 4)

changes in char strength due to air (moisture) exposure following the complete heating up and cooling down. The fast heating rate is assumed to occur because the outer char layer is suddenly removed, as illustrated in Figure 4.1. The residual coating is assumed to be identical to the initial coating. Following this damage, an underlying layer of intumescent coating, having a lower temperature, is exposed. One factor at a time variation is used in the investigation. A very rapid heating rate of the coating is obtained by direct insertion of a free film into a hot oven. After heating and subsequent cooling the mechanical stability of the coating is measured with a Texture Analyzer recording the work necessary to move a cylindrical piston to a certain depth of the char. Comparison of samples exposed to moisture is done by moving some samples to a desiccator after heating.

4.5 Experimental procedures

Sample preparation

A generic solvent-based acrylic intumescent coating was selected for the investigation. The coating contains the usual intumescent compounds - blowing agent, TiO_2 pigmentation, carbon- and acid sources which provide the intumescence. The coatings used for the experiments were all taken from the same batch. Samples of the coating were prepared by drawdown using a CoatMaster 509 MC from Erichsen. The samples were prepared on conventional overhead transparencies, with draw down velocity of 10 mm/s. The area of the overhead transparencies was 210x297 mm^2. After curing, the film could easily be detached from the overhead transparencies. Wet film thicknesses of 300 and 1000 µm were used. The samples were dried for at least 72 hours before use. To investigate the drying behavior, samples of the coating and substrate were placed on scales (ScoutTM Pro) in a fume cupboard and the mass was continuously logged every minute for 60 hours. To avoid fluctuations, due to air flow, the scales were partly covered with the concomitant plastic cap and measurements with empty scales for 20 minutes showed fluctuations within ±0.01 g, corresponding to 0.7 % of the initial coating mass. The cured free films were cut using a round sharp metal template with a diameter of 14 mm. Dry film thickness of the coatings was measured using the Texture Analyzer.

Heating – Muffle oven

Samples were heated in a muffle oven (Nabertherm LVT 5/11/180) in atmospheric air. The muffle oven is an electrically heated oven where the heating elements are separated from the oven room. The muffle oven can be opened at the front during operation so samples can be inserted or removed using pliers. The internal dimensions of the muffle oven are 220x175x130 mm^3. The temperature was measured using a K-type which pierces 60 mm into the oven through the back wall, at 20x20 mm^2 from the upper left corner. The crucibles were placed in the hot oven at the center of the bottom plate so that the samples were heated from all sides. A small mark at the center of the bottom of the oven makes it possible to place the samples at the same position in all experiments. Two sizes of cylindrical crucibles, made from alsint and purchased from W. Haldenwagner, were used. Small and large crucibles have inner diameters of 16 and 26 mm and heights of 30 and 40 mm, respectively. Two heating rates from 800 or 900 ^oC to 1100 ^oC, in 400 and 300 seconds, respectively, were used. These are referred to as HR800 and HR900, respectively. All samples were exposed to 1100 ^oC for 10 minutes before they were removed from the oven. After withdrawal of the sample it was placed on an aerated concrete stone next to the muffle oven to cool down. The samples, which were placed in a desiccator, were allowed to cool to 150 ^oC (measured on the inside of the crucible by a probuilder infrared thermometer, Art no. 59441(KC180) before being placed in the desiccator). The masses before and after heating up and cooling down were determined using a Sartorius Scale with an accuracy of 0.1 mg.

The free films prepared were heated in the muffle oven under the conditions shown in Table 4.1. At least 3 repetitions of each sample were conducted. For the samples showing high standard deviations, with respect to mass loss and vertical expansion after three repetitions, additional experiments were conducted without a significant change in the magnitude of the standard deviations. The number of samples repeated is also shown in Table 4.1. Repetitions of sample sets C1 and C6 were performed with the only difference that the samples were placed in a desiccator after cooling (samples $C1_{des}$ and $C6_{des}$).

When the heating experiments are performed, it is important to take appropriate safety measures. For the experiments performed for this article, welding goggles and alumina foiled heat protective gloves were used.

Table 4.1. Summary of samples and conditions. Subscript "des" refers to samples stored in a desiccator.

Coating Sample	Heating rate	Crucible size	DFT [mm]	Number of repetitions
C1	HR900	Large	0.147	4
C2	HR800	Large	0.147	5
C3	HR900	Large	0.598	3
C4	HR900	Small	0.598	4
C5	HR800	Small	0.598	3
C6	HR900	Small	0.147	7
C7	HR800	Small	0.147	4
C8	HR800	Large	0.598	3
$C1_{des}$	HR900	Large	0.147	3
$C6_{des}$	HR900	Small	0.147	3

Measurement of mechanical stability – Texture analyzer

A TA XT plus – Texture Analyzer from Stable Micro Systems Ltd, was used to measure the mechanical strength of the char against compression at room temperature. A cylindrical piston with a diameter of 2 mm was moved through the sample at a constant velocity of 0.1 mm/s. 500 data points of position and force were recorded per second. As the piston is moved, a strain gauge load cell registers the force exerted on the piston from the sample. The trigger force, at which the Texture Analyzer starts registering the sample, was set to 0.00490 N (corresponding to 0.5 g). To ensure that the trigger force was not reached due to external factors, e.g. dust particles or air currents, it was visually confirmed that the trigger force was reached when the piston touched the sample. Prior to the measurements, the instrument was calibrated using the automatic program from the supplier. The work of destruction, in [mJ], to reach a certain position is calculated by multiplying the sum of the observed forces with the distance of each step. An illustration of the system is shown in Figure 4.2. The texture analyzer is also used to find the maximum expansion by lowering the piston close to the top surface of the char and then move the crucible to the position where the sample is closest to the piston. Note, that an important limitation is that the results are obtained at room temperature and not 1100 ^{o}C. Except for the samples stored in a desiccator, the samples were generally produced during weekdays and following storage over the weekend, compression tests were made. When the samples from the desiccator were compressed, a

maximum time of 5 minutes outside the desiccator was allowed before the piston touched the char.

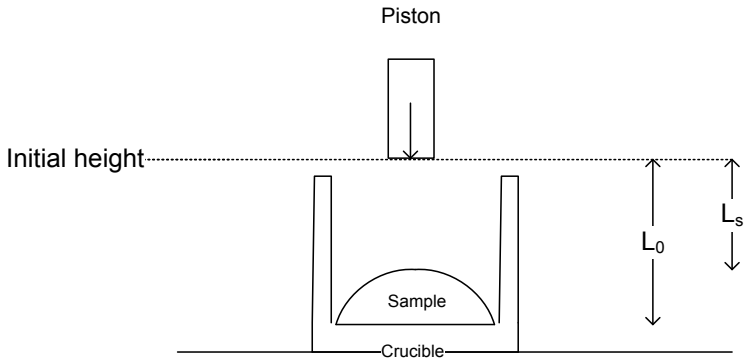

Figure 4.2. Schematic illustration of the Texture Analyzer. L_s and L_0 are the distances to the sample top and sample bottom from a selected initial height, respectively. The height of the sample is the difference given by L_0-L_s.

4.6 Results and Discussion

Solvent content of cured coatings

For thick coating layers above several hundred microns, solvent retention in the lower layers of a coating can cause a range of problems[13]. Due to the high film thicknesses of intumescent coatings, potential solvent retention must be considered. To investigate this, a sample with wet film thicknesses of 1000 µm was followed gravimetrically. A steady state value of the residual mass was reached within 10-15 hours. The solvent retention was found to be no more than 6 wt% of the original solvent content. The dry film thickness of the 300 and 1000 µm coatings was measured at four different places to 147±0 and 598±20 µm, respectively. For the thin film all four measurements showed the same result. It is noted that these film thicknesses are lower than what is used in practice when applying intumescent coatings, where the dry film thickness is typically above 1000 µm. Here, the lower thickness simulates the situation where the expanded char is suddenly removed and "intact" residual intumescent coating exposed as shown in Figure 4.1. In the following, the 147 and 598 µm films are referred to as "thin" and "thick" film coatings,

respectively, not to be confused with the traditional use of these terms, distinguishing between coatings for cellulosic and hydrocarbon fires.

Degree of char expansion

Related to the vertical expansion, a tendency for the thin films (147 µm) to contract horizontally was observed. This horizontal contraction was not observed for the thick films (598 µm). An example of this can be seen in Figure 4.3. A possible explanation for the contraction is that with the sudden increase in temperature, all intumescent reaction steps can happen simultaneously. As an example, the intumescent process of a coating consisting of the typical compounds ammonium polyphosphate, pentaerythritol, and polypropylene has finished char formation at 430 °C[14], which is well below the 800 °C used in this study. If melting and expansion happened at the same time, entrainment (educter) effects, which would carry coating material from the outside into the center of the coating, are possible. Due to the smaller size, the thin films would be more prone to these effects. However, these considerations have not been confirmed.

Figure 4.3. Pictures, looking down in the crucible from above, showing vertical contraction. The inner diameter of the metal ring is the original area of the coating piece. From left the pictures show samples C1 (thin), C6 (thin) and C3 (thick) and C4 (thick).

The average vertical expansion factors, defined as the final height (from substrate to top of char layer) divided by the initial dry film thickness, are seen in Figure 4.4. Comparing the results shown in Figure 4.4, there is not an obvious single factor effect which can be said to influence the vertical expansion factor. In small crucibles, film thickness makes a big difference, where thin films expand much more, relative to the initial coating thickness, than thick films (about 100 % more in this case). For the thin films, a decrease in heating rate shows a reduction in the vertical expansion factor (compare C6 to C7 and C1 to C2), but the effect is not significant because the error bars overlap. These effects are only observed for samples not stored in a desiccator. It can be seen that

the standard deviations of the expansion are largest with the samples of low film thickness. This is expected because the final heights of the thin films are smaller than for the thick films. Therefore, a small (absolute) deviation in the measurement would have a larger impact on the results. The observations related to contraction may be of importance when studying free films in various laboratory equipment, such as fast heating thermogravimetric analyzers, where samples in powder form can be used.

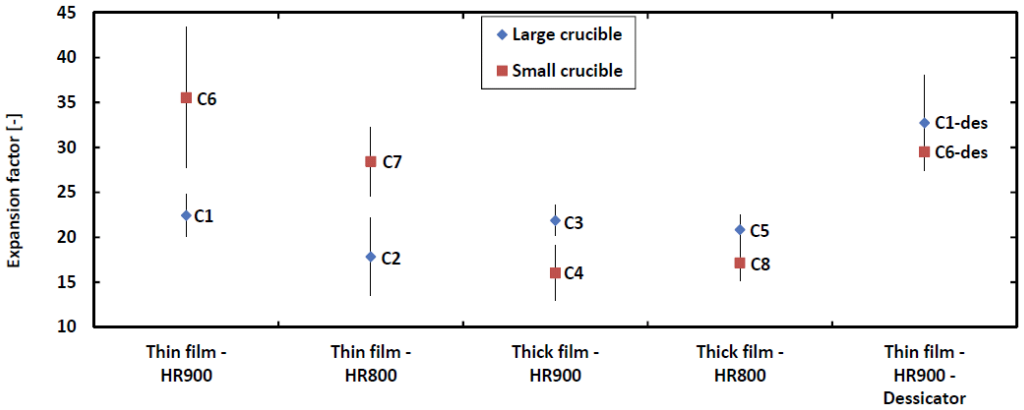

Figure 4.4. Average vertical expansion factor of the coating samples after heating from 800 °C or 900 °C to 1100 °C followed by 10 minutes exposure at 1100 °C. Labels (C1-C8) at each point refer to the conditions in Table 4.1.

Residual mass of the samples

The residual mass fractions after heating are seen in Table 4.2. Residual mass fractions were not determined for the samples stored in desiccator in order not to expose the samples unnecessarily to the surrounding environment. For samples with large film thicknesses (C1, C2, C6 and C7), the uncertainty of the samples with the low film thickness is rather large, except for sample group C7. It is evident from Table 4.2 that the residual mass fraction is not a function of film thickness, crucible size or small changes in heating rate.

Force pattern

A typical curve of the destruction force as function of distance, for another cellulosic coating heated under a radiant heater, was presented in Berlin et al.[6] . The char produced is described to consist of a pyrolysis zone closest to the substrate, a pre-pyrolysis zone, and an upper char layer closest to the heat source. The upper char layer was the mechanically weakest zone and the pyrolysis zone the strongest. Similar profiles are presented in Duquesne et al.[15] for intumescent formulations of polyurethane with expandable graphite or ammonium polyphosphate. To compare the force behavior of shock heated samples, a dimensionless length and force for each sample are introduced. The dimensionless length is defined from 0 to 1, where 0 is at the top of the char and 1 is the bottom of the crucible, shown in Figure 4.2 as L_s and L_0, respectively. The dimensionless force is defined as the actual force divided by the maximum force measured within 90% of the char height. This makes it possible to compare the behavior without considering the differences in expansions and absolute work of destruction. For the comparison, every 10 data point is used. As examples of the normalized force behavior of two repeated C3 samples (HR900, large crucible, 0.147 µm) and C7 (HR800, small crucible, 0.598 µm) are shown in Figure 4.5 and Figure 4.6, respectively. It is seen that the outer layer of the char is stronger than the underlying char. The reason only to focus on 90% of the distance is that a steep increase was observed in the last part of the char which will obscure the plot if included. This is because of solid debris material collecting below the piston. On a qualitative basis, similar behaviors are found for the other samples, including those stored in desiccator.

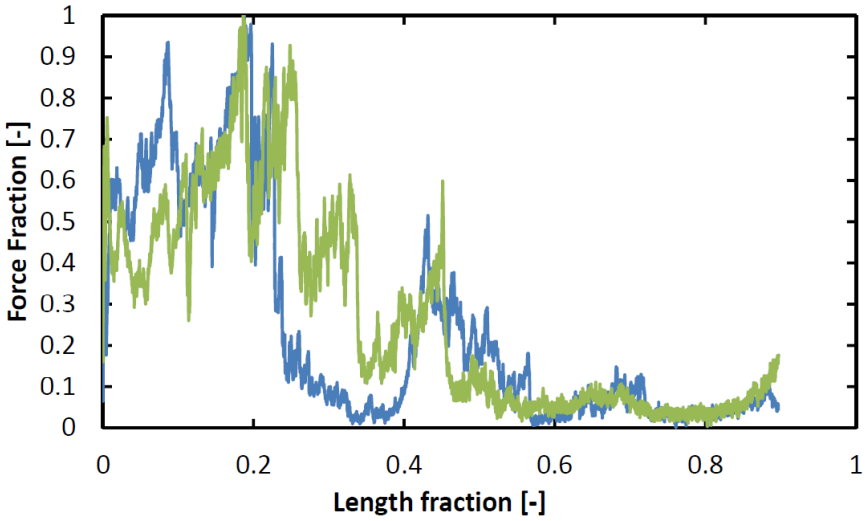

Figure 4.5. Two repetitions of force curves for the C3 sample. The force fraction corresponds to the fraction of force observed within 90% of the distance. Length fraction 0 corresponds to the top of the sample and length fraction 1 corresponds to the crucible.

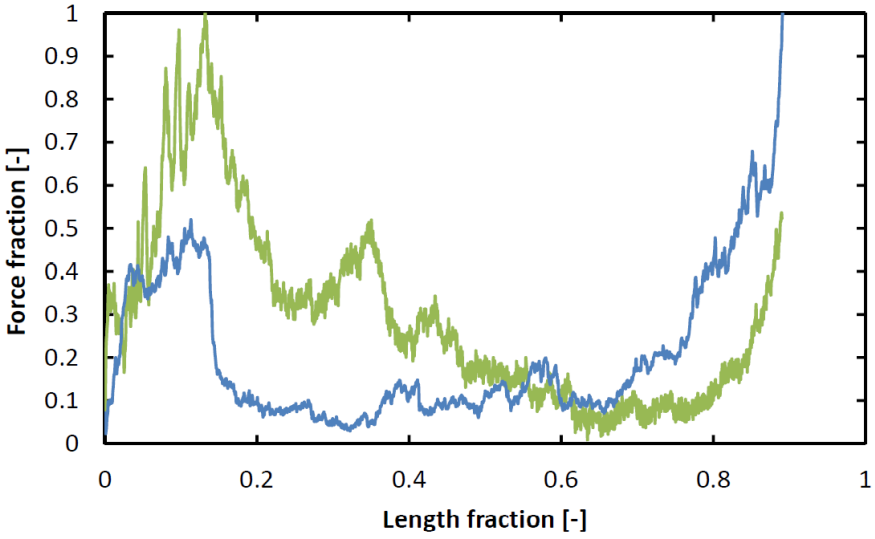

Figure 4.6. Two repetitions of force curves for the C7 sample. The force fraction corresponds to the fraction of force observed within 90% of the distance. Length fraction 0 corresponds to the top of the sample and length fraction 1 corresponds to the crucible.

Work of destruction

To evaluate the mechanical stability of the char against compression, three different measures for the work of destruction are used.

1. W_{90}: The accumulated work necessary to destroy the char – This is the work necessary to reach from the top and 90% of the expanded char height. 90% is chosen to reduce effects of the bottom of the crucible and debris char material assembled below the piston.
2. W_{Dist}: The average work of destruction per distance – This is the work found from bullet 1, divided by 90% of char cap height. This measure corresponds to the average force exerted on the piston.
3. $W_{1\,mm}$: This is the work necessary to destroy the outer layer of the char, defined here as the first 1 mm.

Work of destruction based on the parameters investigated

W_{90} and W_{Dist} are shown in Table 4.2, from which it is clear that neither of the parameters investigated can be seen to affect the values of W_{90} and W_{Dist}. This means that the work of destruction for the char formed does not change significantly with the initial film thickness. One might expect that char formed from a thicker coating film would require more energy to be destroyed, however, this does not appear to be the case.

Table 4.2. Results from the experiments. The residual mass fraction is shown for the samples stored in desiccator. W_{90} is the work necessary to penetrate 90 % of the char height. W_{dist} is the average work per millimeter, which is the same as the average force.

Coating Sample	Heating rate	Crucible size	DFT [mm]	Residual mass fraction [-]	W_{90} [mJ]	W_{dist} [mJ/mm]
C1	HR900	Large	0.147	0.33±0.029	0.15±0.97	0.05±0.04
C2	HR800	Large	0.147	0.33±0.032	0.32±0.23	0.14±0.12
C3	HR900	Large	0.598	0.36±0.007	0.31±0.04	0.03±0.01
C4	HR900	Small	0.598	0.36±0.005	0.19±0.09	0.02±0.01
C5	HR800	Small	0.598	0.37±0.006	0.44±0.20	0.05±0.02
C6	HR900	Small	0.147	0.36±0.021	0.08±0.09	0.02±0.02
C7	HR800	Small	0.147	0.35±0.005	0.10±0.11	0.03±0.02
C8	HR800	Large	0.598	0.35±0.009	0.26±0.08	0.02±0.01
$C1_{des}$	HR900	Large	0.147	N/A	0.08±0.01	0.02±0.002
$C6_{des}$	HR900	Small	0.147	N/A	0.04±0.01	0.01±0.002

From Table 4.2 it can be seen that the standard deviations concerning the works of destruction for the samples stored in desiccator are low compared to the other values. The low standard deviations should also be seen in comparison with the expansion of $C1_{des}$, shown in Figure 4.4 which has a standard deviation in the same range as the other samples. It should also be noted that for $C1_{des}$, due to variation in the expansion, the standard deviation of W_{90} is higher than for W_{dist}. As already mentioned, an important limitation to the work is that the properties are measured at room temperature and not at elevated temperatures. This point is addressed in the literature by reshetnikov et al.[7] and Le Bras et al.[12], but without quantifying the potential change that may take place in the chars. However, a crude estimate of a change in mechanical stability, due to cooling, may be found by comparing data in Berlin et al.[6] and Reshetnikov et al. [7], the force/area ratio, for an intumescent coating (carbamide-formaldehyde resin and carbamide-formaldehyde with ammonium polyphosphate sorbitol ratio 7:3), measured at temperatures between 350 and 1250^{o}C in a gas atmosphere is found to be $0.2\text{-}1\cdot10^{5}$ N/m^{2}. In Berlin et al.[6], using a similar coating heated under a radiant heater, the corresponding values, measured at room temperature, are found to vary between $0.04\cdot10^{5}$ and $0.08\cdot10^{5}$ N/m^{2}. Therefore, the values measured at high temperatures appear to be substantially higher than those measured at room temperature. It is interesting that storage in a desiccator reduces the uncertainty and it can therefore be speculated that the difference in mechanical properties between chars at high and low temperatures will be smaller than the difference observed for storage with or without a desiccator. The reason is probably that chars at temperatures well above 100 ^{o}C can be assumed not to have any condensed water on the surface and that water appear to weaken the char.

4.7 Expansion factor and work of destruction

It would generally be expected that a more expanded char would be weaker than a less expanded char[5, 11]. A plot of the expansion factor against the work of destruction per distance is shown in Figure 4.7. The points in the two figures are based on all the individual measurements from samples stored in free air. It seems reasonable, because of the large scatter seen in the plot, to conclude that there is no direct correlation between the expansion factor and the work of destruction. Similar plots were obtained for the work of destruction in the char cap and the total

work of destruction (not shown). The same conclusions are obtained by plotting the absolute char height instead of the expansion factor (not shown). These findings are in agreement with those presented Nørgaard et al.[10] (addressed in Chapter 5) for the positional dependence of W_{1mm}.

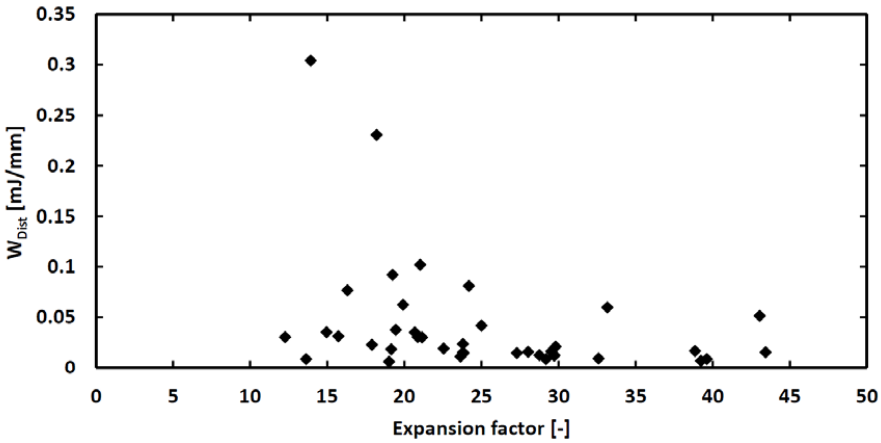

Figure 4.7. W_{Dist} for the individual measurements plotted against expansion factor. The plot shows all data points for C1-C8, $C1_{des}$ and $C6_{des}$. The total number of measurements is 39 (see Table 4.1). Several repetitions for each coating sample are included.

4.8 Conclusions

A generic solvent-borne intumescent coating, suited for cellulosic fires, was studied under shock heating conditions at two film thicknesses of 147 and 598 µm. Two different crucibles were applied and small changes in shock heating rate were investigated. The effect of char storage in a desiccator, prior to char strength measurements, was found to increase repeatability of the work of destruction. The qualitative behavior of the mechanical stability was observed to be the opposite of that previously reported with the outer char layer being the strongest part. The combination of very thin coatings (147 µm) and shock heating showed contraction of the coating in the horizontal plane. Disregarding experiments with char storage in a desiccator, the work of destruction could not be correlated to the following parameters; crucible size, small changes in shock heating rate, and film thickness. Furthermore, the expansion could not be related to the work necessary to compress the char and the mass loss and vertical expansion factor could not meaningfully be correlated to the parameters investigated. The results presented in this work are of importance for cellulosic coatings applied below potentially falling objects and for the use of

screening tests, where coatings may be exposed to fast heating rates. Finally, the char structure, that develops in a muffle oven under the conditions of this work, may differ from that found under a slower heating radiant heater.

4.9 References

[1] J.E.J. Staggs, Thermal conductivity estimates of intumescent chars by direct numerical simulation, Fire Saf. J. 4 (45) 228-237 (2010).

[2] T.T. Lie, C.E. American Society of, Structural fire protection, New York,N.Y., 1992, ISBN 0872628884.

[3] M. Jimenez, S. Duquesne, S. Bourbigot, High-throughput fire testing for intumescent coatings, Ind Eng Chem Res 22 (45) 7475-7481 (2006).

[4] M. Jimenez, S. Duquesne, S. Bourbigot, Multiscale experimental approach for developing high-performance intumescent coatings, Ind Eng Chem Res 13 (45) 4500-4508 (2006).

[5] I.S. Reshetnikov, M.Y. Yablokova, E.V. Potapova, N.A. Khalturinskij, V.Y. Chernyh, L.N. Mashlyakovskii, Mechanical stability of intumescent chars, J Appl Polym Sci 10 (67) 1827-1830 (1998).

[6] A.A. Berlin, N.A. Khalturinskii, I.S. Reshetnikov, M.Y. Yablokova, , in: M. Le Bras, G. Camino, S. Bourbigot, R. Delobel (Eds.), Fire Retardancy of Polymers: The Use of Intumescence, The Royal Society of Chemistry, Cambridge, 1998, ISBN 9781855738041.

[7] I.S. Reshetnikov, A.N. Garashchenko, V.L. Strakhov, Experimental investigation into mechanical destruction of intumescent chars, Polym. Adv. Technol. 8-12 (11) 392-397 (2000).

[8] H. Horacek, Reactions of stoichiometric intumescent paints, J Appl Polym Sci 3 (113) 1745-1756 (2009).

[9] B. Li, M. Xu, Effect of a novel charring–foaming agent on flame retardancy and thermal degradation of intumescent flame retardant polypropylene, Polym. Degrad. Stab. 6 (91) 1380-1386 (2006).

[10] K.P. Nørgaard, K. Dam-Johansen, P. Català, S. Kiil, Testing of intumescent coatings under fast heating, European Coatings Journal (June Issue) 34-39 (2012).

[11] E.D. Weil, Fire-Protective and Flame-Retardant Coatings-A State-of-the-Art Review, J. Fire Sci. 3 (29) 259-296 (2011).

[12] M.L. Bras, M. Bugajny, J. Lefebvre, S. Bourbigot, Use of polyurethanes as char-forming agents in polypropylene intumescent formulations, Polym. Int. 10 (49) 1115-1124 (2000).

[13] S. Kiil, Quantification of simultaneous solvent evaporation and chemical curing in thermoset coatings, Journal of coatings technology and research 7 (5) 569-586 (2010).

[14] S. Bourbigot, M. Le Bras, S. Duquesne, M. Rochery, Recent advances for intumescent polymers, Macromolecular Materials and Engineering 6 (289) 499-511 (2004).

[15] S. Duquesne, R. Delobel, M. Le Bras, G. Camino, A comparative study of the mechanism of action of ammonium polyphosphate and expandable graphite in polyurethane, Polym. Degrad. Stab. 2 (77) 333-344 (2002).

Chapter 5 - Investigation of the influence of heating conditions on cellulosic intumescent char characteristics

This chapter was published with the title “Intumescent coatings under fast heating” in European Coatings Journal, June issue, 2012 34-39. (authors Kristian Petersen Nørgaard, Kim Dam-Johansen Pere Català and Søren Kiil).

5.1 Abstract

Effects of different heating conditions on a generic acrylic solvent based intumescent coating for cellulosic fires are investigated. The heating conditions are described by gas composition, heating rate, temperature, and residence time. Intumescent chars formed in an electrically heated oven are evaluated with respect to char strength, measured as work of destruction, and the char structure, described by vertical expansion and homogeneity of resistance against compression. The coating samples are heated in gas flows consisting of pure atmospheric air, pure nitrogen, or a mixture of the two. The effect on the char of heating rates, using either shock heating or a heating rate around 10 ^{o}C/min, is investigated for coatings heated to a temperature close to 1100 ^{o}C. The effect of residence time, at the final temperature, on the char characteristics is also investigated. The method proposed is a useful way to produce intumescent chars, when using very fast heating rates.

5.2 Introduction

When structural steel is exposed to the elevated temperatures of a fire, the load bearing strength of the steel is reduced significantly[1]. Potentially, this causes collapse of the structure with loss of lifes or assets. To postpone the collapse and allow more time for evacuation, the steel can be coated with a fire protective intumescent coating. Intumescent coatings expand to a thermally insulating char when exposed to sufficiently high temperatures, as for instance in the event of a fire. Approval of an intumescent coating before use is done by third party organizations, where fire tests at well-defined heating rates, are carried out. A frequently used heating rate is the ISO

834 curve which has a fast increase in temperature in the beginning and then levels out from around 500 °C. A temperature of 1100 °C is reached after about two hours[1]. However, in practical applications, special cases where the coating is suddenly exposed to temperatures around 1100 °C may occur. Such a situation may arise when the char formed is damaged by a moving object which exposes the residual underlying coating. The situation is illustrated in Figure 5.1. A moving object could for instance be a fire door which is blown open with high speed. To simplify the investigation it is assumed that the exposed residual coating, below the char, is identical to the initial coating. The damage is assumed to happen when the gas temperature is close to 1100 °C. At this stage of the fire it is very possible that the oxygen content in the surrounding environment is low. Therefore, the investigation also considers the char characteristics as a function of the oxygen level. Another motivation to study the influence of oxygen on intumescent coatings is that in the test furnaces the oxygen content is reported to be around only 4 mol% in a well-tuned gas fired burner[2].

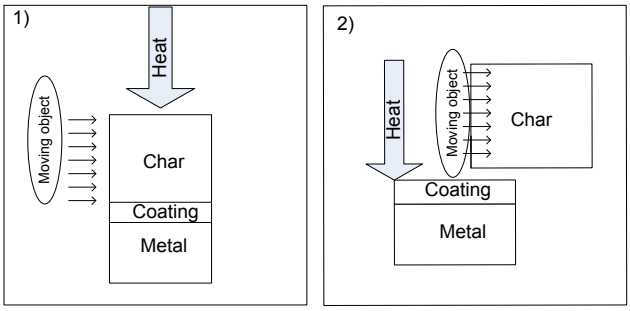

Figure 5.1. Schematic illustration of an incident where the residual coating layer, below the char, is suddenly exposed to a high temperature. The left hand illustration shows the situation before the char is damaged and the right hand one shows the situation right after.

5.3 Strategy of investigation

The purpose of this work is to investigate how the two parameters, gas composition and residence time at the final temperature, affect an intumescent coating exposed to shock heating, in the situation illustrated in Figure 5.1. Reference samples heated at a heating rate of approximately 10 °C/min are prepared for comparison. A very rapid heating rate, shock heating, in various gas compositions is obtained by direct insertion of free coating films in crucibles, into an electrically

heated horizontal ceramic tube. To investigate the mass change, the samples are weighed before and after heating. The final height of the expanded char and the mechanical stability were measured with a texture analyzer which records the work necessary to move a cylindrical piston to a certain depth in the char. Char structure is investigated with respect to the homogeneity of the mechanical resistance against compression. One at a time factor variation is used to investigate the influence of the parameters. Two important assumptions of the work are that the char characteristics are the same at room temperature after cooling and at high temperatures and that the exposed coating is identical to the initial coating.

5.4 Experimental procedures

Sample preparation

A generic solvent-based acrylic intumescent coating was selected for the investigation. Samples of the coating were prepared by drawdown using a CoatMaster 509 MC from Erichsen. The samples were prepared on overhead transparencies, produced by Folex, with draw down velocity of 10 mm/s. The area of the overhead transparencies was 210x297 mm^2 and the average specific surface area was 0.00763 m^2/g. After curing the film could easily be detached from the overhead transparencies. Samples with a target wet film thickness of 300 µm were prepared and cured for at least 2 weeks. The cured free films were cut using a round sharp metal fitting with a diameter of 14 mm. Dry film thickness of the coatings was measured using the Texture Analyzer to be 147 µm. The coating films used for the experiments were all prepared from the same batch.

Heating equipment

The samples were heated in the Entech electrically heated oven, shown in Figure 5.2. The length of the ceramic pipe is 1150 mm. The inner and outer diameters are 50 and 60 mm, respectively.

Figure 5.2. Photo of the heating oven.

The oven is heated with three electrical heaters and the samples are inserted in the small "sledge" shown in Figure 5.3. The oven enables heating in dewatered atmospheric air or nitrogen atmospheres. The nitrogen is purity grade 5.0 from AGA. The gas flows are controlled by mass flow controllers with a 100% capacity of 10 NL/min. For all experiments described in this article the total gas flow was constant at 5 NL/min. A water cooled chamber makes it possible to remove and insert the sample while the oven is hot and while maintaining the specified gas composition. For all the experiments a minimum time of 5 minutes after sealing the oven was kept to ensure the desired atmosphere had reestablished after the pipe had been opened. The samples were heated in porcelain crucibles from VWR-Bie og Berntsen with dimensions of 16 mm at the bottom and 28 mm at the top. To obtain shock heating the samples were pushed 63 cm into the ceramic tube using a metal stick. Insertion of the sample was done within 3 seconds. Before the sample was inserted, a K-type thermocouple (1 m in length and 1 mm in diameter) was inserted with an empty sledge and a steady state temperature of 1082 ^{o}C was measured.

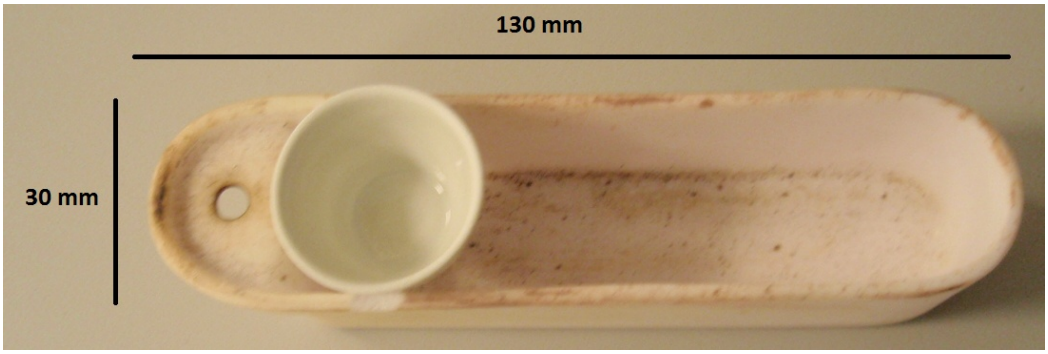

Figure 5.3. Photo of sledge with porcelain crucible. The length and width of the sledge are 130 and 30 mm, respectively.

Two experiments where three samples in the sledge were heated at a target set point heating rate of 10 °C/min were conducted. During the first heating, the thermocouple was inserted with the sledge. The measured temperature and heating rates are seen in Figure 5.4.

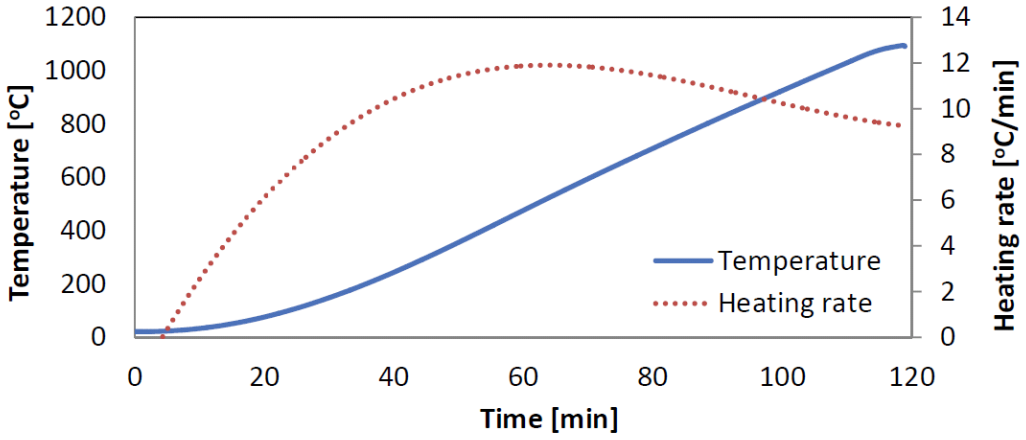

Figure 5.4. Measured temperature (solid line) and heating rate (dotted line) measured when the oven was adjusted to 10 °C/min set point heating rate.

Measurement of mechanical stability – Texture analyzer

A TA XT plus - Texture Analyzer, from stable Microsystems, was used to measure the compression force from which the work necessary to compress the cold sample can be calculated. The piston was set to move at a constant speed of 0.1 mm/s and 500 data points where recorded per second.

The end of the piston was circular with a diameter of 2 mm. The trigger force at which the texture analyzer starts registering the sample is set to 0.00490 N. Before the measurement the Texture analyzer was calibrated using the automatic program, with respect to force and height. In the remainder of this article the work of destruction is defined as the necessary work to reach 1 mm vertical position in the char. Further discussions on testing mechanical resistance of chars are available elsewhere[3, 4]. The texture analyzer is also used to measure the height of the sample, by recording the position at which the trigger force is met. Calibration with the crucible bottom height was made for each sample.

5.5 Results

Results obtained from the experiments are shown in Table 5.1. The vertical expansion and work of destruction presented in Table 5.1 are measured at the highest point of the sample (expansion was not uniform). Each heating experiment was repeated three times. For determination of residual mass fractions all sets are based on three repetitions. For the texture measurements, in a few cases it was not possible to conduct the experiments, because the sample was damaged. Therefore, Table 5.1 shows the number of repetitions of texture measurements. It is generally seen that there are large deviations in the work of destruction in all the sets.

Table 5.1. Summary of results. For mass determination three repetitions were made. The residence time is the time the sample was kept at 1082 ^{o}C. Work of destruction is the work necessary to reach 1 mm into the sample.

Coating Sample	Repetitions for texture analysis	Gas flow [L/min] (gas type)	Residence time [min]	Residual mass fraction [%]	Vertical expansion [mm]	Work of destruction [mJ]
C1	3	5 (N_2)	5	27.6±3.8	5.8±0.8	0.03±0.02
C2	2	5 (Atm)	5	37.6±0.5	4.0±0.2	0.02±0.01
C3	3	2.5 (Atm) + 2.5 (N_2)	5	37.5±0.2	4.5±0.4	0.01±0.004
C4	2	5 (N_2)	15	22.9±2.0	5.8±0.1	0.01±0.01
C5	3	5 (Atm)	15	37.7±1.6	4.1±0.6	0.01±0.004
C6	2	2.5 (Atm) + 2.5 (N_2)	15	38.4±1.1	4.1±0.2	0.03±0.04
C7	3	5 (N_2)	5	36.5±0.7	0.7±0.1	-
C8	0	5 (Atm)	5	19.1±1.1	-	-

Effect of gas composition

Three levels of gas compositions are investigated, 1) nitrogen, 2) atmospheric air and 3) 1:1 mixture of these. Comparing the numbers, it is seen that generally the residual mass fraction is lower for the samples heated in N_2 than for the samples heated in the presence of atmospheric air. In addition the vertical expansion of the samples is higher for the samples in nitrogen. From Table 5.1 it is seen that variation from diluted atmospheric air to normal atmospheric air does not seem to affect the results. This can be seen by comparison of C2 with C3 and C5 with C6, respectively. One possible reason that there are small differences between the samples heated at different oxygen contents could be that the concentration is above the limiting oxygen index at which is the lowest oxygen concentration at which the coating can sustain a flame[5]. The observation that a lower residual mass is present in the N_2 atmosphere may seem surprising. However, this has also been reported for other intumescent coatings, e.g. in reference[2]. A possible explanation for the lower residual mass could be that in the presence of oxygen, decomposition, due to oxidation of the char, may take place, whereas in nitrogen the decomposition could be dehydrogenation, deoxygenation and aromatization, as suggested in Kandola and Horrocks[6].

Effect of heating rate and residence time

Coating samples heated at 10 ^{o}C/min in atmospheric air (C7) and nitrogen (C8) were expanded very little after the heating. Furthermore, the samples heated in nitrogen (C8) were shattered, and therefore it was not possible to make compression measurements on that particular sample. From Table 5.1 it is seen that the slow heating does not seem to affect the residual mass significantly compared to samples heated with shock heating. However, a small reduction in residual mass is seen for the sample heated in nitrogen. Potentially, this could be due to the longer residence time to reach 1100 ^{o}C, where the aforementioned degradation reactions could take place. For shock heating, it is seen that there does not seem to be a significant difference between the samples which had a residence time of 5 minutes or 15 minutes.

Homogeneity of the char

From Table 5.1 the work of destruction is seen to vary among the samples causing a large standard deviation. In total 18 different samples were used to measure the work of destruction. When possible, repetitions at different horizontal positions were made for each sample. These results are collected in Table 5.2. C refers to samples exposed to the conditions shown in Table 5.1. S

refers to individual repetitions and the number in parenthesis refers to the number of compressions on each sample. An example of Sample C1, S1 after three compressions is seen in Figure 5.5.

Table 5.2. Averages and standard deviations in the work of destruction for each sample. The number in parenthesis shows the number of repetitions made on each sample. Group refers to the groups from Table 5.1. Sample refers to the repetitions in each group. For the samples where a single repetition is made the average and standard deviations are not calculated. Gas composition and residence times are shown in parentheses corresponding to the description in Table 5.1.

Sample→ Group↓	S1 [mJ]	S2 [mJ]	S3 [mJ]
C1 (N_2, 5 min)	0.031 ± 0.019 (3)	0.013 ± 0.005 (3)	0.0159 ± 0.0072 (3)
C2 (Atm, 5 min)	0.023 ± 0.008 (3)	0.015 ± 0.002 (2)	-
C3 (N_2+Atm, 5 min)	0.011 ± 0.001 (2)	0.013 ± 0.001 (2)	- (1)
C4 (N_2, 15 min)	0.005 ± 0.002 (2)	0.011 ± 0.006 (2)	-
C5 (Atm, 15 min)	0.018 ± 0.010 (2)	0.015 ± 0.003 (2)	- (1)
C6 (N_2+Atm, 15 min)	0.007 ± 0.005 (2)	0.045 ± 0.019 (2)	-

From these data it is seen that the chars produced by the shock heating are fairly inhomogeneous with respect to the work of destruction, both between each sample and within the horizontal plane in the same sample. A similar finding for samples heated with small variations in shock heating rate and dry film thicknesses of 147 to 598 µm was found in Nørgaard et al. [7] (addressed in Chapter 4).

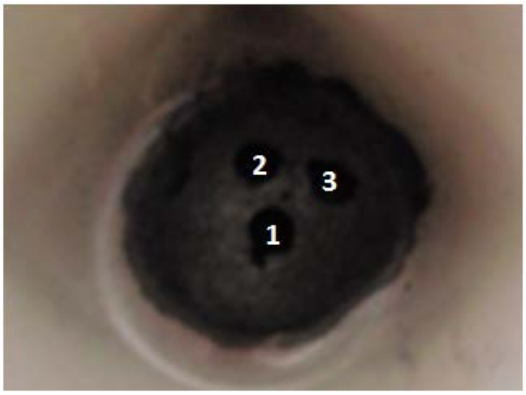

Figure 5.5. Example of sample C1,S1 after compression (expanded char in crucible seen from above). The three holes, labeled 1, 2 and 3, correspond to the number of repetitions in the sample.

5.6 Conclusions

For the selected acrylic coating exposed to shock heating it has been found that the most important factor on vertical expansion and residual mass is the gas composition. The samples heated in pure nitrogen showed both a higher vertical expansion and a higher mass loss than the samples heated in the presence of atmospheric air.

It was found that the chars were inhomogeneous with respect to work of destruction, both in the horizontal plane and between samples measured at the maximum vertical expansion point. The variation in the work of destruction at different points of the sample was found to exceed the effect of the investigated parameters. The samples heated with shock heating, showed higher expansion in both nitrogen and atmospheric air than the samples heated at approximately 10 ^{o}C/min. It has also been shown that if the selected acrylic intumescent coating is exposed to the very fast heating rate, due to damaged char, an evaluation of the char should necessarily be made at the exact heating conditions.

The method presented is of practical importance in the investigation of what happens if the coating is damaged and the residual coating exposed to rapid heating. The results also show the importance of choosing the correct gas composition when developing intumescent coatings for long term fire protection.

5.7 Acknowledgements

Financial support by The Hempel Foundation is gratefully acknowledged.

5.8 Remarks to chapters 4 and 5

The two chapters 4 and 5 have investigated the use of shock heating in relation to char expansion and strength. In chapter 4, which was prepared following the results presented in chapter 5, it was learned that char strength measurements at room temperature, at least for the fragile char produced from the cellulosic coating used, was affected by the moisture adsorbed on the char. Therefore, it is noted that if this knowledge had been available earlier, the char strength measurements could have been performed after storage of chars in a desiccator, which would have increased the repeatability of the char strength measurements presented in chapter 5. In summary, the conclusions regarding char strength in chapter 5 are valid, however, if the experiments were to be repeated, it would be preferable to use a desiccator to increase accuracy of the data obtained.

In addition, after the article in chapter 5 was published and during the review process of the article presented in chapter 4, an article about char strength was published by another research group, Muller et al.[8]. In this work, the char strength for polyurethanes was investigated in different heating scenarios and temperatures up to 700 ^{o}C. It was found that there is a difference between the char strength at room temperature and high temperature. Although it has not been investigated, it is very possible that storage of the samples in a desiccator would have affected also the conclusions of Muller et al.[8]. Muller et al. found that heating rate and temperature are of importance to the mechanical stability. This finding is interesting because it supports the use of shock heating to experimentally simulate the effect of damages on the char.

Another comment, to this thesis of the shock heating method described in chapters 4 and 5 which has often been received during presentations given by the author of this thesis is that the heating occurs from all sides. However, in practical applications such situations are easy to imagine, for instance if a thin steel column is covered with an intumescent coating the coating surrounds the substrate. The situation may also occur when steel joints are protected by intumescent coatings.

5.9 References

[1] T.T. Lie, C.E. American Society of, Structural fire protection, New York,N.Y., 1992, ISBN 0872628884.

[2] G.J. Griffin, A.D. Bicknell, T.J. Brown, Studies on the effect of atmospheric oxygen content on the thermal resistance of intumescent, fire-retardant coatings, J. Fire Sci. 4 (23) 303-328 (2005).

[3] I.S. Reshetnikov, M.Y. Yablokova, E.V. Potapova, N.A. Khalturinskij, V.Y. Chernyh, L.N. Mashlyakovskii, Mechanical stability of intumescent chars, J Appl Polym Sci 10 (67) 1827-1830 (1998).

[4] I.S. Reshetnikov, A.N. Garashchenko, V.L. Strakhov, Experimental investigation into mechanical destruction of intumescent chars, Polym. Adv. Technol. 8-12 (11) 392-397 (2000).

[5] E.D. Weil, N.G. Patel, M. Said, M.M. Hirschler, S. Shakir, Oxygen index: correlations to other fire tests, Fire Mater. 4 (16) 159-167 (1992).

[6] B.K. Kandola, A.R. Horrocks, Complex char formation in flame-retarded fibre-intumescent combinations--II. Thermal analytical studies, Polym. Degrad. Stab. 2-3 (54) 289-303 (1996).

[7] K.P. Nørgaard, K. Dam-Johansen, P. Català, S. Kiil, Investigation of char strength and expansion properties of an intumescent coating exposed to rapid heating rates, Prog. Org. Coat. 12 (76) 1851-1857 (2013).

[8] M. Muller, S. Bourbigot, S. Duquesne, R.A. Klein, G. Giannini, C.I. Lindsay, Measurement and investigation of intumescent char strength: Application to polyurethanes, J. Fire Sci. 4 (31) 293-308 (2013).

Conclusions

Intumescent fire protective coatings are an efficient mean to protect steel structures from high temperatures and subsequent collapse in the event of a fire. The coating expands according to a complex mechanism of temperature triggered reactions and accompanying physical phenomena. Apart from the intumescent coatings themself, interaction with process parameters are of importance. In this work, process parameters such as damages of the char, interactions with a primer, coating thickness, and oxygen content in the fire are investigated using a single solvent-borne acrylic intumescent coating suited for cellulosic fires. The choice of keeping the formulation constant was made to investigate the influence of process parameters and develop methods without having to consider changes due to coating formulation. In the thesis, epoxy primers for the intumescent coating were investigated and it was found that a combination of primer thickness and the presence of oxygen affected the performance of the primers. The primers were also seen to change color from red to black when heated in nitrogen and remained red in the presence of oxygen. A relatively easy applicable engineering model describing expansion rate and temperatures inside the char and the steel substrate was developed. The model showed good agreement with experimental results from a pilot scale gas-fired furnace, although a quantitative match was not possible. The model was solved in a discretized and non-discretized version and it was shown that increasing the number of input parameters did not improve the match between experimental data and model output. An important learning from the experimental and modeling work was that temperatures inside the char are also important for accurate model validation because even if steel temperatures are simulated correctly, the intra-char temperatures may not be. The model can, qualitatively, explain all temperature-time curves and thereby provides an important learning tool. The strength of chars exposed to shock heating was also investigated. The shock heating is important to simulate special scenarios which may occur in a fire and also it shows a potential to develop fast screening methods for investigating intumescent coatings. It was not possible to meaningfully correlate the work of destruction of the chars with the expansion although a repeatable non-dimensional force profile was observed. The force profile showed that the hardest char was in the top char layer. Close to the substrate, the strength also increased, probably due to debris material, and at the center of the char, a mechanically weak zone was

present. Another interesting finding was that the storage of samples in a desiccator improved the repeatability of the char strength measured at room temperature.

Future work

Based on the results and methods presented in this thesis, several topics would be of interest for further investigation. An obvious extension of the project would be to investigate different coating formulations and map the influences of interesting parameters such as binder type (e.g. water based coatings), pigment content and intumescence chemistry.

To further develop the screening method for primers for intumescent coatings, obtaining a larger set of data (reflecting e.g. primer chemistry, thickness, and time to failure) obtained in the furnace would be interesting. In addition, if a larger number of data from the horizontal oven were available, this could be used for mapping the primers and thicknesses suitable for intumescent coatings. Another topic is how to use the color change of the primer observed in nitrogen to verify whether primers in gas-fired furnaces have been exposed to oxygen.

The mathematical model showed a potential as a practically applicable engineering model. Extending the model, to simulate complex geometries (e.g. steel beams) could be interesting and useful for practical purposes. In addition, the general applicability of the simple model would be relevant to explore. A detailed sensitivity analysis and implementation of optimization algorithms (e.g. Nelder-Mead method) for improving the parameter estimation would be useful.

In relation to char strength, further investigations of chars at lower temperatures would be interesting to get a detailed map of the situations occurring in the earlier stages of the fire, where the expansion is less complete and the temperature is lower than the 1100 ^{o}C used in this study. In the light of the recently published article by Muller et al.[1], it would be very interesting to compare char strength measured at high temperatures with char strength measured at room temperature after storage in a desiccator. Finally, a further development of the new methods to epoxy coatings intended for hydrocarbon fires, where much higher heating rates (room temperature to 1100 ^{o}C in about 5 min) are used, would be an important target to pursue.

Appendix A1 – Contribution of solid, gas and radiation to the effective thermal conductivity

As shown in equation (3-15) the effective thermal conductivity of the intumescent char is affected by conduction through the solid and the gas contained in the pores of the chars. In addition, radiation across the pores is also included. In Figure 3.16 the effective thermal conductivity, which combines all the contributions is shown. In Figure A1.1 a comparison of the contribution from the gas/solid part and the radiation part is shown. The comparison is made for a fully expanded char with a porosity of 0.975. The input parameters are the same as the base case shown in Table 3.2 and for the non-discretized model in Table 3.3. From the figure it is seen that until 420 ^{o}C the contribution from the gas/solid part is the most significant. After this temperature the contribution from the radiation part becomes more and more influential. The contribution of the solid is negligible in the figure.

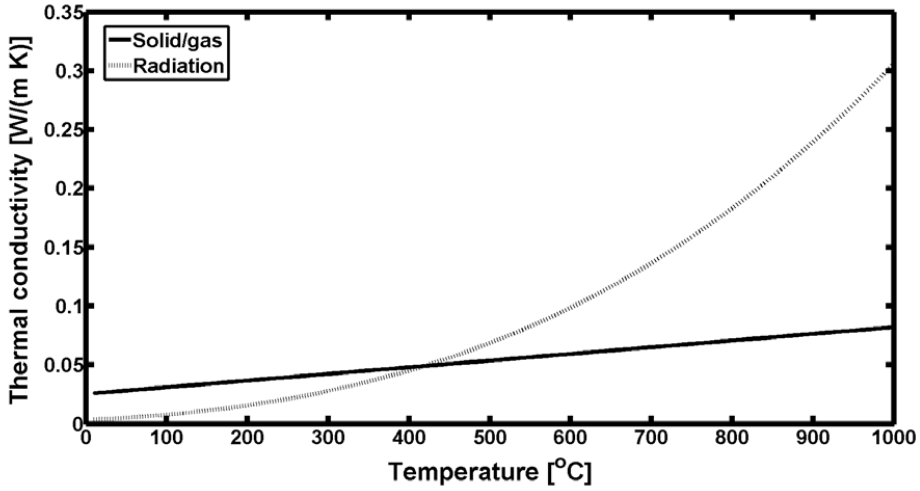

Figure A1.1. Comparison of contributions to the thermal conductivity from the gas/solid part (first term on the right hand side of equation (3-15)) and the radiation part (second term on the right hand side of equation (3-15)).

Centre of Combustion and Harmful Emission Control
Department of Chemical and
Biochemical Engineering
Technical University of Denmark
Søltofts Plads, Building 229
DK-2800 Kgs. Lyngby
Denmark

Phone: +45 4525 2800
Fax: +45 4525 4588
Web: www.chec.kt.dtu.dk

ISBN : 978-87-93054-64-6